NTNU
Norwegian University of
Science and Technology

Operando FTIR study of the NH$_3$-SCR reaction over Cu/Al$_2$O$_3$ and Fe/Al$_2$O$_3$ catalysts
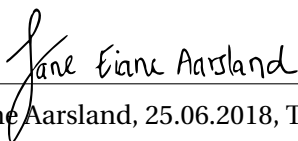
Jane Eiane Aarsland

Preface

This master thesis has been written for the department of Chemical Engineering at the Norwegian University of Science and Technology as a continuation of the specialization project course TKP 4580 in chemical engineering.

Foremost, I would like to thank my supervisor, Professor Magnus Rønning, for his help and guidance during the work of this thesis. I would also like to express my sincere gratitude to my co-supervisor, PhD candidate Samuel K. Regli, for his support, knowledge and assistance in experimental methods and data analysis. I would like to thank Ole Håvik Bjørkedal for kindly providing the catalyst samples used in the work of this thesis. Last, but not least, I would like to thank my family and friends for their amazing support, inspiration and encouragement, and my fellow classmates for making my years as a student in Trondheim unforgettable.

Declaration of compliance:
I declare that this is an independent work according to the exam regulations of the Norwegian University of Science and technology (NTNU).

Jane Eiane Aarsland, 25.06.2018, Trondheim

Abstract

The aim of this thesis was to perform an *operando* study of the NH_3-SCR reaction using Diffuse Reflectance Infrared Fourier Transform Spectroscopy (DRIFTS) and Mass Spectrometry (MS). The experiments were performed in a Nicolet iS50 FTIR Spectrometer with a Harrick Praying Mantis cell. 3 wt% Cu/Al_2O_3, 3 wt% Fe/Al_2O_3 catalysts and pure m-Al_2O_3 support were used in the experiments. The MS data was used as a qualitative measurement for comparison with the generated IR data. The FTIR spectra showed that the NO gas seemed to react differently with the surface of the different samples. The NO seemed to be weakly chemisorbed on Cu/Al_2O_3 and disappeared when NH_3 was introduced to the system. On the Fe/Al_2O_3 catalyst, the NO reacted with the surface to form ferric nitrates that could further react with NH_3 to form H_2O and N_2. As for the m-Al_2O_3 support, the introduction of NO was almost not noticeable in the spectra. The MS data showed a difference in N_2 production between the three samples, although it was expected to see even more activity in the Cu and Fe samples than on the support alone. However, the IR results indicated that less reaction products were formed on the support.

Sammendrag

Hensikten med denne masteravhandlingen var å gjennomføre et *operando* studie av NH_3-SCR reaksjonen ved å bruke Diffuse Reflectance Infrared Fourier Transform Spektroskopi (DRIFTS) og Masse Spektrometri (MS). Eksperimentene ble utført i et Nicolet iS50 FTIR Spektrometer med en Harrick Praying Mantis celle. 3 vekt% Cu/Al_2O_3, 3 vekt% Fe/Al_2O_3 katalysatorer og m-Al_2O_3 ble brukt i forsøkene. MS-data ble brukt som en kvalitativ måling for sammenlikning med de genererte IR resultatene. FTIR spektrene viste at NO-gass syntes å reagere annerledes med overflaten av de forskjellige prøvene. NO syntes å være svakt kjemisorbert på Cu/Al_2O_3 og forsvant når NH_3 ble introdusert i systemet. På Fe/Al_2O_3 katalysatoren reagerte NO med overflaten for å danne jernnitrater som kunne reagere ytterligere med NH_3 for å danne H_2O og N_2. Når det gjelder m-Al_2O_3 så var introduksjonen av NO nesten ikke merkbar i spektrene. MS resultatene viste en forskjell i N_2 produksjon mellom de tre prøvene, selv om det var forventet å se mer aktivitet på Cu og Fe katalysatoren enn på støttestrukturen. Imidlertid viste IR-resultatene at mindre reaksjonsprodukter ble dannet på m-Al_2O_3.

Contents

List of Symbols

Symbols	Description
A	Absorbance
a	Constant in the Morse function
D_e	Dissociation Energy
Ep	Energy of Photon
e_i	Magnitude of Atomic Changes
F	Spring Force
h	Planck's Constant
I	Intensity of Beam of Electromagnetic Radiation that has passed through the Sample
I_0	Initial Intensity of a Beam of Electromagnetic Radiation
k	Spring Constant in Hooke's law
m	Mass
r_i	Position of Atoms
x_i	Displacement Vectors
ν	Photon Frequency
ω	Constant used to express periodical motions in Hooke's law
μ	Dipole Moment

List of Abbreviations

Abbreviation	Description
Ar	Argon
DRIFTS	Diffuse Reflectance Infrared Fourier Transform Spectroscopy
FTIR	Fourier Transform Infrared Spectroscopy
He	Helium
N_2	Nitrogen
NH_3	Ammonia
NIST	National Institute of Standards and Technology
NO	Nitrogen Oxide
NO_x	Nitrogen Oxides
MFC	Mass Flow Controllers
MS	Mass Spectrometry
m/z	Mass to charge ratio of an ion
SCR	Selective Catalytic Reduction
S/N	Signal-to-noise

List of Figures

List of Tables

Chapter 1

Introduction

Nitrogen Oxides (NO_x) are defined as a group of molecules containing nitrogen and oxygen which are byproducts from high-temperature combustion of fossil fuels. They are unwanted pollutants in the atmosphere because they contribute to acid rain and thus acidification of aquatic systems [1], [2], tropospheric ozone production [3], and formation of carcinogenic particles [4]. The main sources of NO_x are emissions from combustion of fossil fuels in the transportation sector and from industrial activity. About 46% of the total NO_x emissions come from electrical power plants, while 49% of the total emission quantity come from transportation vehicles [5]. Reducing emissions from power plants, factories and automotive vehicles is therefore of great importance. Selective catalytic reduction of NO_x by ammonia (NH_3-SCR) is one of the most widely used technologies for NO_x reduction today [6], [7], and it is still an important research area due to its environmental impact. Understanding the kinetics and the mechanism of the reaction is important in order to develop good catalysts. *In situ* and *operando* FTIR spectroscopy has therefore been used by several scientists to study the mechanism of the SCR reaction by studying the catalyst surface adspecies and their reaction activity [8]–[12].

The term *in situ* means that the measurements are carried out under reaction conditions, or under conditions that are similar as to the relevant reaction conditions [13]. *Operando* methodology is a form of *in situ* measurements where the spectroscopic characterization is compared to information from measurements of catalytic performance [14]. *Operando* studies are important in order to understand the chemistry that takes place under reaction conditions. An *operando* study of the NH_3-SCR reaction was therefore performed in this thesis under operating conditions

using FTIR spectroscopy with simultaneous monitoring of the gas composition by using a mass spectrometer.

1.1 Motivation

1.1.1 Infrared Spectroscopy

When it comes to characterization of catalytic systems, infrared absorption spectroscopy was one of the first techniques in use, and it is still one of the most widely used techniques today. This is because of its ability to provide important information about the catalyst itself, but also about the reaction mechanism taking place on the catalyst surface [15]. Infrared spectroscopy can be used on catalysts for many purposes. One of them is to identify adsorbed species on the surface since all molecules have its own vibrational energy. By looking at the peaks generated by the vibrational energy in the IR spectrum and assigning them to known vibrational modes, such as C-O or O-H stretches, one can identify unknown species. The IR spectrum can in other words be seen as the fingerprint of the molecules [16]. The IR technique can also be used to calculate the surface coverage of the adsorbed species as it follows the Beer-Lambert law where the absorption is proportional to the number of molecules adsorbed [15]. The catalytic sites of the catalysts are often determined by using probe molecules, with known vibrational frequencies, that only adsorbes to specific sites on the catalyst surface. The adsorption of these probe molecules can then be used to determine if these specific sites are present on the surface, and the intensity of the absorbance can be used to determine the surface coverage [17].

The first IR experiments in the field of catalysis were performed *ex situ*, after exposure to the reactants, in order to retrieve information about chemisorbed species on supported metals. Later, it was attempted to do the same experiments under more realistic conditions, *in situ*. Lately, a lot of focus has been directed towards *operando* studies as well, under actual reaction conditions and in combination with other techniques in order to correlate molecular and structural information. The terms *in situ* and *operando* may not always be easy to differentiate, but the goal of both methodologies is usually to study the connection between surface species identified by IR and the reaction that is taking place on the catalyst surface [15]. This was also the motivation behind using *operando* FTIR as an analysis tool in this thesis.

IR absorption spectroscopy is a powerful tool that can provide important information about the molecular structure of the catalyst surface, the active sites and the adsorbed

species under actual reaction conditions which are difficult to obtain by other techniques. In principle, the same information could also have been retrieved by other techniques such as Raman spectroscopy. However, this is more often used as a complementary technique to the infrared spectroscopy as it often provides weaker signals, although it is better than IR on detecting low-frequency modes. Also, the FTIR instruments are cheaper than Raman and therefore also a more commonly applied technique [15].

1.1.2 Selective Catalytic Reduction

The motivation behind choosing selective catalytic reduction as the reaction to be studied was its environmental importance. It is also a reaction that is suitable for spectroscopic studies as there is a cyclic switch between oxidizing and reductive environments when ammonia is used as a reductant. Different substances will adsorb to the catalyst when the conditions change, and thus changes will also be seen in the IR spectra.

The United States Environmental Protection Agency, US EPA, has decreased the limits of the amount of harmful emissions that come from diesel fuel in the transportation sector. In 2010 a new regulation came fully into effect where the US EPA emission standards decreased the limits to the amount of NO_x that each vehicle was legally allowed to produce. This caused a need to advance the NO_x reduction technology that was already in use, as all on-road heavy duty diesel engines would require NO_x exhaust control technology by the year of 2010 [18]. Held *et. al.* [19] was among the first to publish an article on how to apply the SCR system into vehicles. They suggested to use non-toxic urea as the reducing agent, where ammonia was released under hydrothermal conditions. This technique is more complicated than the stationary SCR reaction used in power plants as the amount of urea needs to fit the activity of the catalyst in use, the ammonia stored on the catalyst, and the constant variations in NO_x emissions. A lot of work has therefore been preformed in order to improve this technique, and reduction efficiency is in the range of 80-90% today [6].

The importance of SCR technology became very clear when the EPA regulations lead to an incident called "Dieselgate" which refers to the car manufacturing company Volkswagen who claimed that their cars did not need SCR technology as they used a cheaper technology called LNT (Lean NO_x Trap) instead. Later it was revealed that their cars were actually programmed to activate emission controls during laboratory testing to make the cars meet the US emission standards. The emission controls were

turned off, and the emissions were far from meeting the regulation standards when the cars were actually in use. Volkswagen admitted to their scheme, and EPA filed an official notice of violation in 2015 [20]. The Dieselgate incident shows how important the SCR technology is for car manufacturers in order to meet emission standards. NO_x from gasoline is treated efficiently by the three-way catalyst, but this can not be implemented in a diesel engine because it operates under oxygen excess. The SCR technology has been widely used in stationary power plants for many years, and it was first implemented in diesel vehicles in 2005 [10].

Stricter national and international regulations to reduce harmful air emissions and growing awareness of the environmental impact of global shipping activity have also caused increased interest for the installation of abatement systems in the marine sector. Currently, SCR is considered as one of the best technologies in this industry as well, as it does not need to be complemented by other technologies due to its high efficiency. Research and development of marine SCR installations have however not come as far as in the automotive industry, possible due to lack of legal regulations. It is however expected that stricter regulations will be met in the future [21].

1.1.3 Catalyst choice

Various catalysts have been used for the NH_3-SCR process. V_2O_5/TiO_2 is most widely used today because of its high activity and high resistance to SO_2 [22], [23]. Vanadia is however a toxic compound which can lead to production of volatile compounds at high operating temperatures. Also, the titania support has a low stability at low temperatures. A lot of NO_x is produced during cold start-up of a vehicle or during short travelling distances, and it is therefore important that the catalyst also works well at low temperatures [5], [10]. As a result it is desirable to develop alternative catalysts. Zeolite-based catalysts promoted by transition metals have proven to be a very good alternative to vanadia. Copper and iron are mostly used as transition metals due to their high activity [5], [8], [10]. The zeolites promoted by iron are usually used in high-temperature reactions as it is most active at temperatures higher than 300°C. Copper-based zeolites, on the other hand, are most active at temperatures below 300°C. Both transition metals generally promote high activity, but Kamasamudram *et. al.* [24] have shown that the NO_x conversion is higher in iron-exchanged zeolites than in copper-exchanged zeolites under transient conditions, i.e., when there is constant variations in the concentration of the reactants, which is usually the case in real-life operation. The zeolite-based systems (especially ZSM-5 zeolites) have gained a lot of interest because of their high activity in converting nitrogen oxides

to N_2 and H_2O. However, synthesizing a Cu-ZSM-5 catalyst is around 25-30 more expensive than synthesizing for example a CuO/Al_2O_3 catalyst. It is also harder to make the zeolite-based catalyst meet the industrial requirements that are needed, like for instance mechanical strength [8]. Therefore, it is interesting to look into the use of high-surface-area oxides like Al_2O_3 and how to improve their catalytic behavior. Fe/Al_2O_3 and Cu/Al_2O_3 have therefore been chosen as catalysts in this thesis along with the m-Al_2O_3 support itself for comparison.

1.2 Goal

This master thesis was written as a continuation of a specialization project where the aim was to establish a method for *in situ* characterization of Lewis and Brønsted acid sites on various catalysts by using Diffuse Reflectance Infrared Fourier Spectroscopy (DRIFTS). The goal of this master thesis was to further increase the complexity of those experiments to see if it was possible to do *operando* studies of reactions in the FTIR cell. The specialization project had various bottlenecks in the procedure which could be improved, such as data treatment, data analysis and visualization as these are all very time-consuming procedures. The challenge with *operando* FTIR studies is that it generates a lot of data that has to be processed and analyzed. This has been tackled by Python scripting in order to make the process of data analysis more efficient. The samples used in this thesis were supplied by PhD candidate Ole Håvik Bjørkedal who researches catalysts for use in the NH_3-SCR reaction. Synthesis and characterization beyond IR spectroscopy have therefore not been in the scope of this thesis.

Chapter 2

Theory

2.1 Selective Catalytic Reduction

In SCR technology, a gaseous reductant like ammonia or urea is added to the flue gas and adsorbed onto a catalyst with the means of converting NO_x gases into N_2 and H_2O [2], [25]. Ammonia is most widely used as a reductant because of its availability, although it has its disadvantages like the risk of emission of unreacted ammonia which may lead to NO_x formation again [26]. It is therefore important to achieve as high conversion of the reductant as possible. The process usually occurs at a temperature between 300-400°C [5]. The NO_x produced by diesel engines mostly consist of NO, and only a small fraction of NO_2. Reduction of NO by NH_3 is referred to as the "standard SCR equation" [10]:

$$4NO + 4NH_3 + O_2 \rightarrow 4N_2 + 6H_2O \tag{2.1}$$
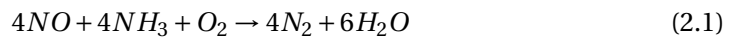
However, it is possible to speed up the SCR reaction by increasing the NO_2/NO_x molar ratio. The reaction is then referred to as "fast SCR reaction" [10], [25]:

$$4NH_3 + 2NO + 2NO_2 \rightarrow 4N_2 + 6H_2O \tag{2.2}$$
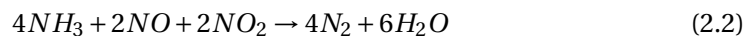
The fast SCR reaction is mostly used in diesel after-treatment systems where an oxidation catalyst, diesel oxidation catalyst (DOC), is used to oxidize NO to NO_2 [10]. Furthermore, there is a third SCR reaction that occurs if only NO_2 takes place in the reaction. This reaction is slower than the two others [25]:

$$4NH_3 + 3NO_2 \rightarrow 3.5N_2 + 6H_2O \tag{2.3}$$
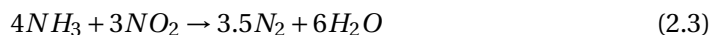
There are also some side reactions that compete with the SCR reaction. For example, NH_3 may be oxidized to NO at high temperatures. This is an undesirable reaction that should be avoided because less NH_3 will then be available for NO_x conversion [25]:

$$4NH_3 + 5O_2 \rightarrow 4NO + 6H_2O \tag{2.4}$$

Also, the formation of N_2O has been reported for the commonly used V_2O_5/TiO_2 catalyst [25]. This is highly undesirable because N_2O is suggested to be the most important ozone-depleting substance (ODS) of the 21st century [27] as 1 kg of N_2O in the atmosphere contribute as much to global warming as 298 kg of CO_2 does [28]. Equation 2.5 shows one of the possible reactions leading to N_2O formation [25].

$$4NH_3 + 4NO + 3O_2 \rightarrow 4N_2O + 6H_2O \tag{2.5}$$
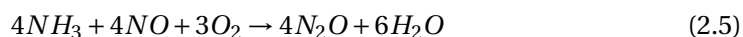
The standard SCR equation, illustrated in equation 2.1, will be the main focus of this thesis.

2.2 Infrared spectroscopy

Infrared spectroscopy is a commonly applied analysis technique due to its ability to identify molecules based on their vibrational energy. In the field of catalysis it is widely used to determine adsorbed species and to see how these species are chemisorbed onto the surface of the catalyst [23].

Infrared radiation falls into three categories: far-infrared radiation (10-200 cm^{-1}), mid-infrared radiation (200-4000 cm^{-1}) and near-infrared radiation (4000-10000 cm^{-1}). It is the mid-infrared region that is of most interest to us [16].

2.3 Molecular Vibrations

The energy of a molecule can be divided into translational energy, rotational energy, vibrational energy and electronic energy. The energy levels are unique for each

molecule. Chemical bonds hold atoms in a molecule bound together, and these bonds vibrate. Absorption bands throughout most of the infrared region of the spectrum come from molecular vibrations [29].

2.3.1 Photon Energy

According to quantum theory photon frequency, v, and photon energy, E_p is related by

$$E_p = hv \qquad (2.6)$$

where h is Planck's constant. This photon energy may be absorbed or emitted by a molecule, causing a transfer of rotational, vibrational and electronic energy by an amount of ΔE:

$$\Delta E = E_p = hv \qquad (2.7)$$

ΔE is positive if the molecule gains energy and a photon is absorbed, and negative if the molecules loses energy and a photon is emitted [29].

2.3.2 Degrees of Freedom of Molecular Motion

The atomic nuclei in a molecule represent centers of mass and the internuclear forces holding the molecule together can be assumed to be similar as to massless springs. Three coordinates, such as x,y and z in Cartesian coordinates, are needed in order to define the position of a nuclei mass. Therefore each nucleus has three degrees of motion, one for each direction. If a molecule consists of N atomic nuclei, then there will be a total of 3N degrees of freedom for all the nuclear masses present in the molecule. The molecule itself also requires three degrees of freedom of motion to determine the position of the center of gravity. These are translations of the center of gravity of the molecule. In addition, a nonlinear molecule has three independent rotational degrees of freedom specifying its molecular orientation about the center of gravity, giving a nonlinear molecule a total of 3N-6 internal degrees of freedom. A linear molecule only has a total of 3N-5 degrees of freedom because it only has two rotational degrees of freedom due to the fact that one of the rotational degrees of freedom about the molecular axis does not displace the nucleus. The internal degrees

of freedom of motion for both linear and nonlinear molecules correspond to the degrees of independent normal modes of vibration, meaning that all the atoms change periodically with the same frequency and pass through their equilibrium positions at the same time. There is no rotation of the molecule and the center of gravity does not shift, but the magnitude and direction of the vibrational amplitudes of the individual atoms may differ [30].

2.3.3   Classical Vibrational Frequency Formula for a Diatomic Molecule

The classical vibrational frequency for a diatomic molecule is a helpful model in order to understand molecular vibrations. A diatomic molecule with two masses m_1 and m_2 connected by a massless spring can be modeled as a classical harmonic oscillator as shown in Figure 2.1. For simplicity, the masses can only move along the molecular axis. The displacement of the masses can be plotted over time, giving a sinusoidal or cosinusoidal wave when the molecule performs one normal mode of vibration [29]. X_1 and X_2 are displacement vectors of each mass from the equilibrium position making $(X_2 - X_1)$ a measure for how much the bond length differ from the equilibrium length.
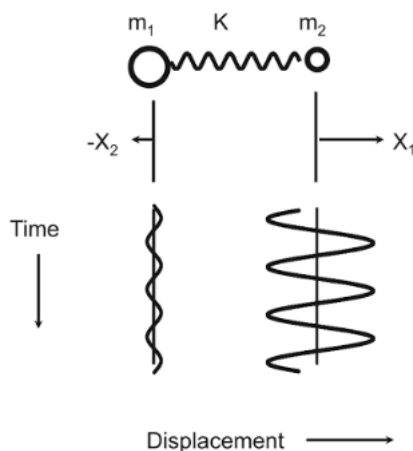
Figure 2.1: Motion of a simple diatomic molecule [29]

It is assumed that the spring obeys Hooke's law, meaning that the spring force on each mass when they are not in their equilibrium position is given by equation 2.8

$$F = -k(X_2 - X_1) \tag{2.8}$$

where k is the spring constant and X_1 and X_2 is the displacement of atom 1 and 2 from their equilibrium position. Hooke's law force can be found through Newton's second law for the two masses:

$$F(X_2 - X_1) = m_1 \frac{d^2 X_1}{dt^2} \tag{2.9}$$

$$-F(X_2 - X_1) = m_2 \frac{d^2 X_2}{dt^2} \tag{2.10}$$

When the spring is stretched and $(X_2 - X_1)$ is positive, the force on m_1 goes in positive X-direction and in negative X-direction for m_2. Since both a sinus or cosine function can be used to express the periodical motions of X_1 and X_2, the equations above can be expressed as the second derivative of one of these functions with respect to time:

$$X = cos(\omega t) \tag{2.11}$$

$$\frac{d^2 X}{dt^2} = -\omega^2 cos(\omega t) \tag{2.12}$$

where ω is a constant. The function will shift with 2π for every cycle, making ω equal to $v2\pi$. By solving the differential equations, we are left with the conclusion that for a diatomic molecule, the classical vibrational frequency can be expressed as:

$$v = \frac{1}{2\pi} \sqrt{\frac{k}{\mu}} \tag{2.13}$$

where

$$\frac{1}{\mu} = \frac{1}{m_1} + \frac{1}{m_2} \tag{2.14}$$

As seen from the equation, increasing bond strength and decreasing mass of the vibrating atoms will increase the intensity of the vibrational frequencies [16].

2.3.4 Change in Dipole Moment

When a molecule is introduced to a disturbing frequency like infrared radiation, and this frequency meets the same frequency that the molecule holds naturally, the molecule absorbs energy and increase its own vibrational energy. Although the molecule is introduced to a spectrum of different frequencies, it is only capable of absorbing the frequencies that match the natural vibrating frequencies in the molecule. Molecular vibrations must cause changes in dipole moment of the molecule in order for it to absorb infrared radiation. The magnitude of this change is decided by how effectively the molecule can absorb the energy from an infrared photon, which gives a measurement of the intensity of the absorption [30]. The dipole moment, μ, can be described by equation 2.15, where (e_i) is the magnitude of atomic changes and (r_i) is their position.

$$\mu = \sum e_i r_i \tag{2.15}$$

A simplified way of looking at the atomic changes is by comparing the electronegativities of the atoms. Diatomic molecules that consist of two equal atoms, like H_2, O_2 and N_2, have no dipole moment because their center of positive and negative charge will coincide at the center of the molecule, giving a dipole moment of zero. The dipole moment will remain zero during molecular vibrations, and thus the molecule cannot absorb IR radiation. In contrast, diatomic molecules that consist of two different atoms, like HCl, NO and CO, have dipole moments because the charge distribution and dipole spacing in the molecule changes during molecular vibrations. These molecules therefore have IR active vibrations [29]. Figure 2.2 describes how the oscillating electric field of the IR photon cause oscillations in the molecular dipole moment with the same frequency as the incident photon.
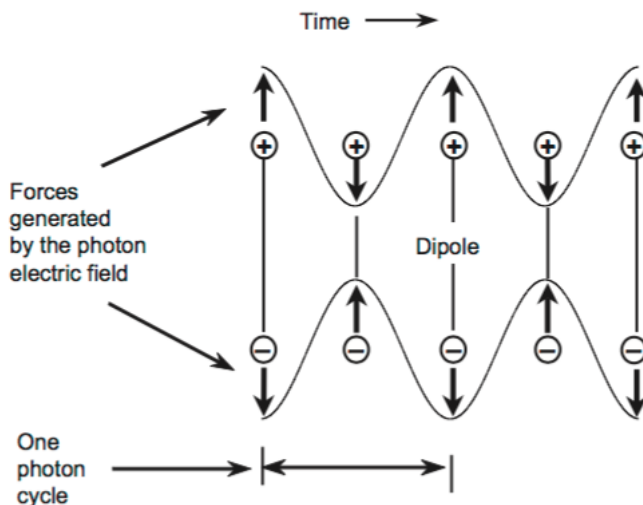
Figure 2.2: Oscillating electric field of IR radiation cause oppositely directed oscillations of the molecular dipole [29]

2.3.5 Anharmonicity

Hooke's law is as previously stated a useful simplification for understanding the vibrational frequencies for a diatomic molecule. However, it is not always an adequate representation of the potential energy with respect to a real displacement of a bond between two atoms ($x = r - r_e$). If r moves under the equilibrium bond distance and the atoms collide, the potential energy has to increase so that some singular behaviour must occur before r reaches zero. If r increase, on the other hand, the potential energy does not increase without a limit. Instead, it moves towards the dissociation energy which is the energy that is required in order to split two atoms so that there is no bond between them. The Morse function, given in equation 2.16, gives a reasonable approximation for explaining the behaviour of a "real" bond.

$$V(x) = D_e[1 - exp(-ax)]^2 \qquad (2.16)$$

where D_e is the dissociation energy and a is a constant. For a simple harmonic the vibrational energy levels associated with a particular vibration are equally spaced, while this is not the case for anharmonic oscillators [31]. This is shown in Figure 2.3
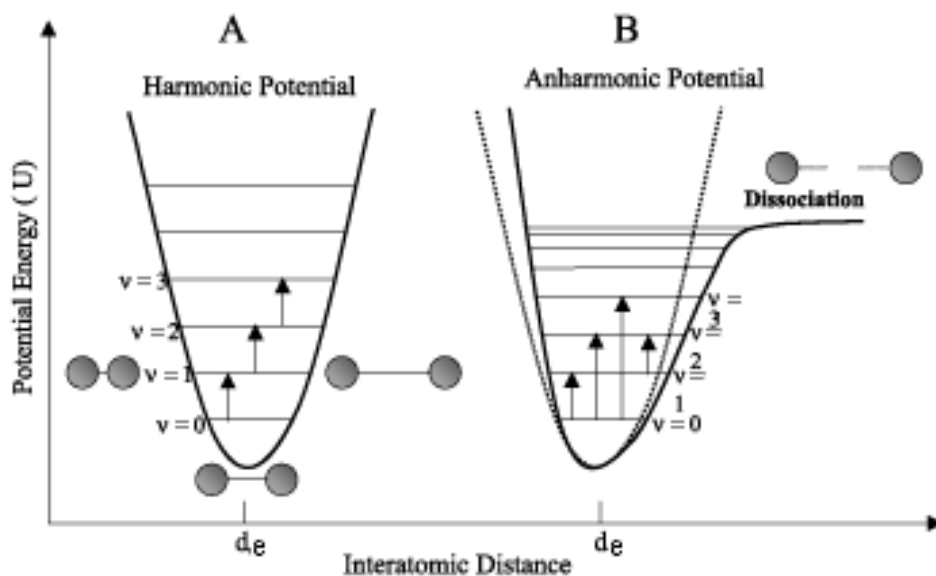
Figure 2.3: Schematic representation of the potential energy of a diatomic molecule for the (A) harmonic and (B) anharmonic (morse) models [32]

2.4 Fourier Transform Infrared Spectroscopy (FTIR)

FTIR spectroscopy is a widely used technology today because of its ability to obtain the entire spectrum for each scan, making the process of obtaining a spectrum much less time-consuming. The core of FTIR spectroscopy is the Michaelson interferometer, which consists of one fixed and one movable mirror and a beam splitter. The IR radiation from the source is split into two beams, where one is transmitted and one is reflected. The transmitted and reflected beams then hit the stationary mirror and the movable mirror respectively, and are reflected back to the beam splitter where they are recombined. By moving the mirror back and forth, the intensity of the signal increase and decrease, giving rise to a periodical interference pattern called an interferogram which is generated by the software. The sample is placed between the beam splitter and a detector. The signal of the combined beam changes when it interacts with the sample because some frequencies are absorbed by the sample. The detector measures the altered signal, and a spectrum is generated by fourier transform of the detected interferogram. A complete single-beam spectra can be obtained by a single scan of the moving mirror [30]. A schematic of the FTIR is given in Figure 2.4.
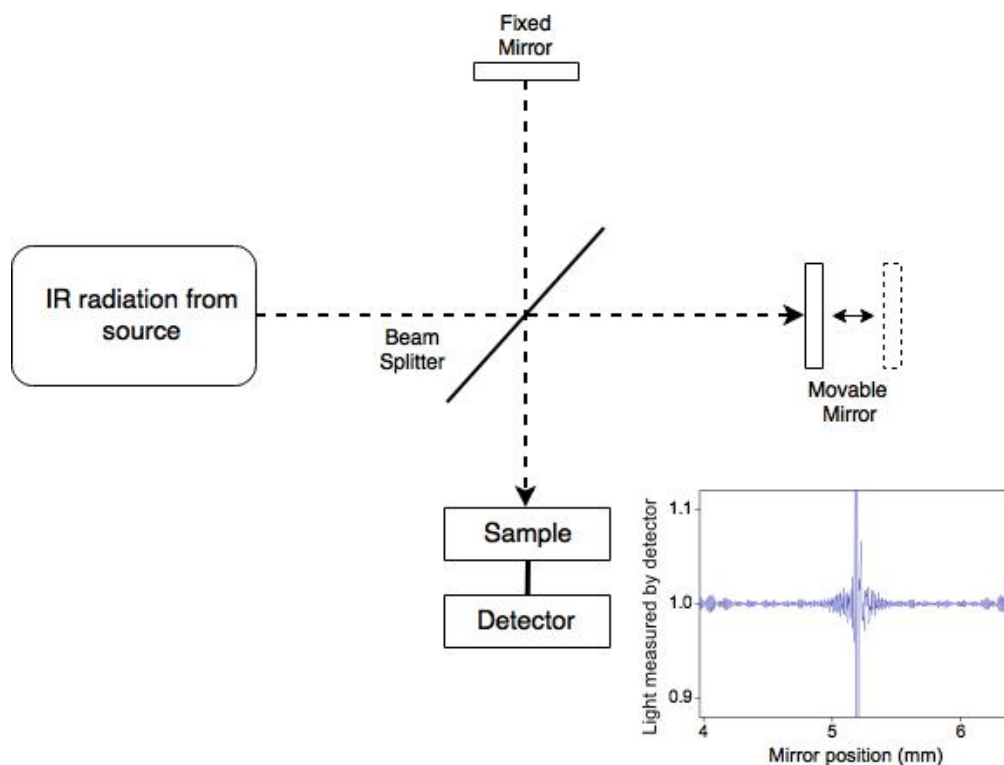
Figure 2.4: Schematic of a typical FTIR spectrometer with interferogram

2.4.1 Diffuse Reflectance Infrared Fourier Transform Spectroscopy, DRIFTS

There are several modifications of the FTIR spectroscopy method including transmission, attenuated total reflection (ATR) and diffuse reflectance. The latter was used in this thesis.

The DRIFTS technique has several advantages over the other techniques. Sample preparation is easier because powdered samples can be used without having to press them into disks, and also not all catalysts are capable of being compressed into disks that are thin enough to transmit IR radiation and at the same time strong enough to encounter *in situ* treatment. Samples that scatter too much in order to use transmission or ATR techniques give good DRIFT spectra, and also powdered samples are less sensitive to diffusion limitations [13].

IR radiation from the source interacts with a powdered sample and reflects off its surface causing light to diffuse or scatter in different directions as shown in Figure 2.5.
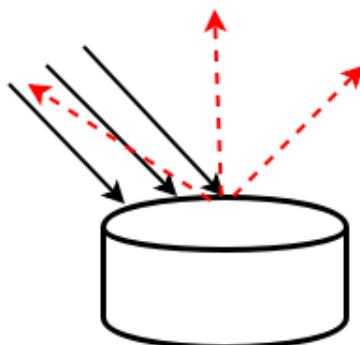
Figure 2.5: IR beam hits sample and is diffused in different directions

The sample is placed in a sample cup equipped with a heater and gas inlet and outlet lines. A dome is placed on top of the sample cup where the incident and the diffusely reflected IR beam can pass through infrared transparent windows [13]. Figure 2.6 shows what a typical DRIFTS cell looks like.
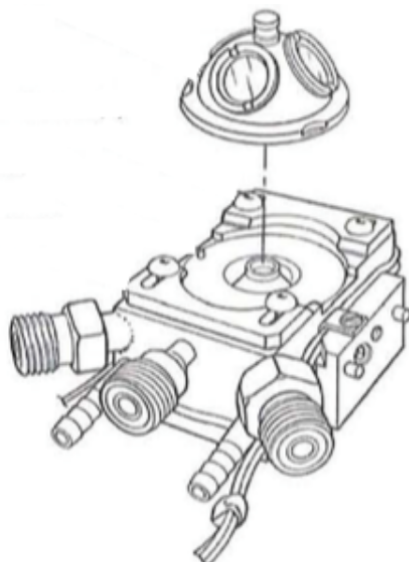
Figure 2.6: Schematics of a typical DRIFTS cell [33]

2.4.2 The Beer-Lambert Law

The Beer-Lambert law is used to calculate the absorbance, A, by using the relationship between the initial intensity of a beam of electromagnetic radiation, I_0, and the intensity of the beam that has passed through the sample, I [34].

$$A = -log_{10}\frac{I}{I_0} \tag{2.17}$$

2.4.3 FTIR in Nitrogen Chemistry

In the field of catalysis, infrared spectroscopy is most commonly used to identify adsorbed species on the surface of a catalyst. It can also be used to see in which way these species are chemisorbed onto the surface. Molecules with different combinations of atoms will produce a unique spectra, and information about the molecular structure can therefore be gained from the spectra [23]. The technique is also used to identify the strength, type and number of acidic sites on a catalyst. The acidic sites are of great interest because they can affect the catalytic properties of a catalyst [17]. The acid sites can be divided into two groups; Brønsted and Lewis acid sites. Brønsted acids are defined as proton donors while Lewis acids are defined as electron acceptors [23]. Brønsted acid sites can in most cases be observed directly with IR spectroscopy through their vibrating $\nu(OH)$ bands. Lewis acid sites on the other hand can not be observed directly by IR since Lewis acids often are cations that are coordinatively unsaturated and does not act as vibrators [35]. This problem can be solved by using a suitable probe molecule with known vibrational frequencies. The probe molecule, which is often a Lewis base, can adsorb to the acid sites on the surface giving an IR spectra specific to the interaction with the site. The change in vibrational frequencies in the sample will give information about the nature of the acid site. Finding an appropriate probe molecule is crucial in order to obtain an overall view of the acidic sites on the surface. It's size should be small enough to react with all active sites on the surface, and its basic strength should be strong enough to interact with even the weakest sites. NO, CO, NH_3 and pyridine are most commonly used as probe molecules [35].

Ammonia is used as a probe molecule, but it can also be used in reactions and not just in acidity measurements. As ammonia is one of the reactants in the SCR reaction, the studies where ammonia was used as a probe can be used to assign some of the peaks found in the IR spectra in this thesis. Ammonia is a strong base

and will therefore react with extremely weak acid sites. When ammonia reacts with a Brønsted acid it gets a proton from the acid to form ammonium ion where NH_3 is transformed into NH_4^+. When ammonia reacts with a Lewis acid a free electron-pair from the nitrogen in ammonia binds to the acid, or the NH_3 can be hydrogen bonded. Bands centered around 1450, 1700, and 3130 cm^{-1} are typical for ammonium ions, i.e., Brønsted acids and coordinately bonded NH_3 gives bands near 1250, 1630, and 3330 cm^{-1} [12], [17], [36]–[38].

J.B Peri [39] did a study of the mechanism of adsorbance of ammonia on alumina with infrared spectroscopy and found that ammonia adsorbed on alumina give broad bands at 3400, 3350, 3100, and 1620 cm^{-1}, and smaller bands at 3540, 3485, 3260, 3210, 1560, and 1510 cm^{-1}. N-H stretching vibrations caused bands at 3355, 3400, 3485, 3540, 3210, 3260, and 3100 cm^{-1}. The bands near 1620, 1560 and 1510 cm^{-1} were assigned to -NH_2 or NH_3 deformation modes. N-H bending vibrations in the NH_4^+ ion gave a band at 1400 cm^{-1}.

Barzetti *et. al.* [17] did a study where they used pyridine and ammonia as probes for FTIR analysis of solid acid catalysts and found that ammonia was a less reliable probe molecule than pyridine, as the absorption bands of ammonia overlapped. However, they were able to assign some of the bands that appeared from ammonia adsorption. A band at 1630 cm^{-1} was assigned to ammonia coordinated to Lewis-acid sites, and two bands appeared at 1681 and 1450 cm^{-1} due to formation of ammonium ions, i.e. Brønsted acid sites.

2.4.4 FTIR Studies of the NH_3-SCR Reaction

The vanadia SCR catalysts have been extensively studied using *in situ* DRIFT spectra in order to determine the mechanism of the reaction [40], [41]. There is a general agreement among researchers that the reaction follows the Eley-Rideal mechanism, meaning that molecular N_2 is formed by the reaction of strongly adsorbed ammonia species with gaseous or weakly adsorbed NO molecules. There is still a disagreement about which ammonia adspecies (Brønsted or Lewis) that is present in the reaction [9]. However, several researchers have found that NO molecules also adsorbed to the catalyst surface and was oxidized to NO_2, nitrite and nitrate species when zeolite based, Fe_2O_3 and CuO doped catalysts were used for the SCR reaction [8]. These findings suggest that the reaction could also follow the Langmuir-Hinshelwood mechanism where it is assumed that all species adsorb to the surface before taking

part in any reactions [23].

There are several examples of in situ studies of the NH_3-SCR reaction [8], [10]–[12]. One example is Ruggeri *et. al.* [10] who did a FTIR *in situ* study of the "fast SCR" equation presented previously in equation 2.2 over a Fe-ZSM-5 catalyst. Their aim was to study the mechanism and development of surface intermediates during adsorption of NO_2 and how surface NO_x reacted with NH_3 and NO. Their study showed that formation of surface ferric nitrates was a key step in the fast SCR reaction and that these surface nitrates were further reduced by NO. NO_2 adsorption showed that ferric nitrates were formed on the surface with assigned bands at 1620 cm^{-1} and 1574 cm^{-1}. During NH_3 adsorption, a broad band between 3500-1550 cm^{-1} appeared due to various forms of adsorbed ammonia, mostly hydrogen bonded, along with a negative OH band at 3610 cm^{-1}. They associated the negative OH band to ammonium ions, NH_4^+, as the formation of ammonia ions compensated for the negative charge of the zeolite and thereby neutralized the hydroxyl bands ($NH_4^+ + OH^-$).

2.5   Mass Spectrometry

Mass spectrometry (MS) is an analytic method for determining the characteristics of individual molecules based on their molecular weight. A wide range of chemical substances can be studied based on their chemical properties by this technique due to a high resolution level and its ability to detect compounds at very low concentrations [42]. The basic principle of MS is that the molecules are converted into ions, usually by the loss of an electron, and then separated according to their mass and charge by external electric and magnetic fields. There are several types of MS instruments but they all generally involve four elemental stages, namely the introduction of the sample, ionization, analysis, and detection [42]. A schematic of the stages is shown in Figure 2.7.
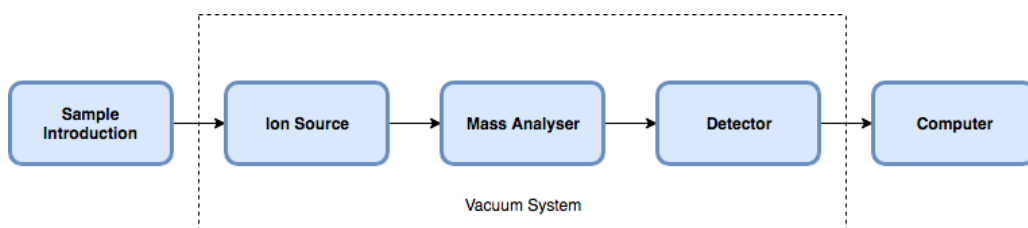
Figure 2.7: General steps in Mass Spectrometry

The sample is first introduced to the ionization chamber where the molecule is exposed to a beam of high energy electrons which gives the molecule a positive charge either by removal of an electron or by addition of a proton. The charged molecular ions are then passed on to an analyzer where the ions are sorted according to their mass-to-charge ratio (m/z). Several methods can be used for analysis of generated ions, including the time-of-flight method, electrostatic and Fourier-transform [42]. In the time-of-flight method, the charged molecules move through a long vacuum chamber due to a rapid increase in voltage inside the chamber. It is assumed that the voltage application gives the same amount of kinetic energy to each particle. The different ion masses will thus have different travelling speeds and thereby different travelling time through the vacuum chamber because lighter ions acquire greater velocity. The electrostatic analysis technique uses a device called quadrupole which retains all the ions, except ions with a specific mass range. These ranges are determined by the operating parameters of the apparatus. The Fourier-transform analyzer uses a strong magnetic field to make the ions move in circular paths according to the mass-to-charge ratio. Radiofrequency signals are produced by the ion movements and analyzed by Fourier transform in order to obtain a mass spectre [42].

Finally, there is a detection step, which detects and quantifies the separated ions. The ions collide with an electron emitting material which generates a stream of electrons that is proportional to the number of ion impacts which generates the signal that is to be analyzed [42].

The National Institute of Standards and Technology (NIST) provides mass spectra in the form of bar graphs in which each bar shows a specific mass-to-charge ratio of an ion, and the length of the bar implies the relative abundance of the ion. The m/z value of the ions are usually corresponding to mass itself, as most of the ions formed in a mass spectrometer have a single charge. A mass spectrometer can therefore easily separate ions that differ by only a single atomic mass unit, and give exact values for the molecular mass of a compound [43]. An example of a mass spectre from NIST is shown in Figure 2.8 for NH_3. The rest of the mass spectres used in this thesis can be found in Appendix B.
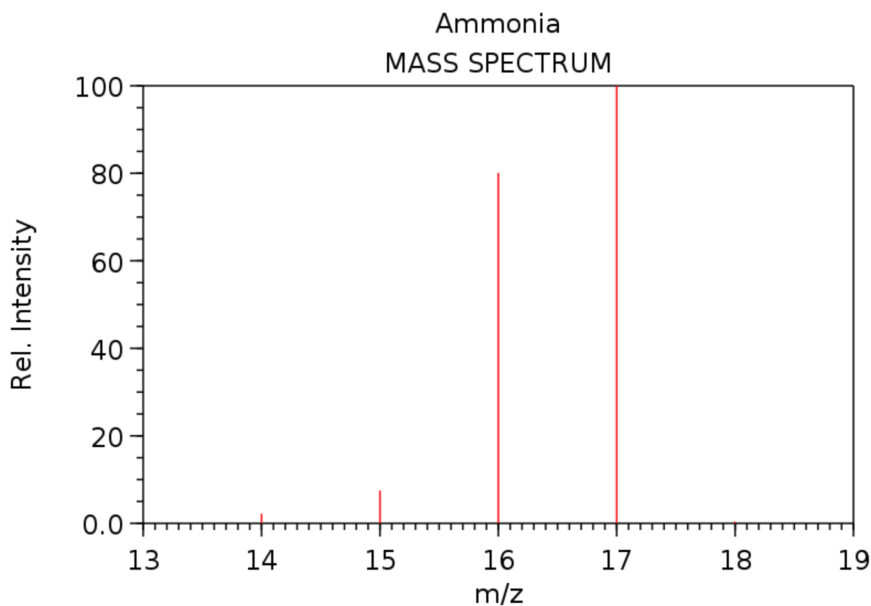
Figure 2.8: NH_3 mass spectrum from NIST Chemistry WebBook [44]

The relevant m/z ratios and the approximate relative intensity of the gases used in this thesis are summed up in Table 2.1.

Table 2.1: Relative intensity of compounds found at relevant m/z ratios

m/z	Gasses Occuring (Relative Intensity)
m4	He (100)
m14	N_2 (15), NO_2 (10), NO (10), NH_3 (>5)
m15	NH_3 (10), NO (>5)
m16	NH_3 (80), NO_2 (20), O_2 (20), NO_2 (20), CO_2, NO (>5)
m17	NH_3 (100), H_2O (20)
m18	H_2O (100)
m28	N_2 (100), N_2O (10), CO_2 (10)
m30	NO (100), NO_2 (100), N_2O (30)
m32	O_2 (100)
m40	Ar (100)
m44	CO_2 (100), N_2O (100)
m46	NO_2 (35)

Chapter 3

Experimental

3.1   Setup

IR spectroscopy was performed by using a Nicolet iS50 FTIR Spectrometer with a Harrick Praying Mantis cell and a Harrick HVC-DRP-3 high temperature reaction chamber. The praying mantis cell was heated by a 220V Harrick ATC-024-4 temperature controller and water-cooled. 6 mass flow controllers, MFCs, were used to flow gasses through the sample cell, and LabVIEW was used to control the temperature and the different mass flow controllers. National instruments LabVIEW control was written by Samuel K. Regli for control of MFCs. OMNIC v.9 was used to collect spectras. The gas was flowed through the IR cell and then through a line heated to 150°C into a mass spectrometer from ThermoStar with Quadera software. A block diagram of the experimental setup is shown in Figure 3.1
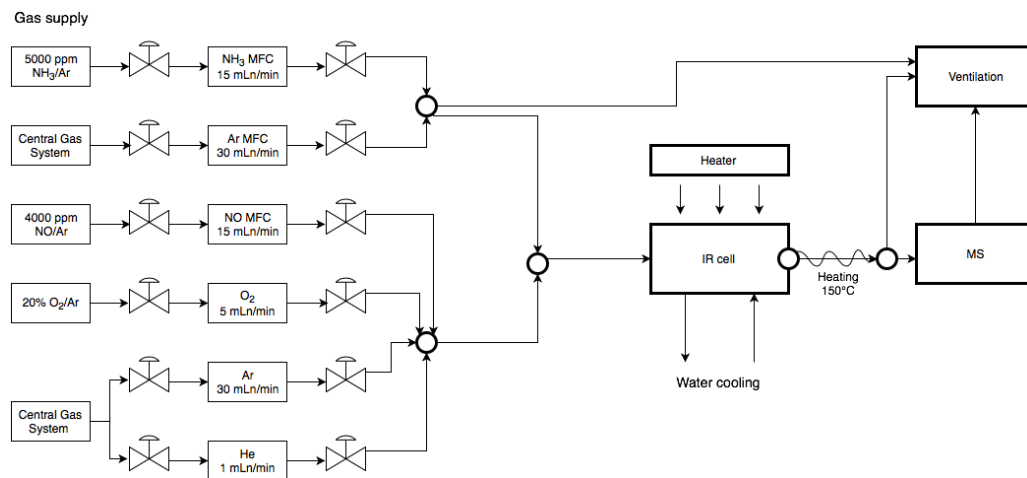
Figure 3.1: Block diagram of the experimental setup used in experiments

3.1.1 Experimental Procedure

The cell was first heated to 350°C and held there for 1 hour in order to dehydroxylate the surface and remove any adsorbed species on the catalyst. A temperature profile was then programmed to see how the SCR reaction proceeded with decreasing temperatures. 1500 ppm of NO was first introduced at 350°C. After 30 minutes, 1500 ppm of NH_3 was added to the gas mixture for 45 minutes before both gasses were turned off. Only Ar, He and O_2 was flowed for 15 minutes, before the temperature was decreased by 50°C. The temperature was held steady for 30 minutes before NO was introduced again. This cycle was repeated at 300°C, 250°C, 200°C, 150°C and then at room temperature. The temperature was increased to 350°C between every temperature step and held there for 30 minutes in order to start every cycle with a clean surface. A total gas flow of 30 mLn/min was used during the whole experiment, with a constant concentration of 5% of O_2 as there will always be some oxygen present in the system after combustion. The rest of the gas mixture consisted of Ar and He. The temperature profile used in the experiments is shown in Figure 3.2.
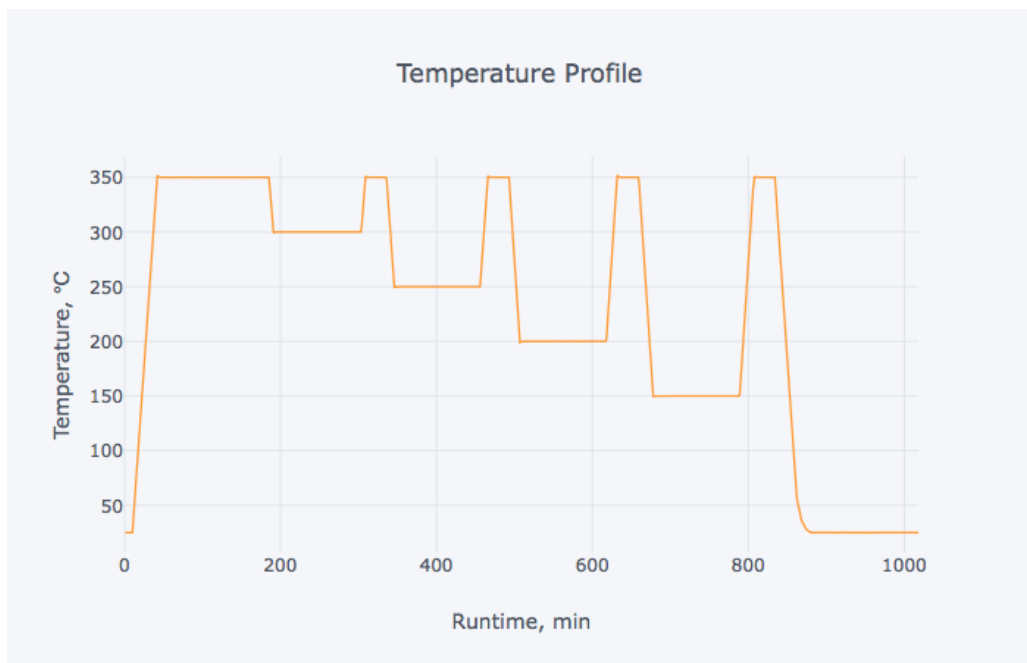
Figure 3.2: Temperature profile used in FTIR experiments

Spectra were collected by a built in sample collection macro in the OMNIC software. A single spectrum was recorded within 30 seconds and consisted of 8 scans with 4 cm^{-1} resolution.

3.2 Calibration of Mass Flow Controllers

The MFCs needed to be calibrated prior to the experiments in order to make sure that the right amount of gas was flowed at all times, since their working principle is based on the thermal conductivity of the individual gases. This was done by using an ADM flow meter from Agilent Technologies which measures gas volumetrically. The flow meter was connected to the outlet of each MFC and tested at various setpoints with 3 parallels to make a calibration curve that could be implemented into LabVIEW.

3.3 Calibration of Mass Spectrometer

The mass spectrometer was calibrated in three different ways. A single gas mixture of either NO or NH_3 was introduced first at 50, 250, 500, 750, 1000, 1250 and 1500 ppm while the other gas was turned off. This was done for both NO and NH_3. The second step was to use a binary gas mixture of NO and NH_3 where one of the gases was held constant at the concentrations listed above while the concentration of the other gas varied. In other words, NO was first held constant at 50 ppm while NH_3 was introduced at 50, 250, 500, 750, 1000, 1250 and 1500 ppm, then the NO gas was turned up to 250 ppm while NH_3 went through the same range again, and so on. This was then done one more time by holding NH_3 as the constant flow. The third step in the calibration was to use a tertiary gas mixture where step two was repeated, but this time with an addition of a constant flow of 5% O_2.

3.4 Temperature Calibration

There are some possible sources of deviations linked to the DRIFTS technique that have to be eliminated in order to get accurate and representative data. Temperature control throughout the sample bed is difficult due to the fact that the cell is designed to enable the use of spectroscopic techniques. Meunier *et. al.*[45] did a striking observation that the temperature of the surface of the sample bed was significantly lower than the temperature measured by the sample bed thermocouple. Temperature calibration of the cell was therefore performed in the specialization project, and the results were used in this work. The results of the temperature calibration are presented in Appendix A.

3.5 Samples

3wt% Cu/Al_2O_3, 3wt% Fe/Al_2O_3, and mesoporous alumina were used in the SCR experiments. All 3 samples were prepared by Ole Håvik Bjørkedal. The samples were prepared by the sol-gel method. $m\text{-}Al_2O_3$ had a measured surface area of 286 m^2/g with an average pore diameter of 4.1 nm. The $m\text{-}Al_2O_3$ was used as support for the Cu and Fe sample. The synthesis method should essentially give isolated copper and iron atoms, but it still remains to do characterization to check if this is also the case under reaction.

3.6 Data Processing

Spectra from DRIFTS experiments and MS data were imported to, and processed with Python in Jupyter Notebook in order to efficiently align and compare the two different methods. The runtime of the MS data was synchronized with the runtime of the IR log in order to make sure that the two datasets were aligned. All the masses from the MS data were then plotted separately in order to better see the change happening in each of the relevant masses as the reactant gases were introduced and with respect to temperature changes.

The Beer-Lambert law was used to calculate the absorbance from the IR single-beam spectra (raw data). A background spectrum, I_0, was taken for each temperature in flowing Ar, He, and O_2, used in the Beer-Lambert law, and thereby eliminating the absorption features that comes from the structural vibrations of the catalyst from the overall absorption to highlight the changes occurring during reaction. The IR data was separated and studied for each individual temperature step by using contour- and line plots in order to visualize the reaction taking place, and to identify the interesting peaks occurring when all the spectra were put together. The peaks were then identified and compared to the relevant MS data occurring in the same time frame. The Python code used in these experiments is included in Appendix E.

Chapter 4

Results and Discussion

4.1 MS Calibration

The MS calibration revealed that it was not possible to do a proper calibration of this instrument to use in this kind of study. The goal of the calibration was to be able to calculate the selectivity, consumption, and conversion levels on the two catalysts and the support in use, and to see how the activity changed with decreasing temperatures. However, this was not possible because the filament in the MS instrument reacts differently to oxidative and reductive environments. The atmosphere changed as oxygen was introduced to the system which caused the signal to change constantly, and the masses to overlap. MS is generally not the best method for nitrogen compounds because the masses overlap which makes it hard to separate them from each other. Thus, it is hard to get quantitative data from this technique in an experiment like this. Therefore, the MS data could only be used as a qualitative comparison between the peak intensity of the relevant masses. Kinetics was not in the scope of this thesis. The focus has therefore been on IR technology.

4.2 Mass Spectrometry Results

Figures 4.1, 4.2 and 4.3 show all the collected MS data for the SCR reactions on the three samples. The orange fill in m30, blue fill in m17, and the green fill m32 shows where NO, NH_3, and O_2, respectively, were flowed through the samples at each temperature step.

The first subplot in each figure shows how the temperature varied from 350°C to room temperature over the whole experiment. The subplots below show the ion current, or raw signal, of the mass numbers that are associated with the present or expected molecules for this experiment, as shown in Table 2.1. The last subplot shows the pressure in the MS measurement chamber.

Figure 4.1: Cu/Al$_2$O$_3$ MS data. The fist subplot shows the temperature profile. The subplots below show the ion current of relevant mass numbers. The last subplot shows the pressure in the MS measurement chamber. The Orange fill in m30 shows where NO was flowed, blue fill in m17 where NH$_3$ was flowed and green fill in m32 shows where O$_2$ was flowed through the sample.
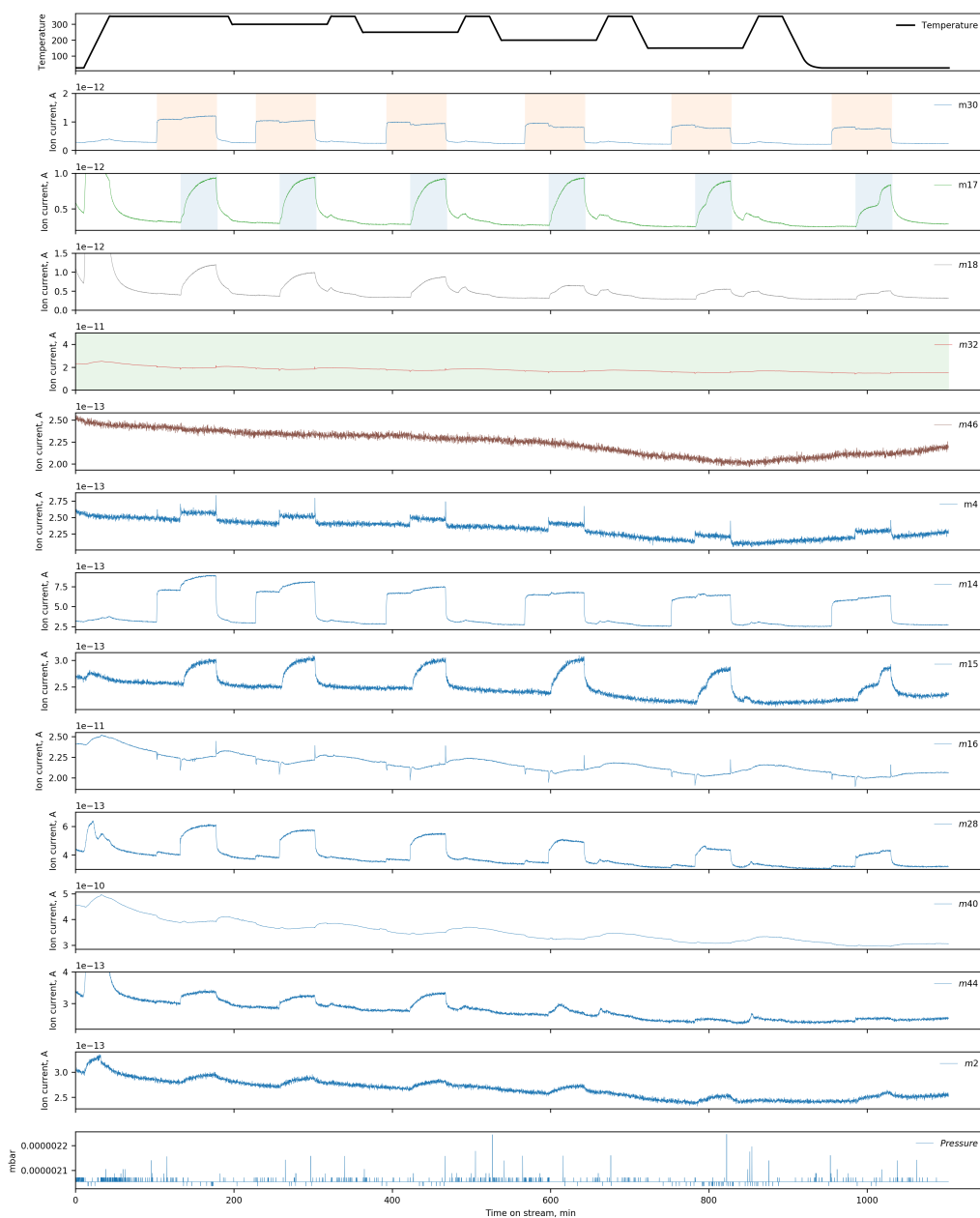
Figure 4.2: Fe/Al$_2$O$_3$ MS data. The fist subplot shows the temperature profile. The subplots below show the ion current of relevant mass numbers. The last subplot shows the pressure in the MS measurement chamber. The Orange fill in m30 shows where NO was flowed, blue fill in m17 where NH$_3$ was flowed and green fill in m32 shows where O$_2$ was flowed through the sample.
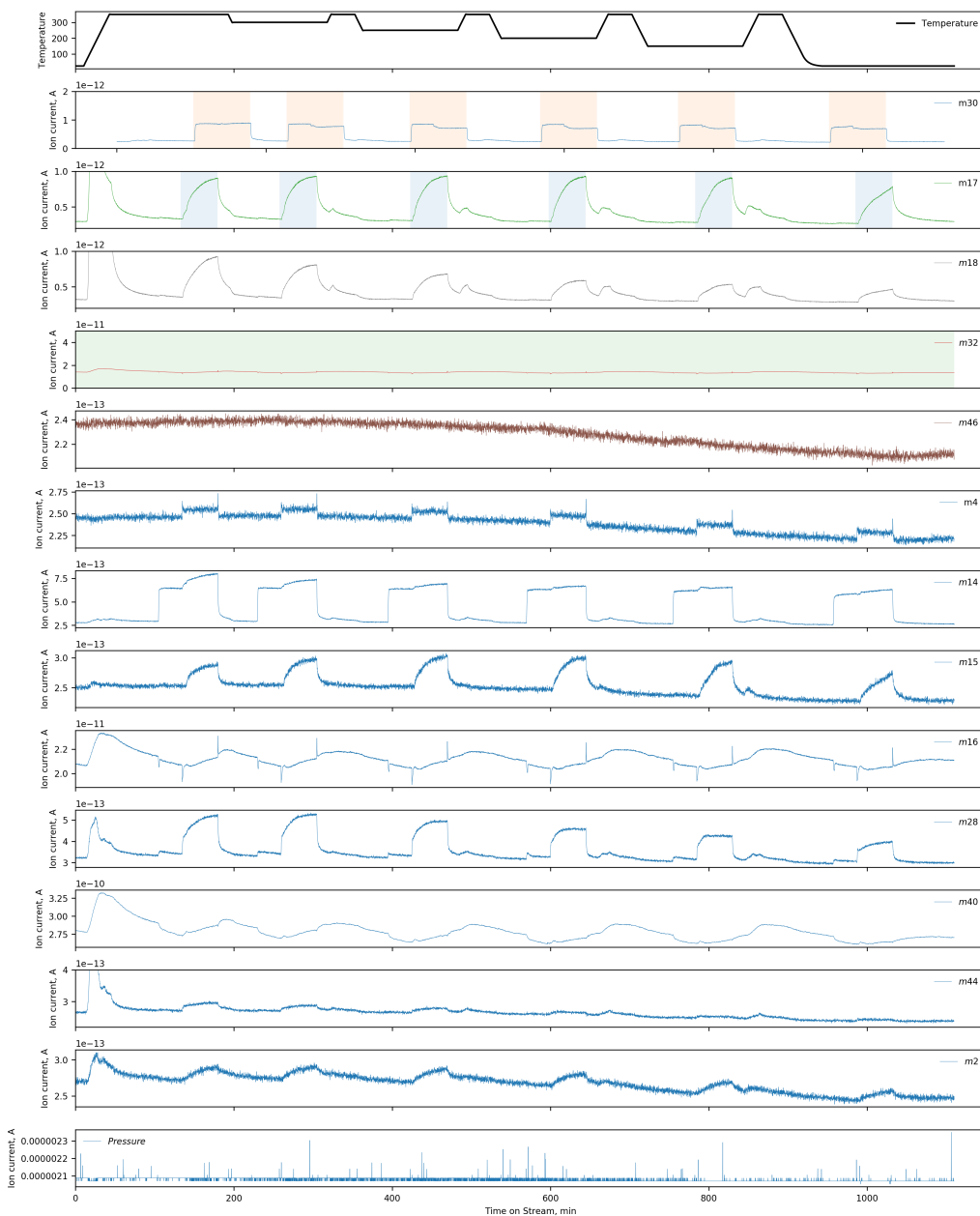
Figure 4.3: m-Al$_2$O$_3$ MS data. The fist subplot shows the temperature profile. The subplots below show the ion current of relevant mass numbers. The last subplot shows the pressure in the MS measurement chamber. The Orange fill in m30 shows where NO was flowed, blue fill in m17 where NH$_3$ was flowed and green fill in m32 shows where O$_2$ was flowed through the sample.
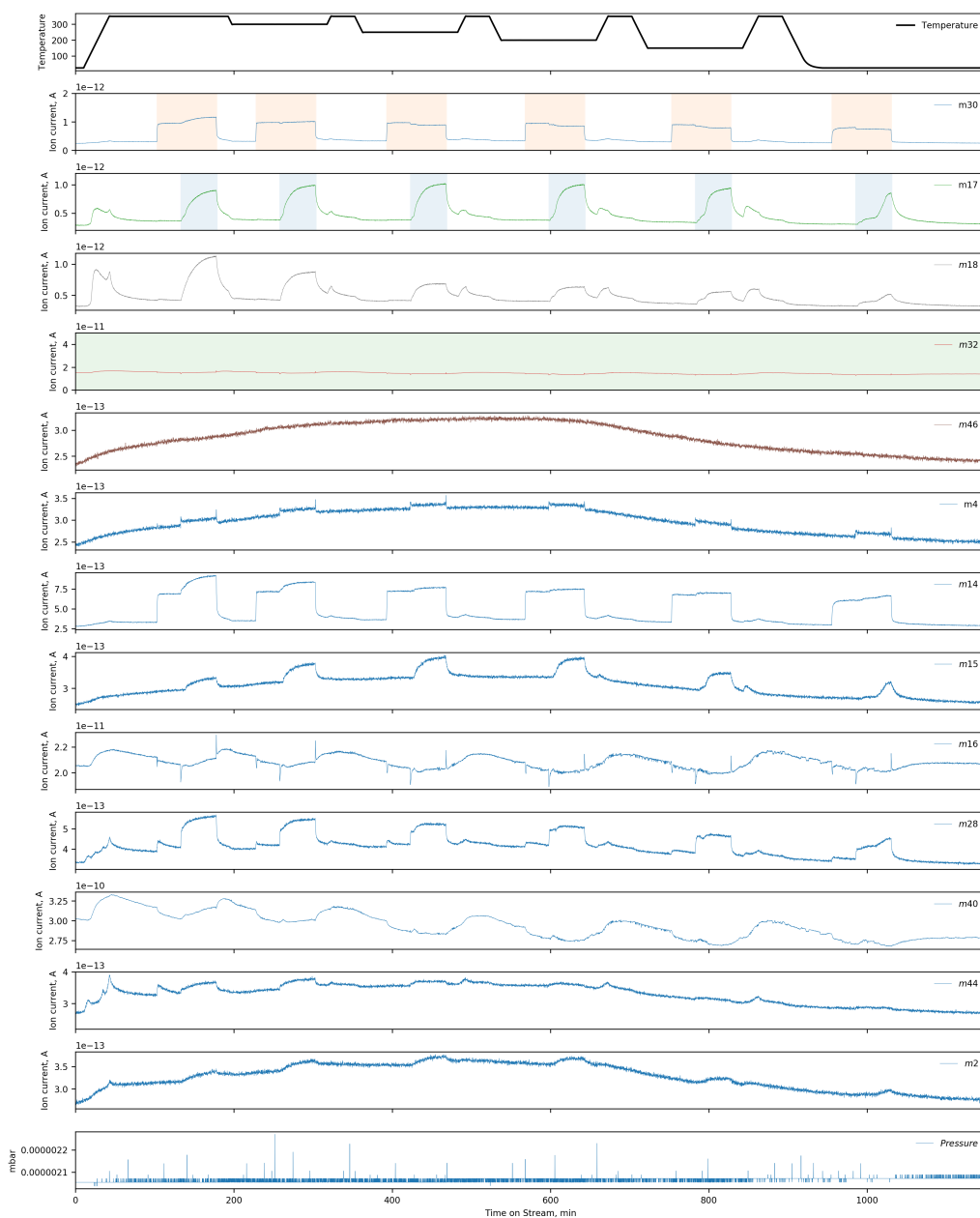
The main products of the SCR reaction are H_2O (mainly m18) and N_2 (mainly m28). m17, m18, m28, and m44 increased during the cleaning step for all three samples because there were some H_2O, N_2 and CO_2 initially adsorbed in the system which were removed with the temperature increase. The height of this spike was not analyzed in detail and is therefore not included in the plots in order to see the change at each temperature step better. An overall shift can be seen in all the figures as the signals generally tail off with decreasing temperatures. Very little H_2O and N_2 is produced at room temperature. It was not expected to see any formation of reaction products at room temperature, as the SCR reaction generally occurs at higher temperatures. But some of the gas may have reacted in the line between the IR cell and the MS as the line between them was heated to 150°C.

Two peaks are seen in m17 and m18 in all three figures at all temperatures between 300-150°C. Water gives a signal to both these peaks. The first peak represents the formation of water occurring during reaction, while the second peak is always found when the sample is reheated to 350°C. The latter is due to the fact that the surface is cleaned, and water is desorbed from the catalyst.

In panel 6 in all three figures, the signal of m46 is very noisy. m46 is mainly associated with NO_2. The figures indicate that there is more NO_2 in the system at high temperatures, but this can also just be noise as the signal generally only varies from 2.2-2.4e^{-13}. It is expected that there will be a gas phase reaction taking place between NO and O_2 that will form some NO_2 which is also seen in the figures above. This is however a slow reaction, which does not give a big contribution to the MS as the signal shows a smooth line that does not spike or vary with the reaction taking place.

m14 gets a signal mainly from N_2, N_2O, NO, and some from NH_3 as there is a little spike occurring when NH_3 is introduced to the system. m15 mainly gets a signal from NH_3 and follows the same trend as m17 in all three figures. m4 also shows some peaks when the reaction is taking place. This could possible be an impact of He in NH_3.

m44 shows some variations at high temperatures. This could be due to some CO_2 residue in the IR cell, but since there is a little maximum in the signal happening simultaneously as the reaction gases are flowed, it is more likely that the signal is due to some N_2O production. N_2O is a very unwanted product in the SCR reaction because of its negative environmental impact. The production of N_2O is however very small for the two catalysts which shows that they have a high selectivity towards

converting NO_x into N_2 and water. More N_2O production is seen on the support in Figure 4.3 for all temperatures.

The pressure looks relatively stable in each of the figures, except for some random spikes. However, the variations are very small.

The MS data is similar for the two catalysts and for the support, with overall decreasing signals at lower temperatures. It was not expected to see any production of water and nitrogen on the support, as copper and iron act as the active materials. There are however some differences between the catalysts and the support as shown in Figure 4.4 which compares the m18, m28, m17, and m30 signals for the three samples. All the signals are highest for the Fe/Al_2O_3 catalyst which indicates that this catalyst was more active for the SCR reaction than the Cu catalyst, which was also expected from literature [24]. But, as the difference is quite small, this should also be looked at in the IR data. The figure shows that the support also produced almost the same amount of water (m18) as the two catalysts, which was unexpected. The formation of water on the support could also be caused by impurities in the cell with residues from previous experiments. It could also be because of a gas phase reaction taking place in the heated line between the IR cell and the MS. There is some background drift in m28 between the reactions taking place and the m-Al_2O_3 therefore does not reach the same zero-level as the two others. This could be an effect of calibration, which is a weakness of the MS technique. However, as the baseline is higher for the support, the distance to the top of the peaks occurring with the reaction is much smaller than for the two catalysts. This shows that less nitrogen was formed on the support, which is a clear indicator that the support was less active.
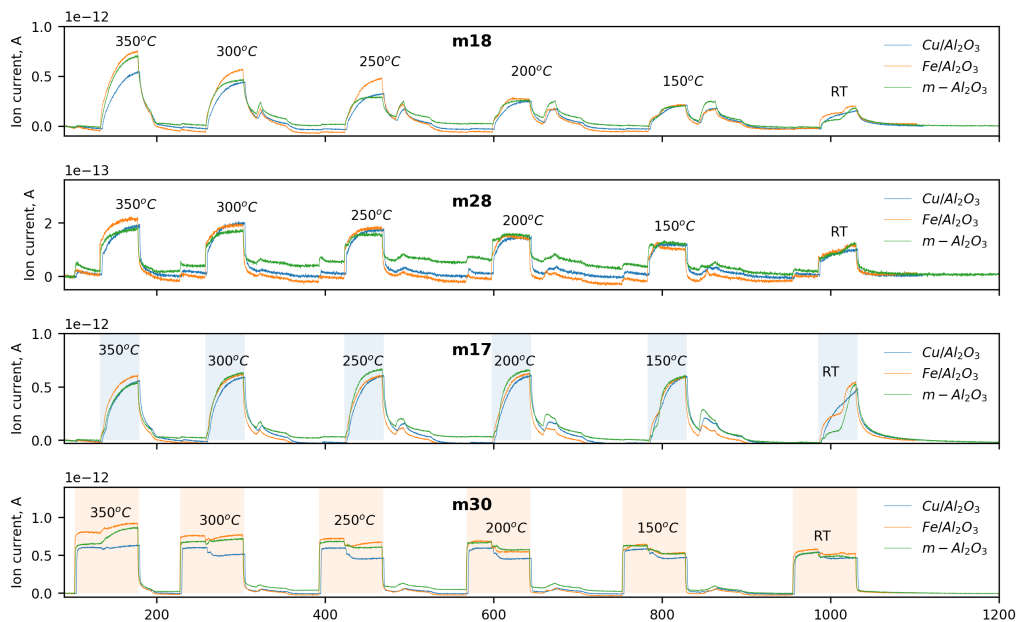
Figure 4.4: Comparison of H_2O (m18) and N_2 (m28) production and signal of NH_3 (m17) and NO (m30) on the three different samples. Blue fill shows where NH_3 was flowed and orange fill shows where NO was flowed.

The MS data indicates that the conversion levels of the SCR reaction are quite low as the collected MS data for both the two catalysts and the support are very similar. The MS data could only be used as a qualitative measurement, and therefore information about consumption, conversion and selectivity could not be retrieved from this data. The MS results can however give an indication of what is going on in the system, and be compared to the IR results in the following chapter.

4.3 Infrared Spectroscopy Results

4.3.1 Cleaning Step

Figure 4.5 shows the absorption spectrum for the entire experiment, using the same background spectrum for all temperatures. This data was not further used in the results, because a new background spectrum was taken for each temperature step in order to get more accurate data. This figure is simply presented to show the importance of reheating the sample between the reactions in order to clean the surface of adsorbed gases and contaminations. As seen in the figure, the catalyst surface was efficiently cleaned in between the reactions as very little absorption was seen when the temperature was increased to 350°C. In comparison, the signal continues to increase after turning of the reactant gases at room temperature where the sample did not get reheated.

There was also a strong absorption seen at the beginning of the experiment. This is due to adsorbed species onto the sample surface like for instance CO_2 and H_2O. O-H bands are known to give a broad peak between 3600-3000 cm^{-1} and CO_2 is known to give a peak between 2500-2000 cm^{-1} [46]. Both peaks decrease rapidly with an increase in temperature, and the catalyst surface is more or less clean after running for about 90 minutes, except for some noise at low wavenumbers which is to be expected due to low signal-to-noise ratio in this region. All IR data in the following chapter has been cut at 1200 cm^{-1} because the detector in the IR apparatus in use is not strong enough to get a sufficient signal at these low wavenumbers.
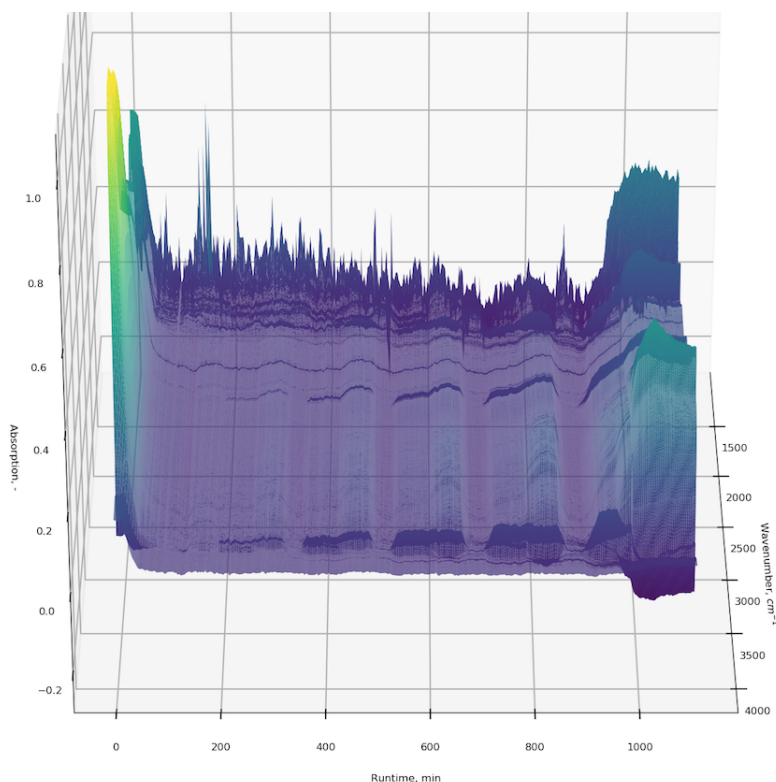
Figure 4.5: Cu/Al$_2$O$_3$ absorption spectra for the entire experiment using background spectrum at 350°C

4.3.2   NH$_3$-SCR

The SCR reaction usually takes place between 400-300°C. As this is an *operando* study, it is most interesting to look at the results generated closest to operating conditions. The spectra at 350°C were quite noisy. A reason for this could be that the sample itself starts to send out IR radiation at high temperatures. Also, the intensity of the spectra were higher at room temperature than for the others, probably because the sample was not reheated after the reaction and the signal therefore continued to increase. The room temperature spectra have therefore not been included in most figures to better see the changes occurring at the more relevant temperatures, as it is not expected to see very much production of reaction products at room temperature which was also seen in the MS results. Therefore, the main focus has been to study the catalysts at 300°C and see the differences that occur for the different samples. An example of the spectra at 350°C and at room temperature is included in Appendix D

In order to look more into the reactions happening at each temperature step, a contour plot was made to see where the interesting peaks were found. Figures 4.6, 4.7, and 4.8 show the reactions happening at 300°C for Cu/Al_2O_3, Fe/Al_2O_3, and $m-Al_2O_3$, respectively. The color of the plots indicates the intensity of the absorption at specific wavenumbers in time. The absorbance is close to zero at the bottom of each plot. This was right after the surface had been cleaned at 350°C, and the temperature had just reached 300°C. A background spectrum was taken here for each sample in order to calculate the absorbance at this temperature. The signal also starts to decrease at the top of each plot as the temperature again starts to increase to 350°C. The most interesting peaks in the figures are marked by letters.
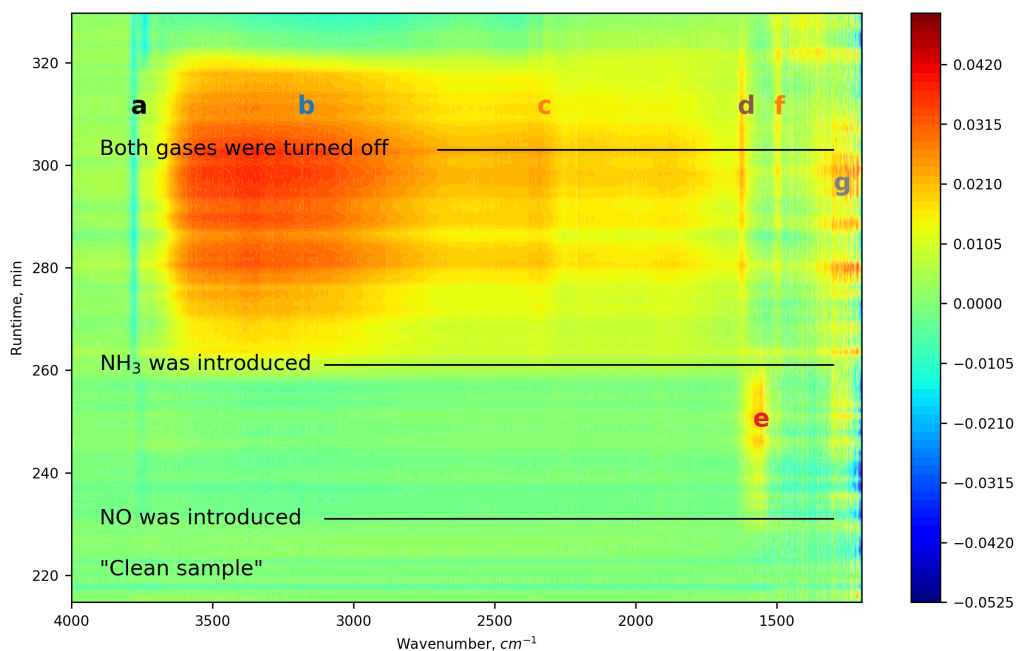
Figure 4.6: Contour plot of SCR reaction at 300°C on Cu/Al_2O_3 catalyst
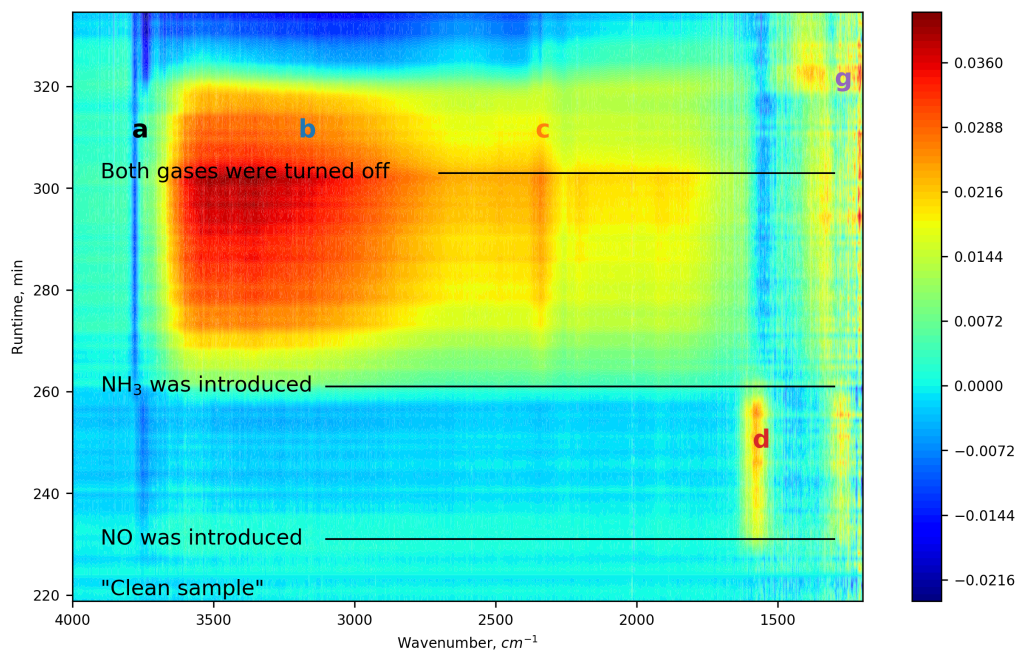
Figure 4.7: Contour plot of SCR reaction at 300°C on Fe/Al$_2$O$_3$ catalyst
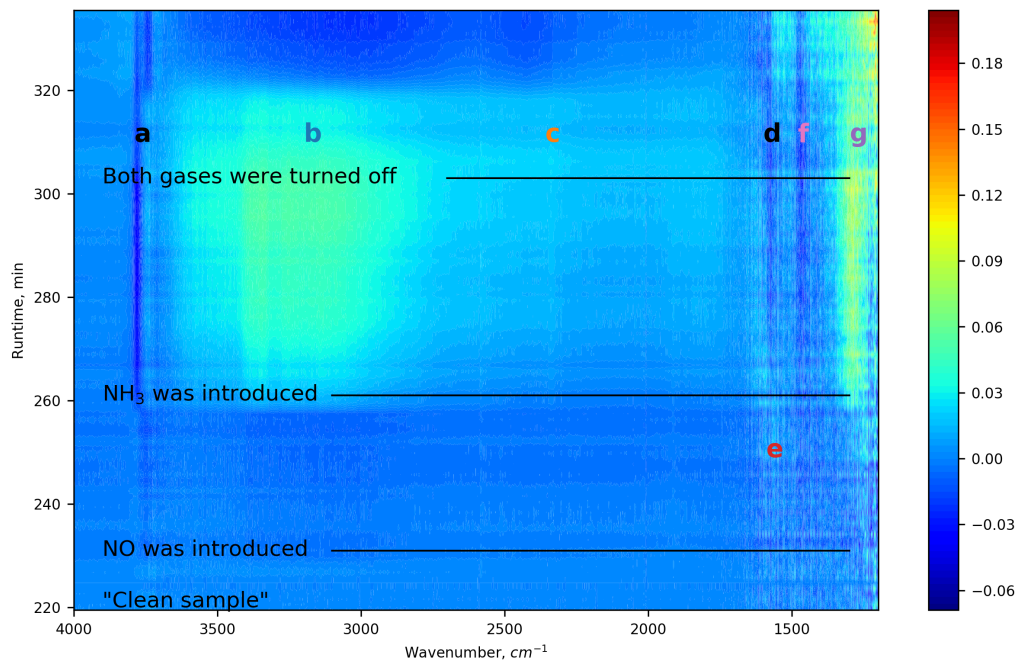
Figure 4.8: Contour plot of SCR reaction at 300°C on m-Al$_2$O$_3$ support

4.3.3 Similarities between the Samples

Peak **a**, **b**, **c**, and **g** are the same for the three samples, although with varying intensities. Peak **a** is a negative peak that appears at 3780 cm^{-1}. This peak corresponds well to OH groups classified by Knözinger and Ratnazami [47]. A negative peak means that something that was initially present on the surface has been removed. The peak is most likely negative because there were some hydroxyl bands initially present on the surface which had been corrected for in the background corrections when calculating absorbance at each temperature step. When these hydroxyl bands decrease in intensity upon ammonia adsorption, the signal becomes negative. As the intensity of the negative peak increase, there is a simultaneous increase in a broad band between 3600-3000 cm^{-1}, marked by **b** in all figures. This is partly due to the formation of hydroxyl bands as a result of the SCR reaction taking place. Also, the formation of different kinds of adsorbed ammonia species contributes to the broad peak. As the temperatures decrease for the Cu and Fe catalysts, the tribute from ammonia to peak **b** becomes more visible as less H_2O is formed at low temperatures. Peak **a** and **b** is plotted for all temperatures right after the two reactant gases were turned off in Figures 4.9, 4.10, and 4.11 in order to see the evolution of these peaks for each of the samples. The peaks marked by **b** are assigned to hydrogen bonded NH_3 as they are centered around 3500, 3370, 3260 and 3140 cm^{-1}, although some of the ammonia could also be bonded to the metal itself.
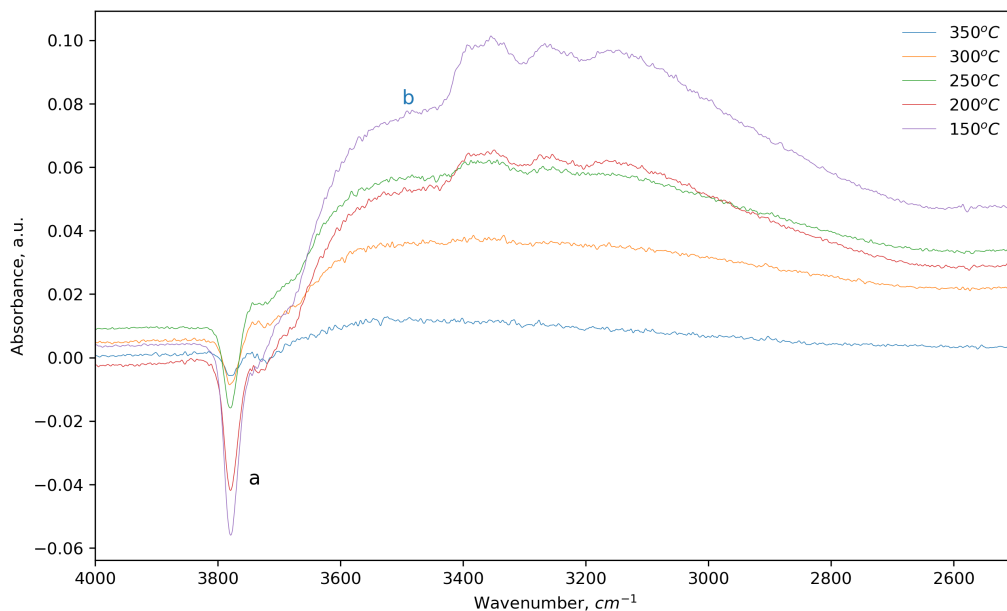
Figure 4.9: Maximum spectra of all temperatures between 4000-2500 cm^{-1} on Cu/Al$_2$O$_3$ to see the evolution of peak **a** and **b** with decreasing temperatures.
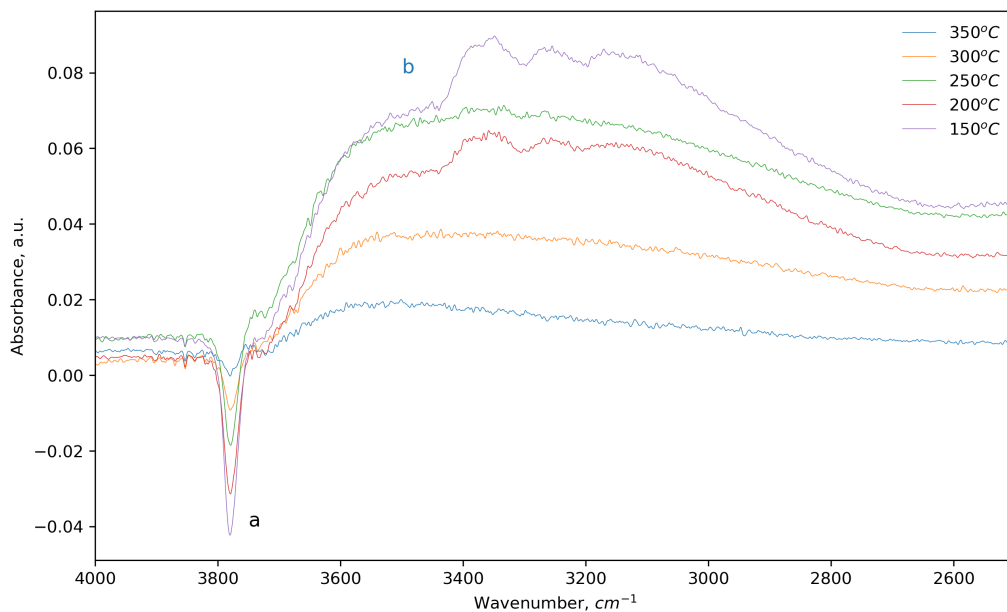
Figure 4.10: Maximum spectra of all temperatures between 4000-2500 cm^{-1} on Fe/Al$_2$O$_3$ to see the evolution of peak **a** and **b** with decreasing temperatures.
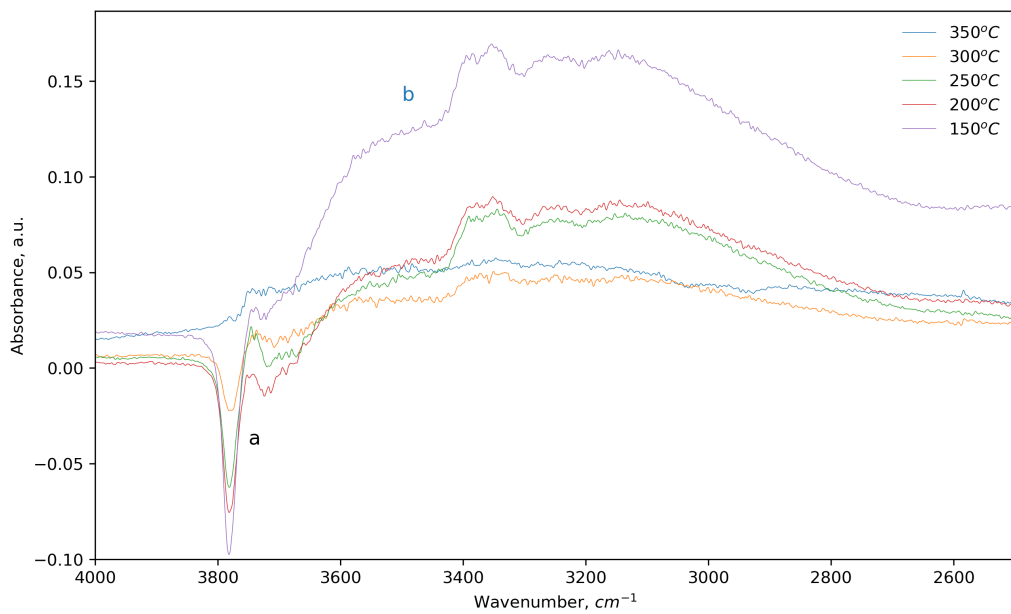
Figure 4.11: Maximum spectra of all temperatures between 4000-2500 cm^{-1} on m-Al$_2$O$_3$ to see the evolution of peak **a** and **b** with decreasing temperatures.

Figure 4.9 and 4.10 look quite similar, as the NH_3 peaks do not become very visible until the temperature has been decreased to 200°C for both catalysts, although one can already begin to see some changes on the Cu catalyst at 250°C in figure 4.9. In comparison, the same peaks are visible for the m-Al_2O_3 support already at 300°C. To get a closer look on the formation of these peaks, Figures 4.12, 4.13, and 4.14 compare the evolution of the negative peak and one of the ammonia peaks (3260 cm^{-1}) with the MS signal of m18 and m28 for the two catalysts and the support. m18 mainly gets a signal from water and m28 from nitrogen. Also, the blue fill in panel C shows where NH_3 gas was flowed, and the orange fill in panel D shows where the NO gas was flowed. Panel C and D in each of the figures show that more water and nitrogen are produced at the highest temperatures. The peaks in panel B increase as the production of reaction products decrease. The intensity of the negative peak in panel A also increases with lower H_2O and N_2 production. Thus, the peaks of hydrogen bonded NH_3 become more clear when less H_2O is produced. Panel C and D in the three figures show that at 200°C the MS signals of m18 and m28 were less than half of the signal at 300°C. The fact that the ammonia peaks in **b** did not become visible on the Cu and Fe catalysts before the temperature was about 200°C could indicate that a smaller amount of H_2O and N_2 was produced on the m-Al_2O_3 although this was only seen for N_2 in the MS results in chapter 4.2.
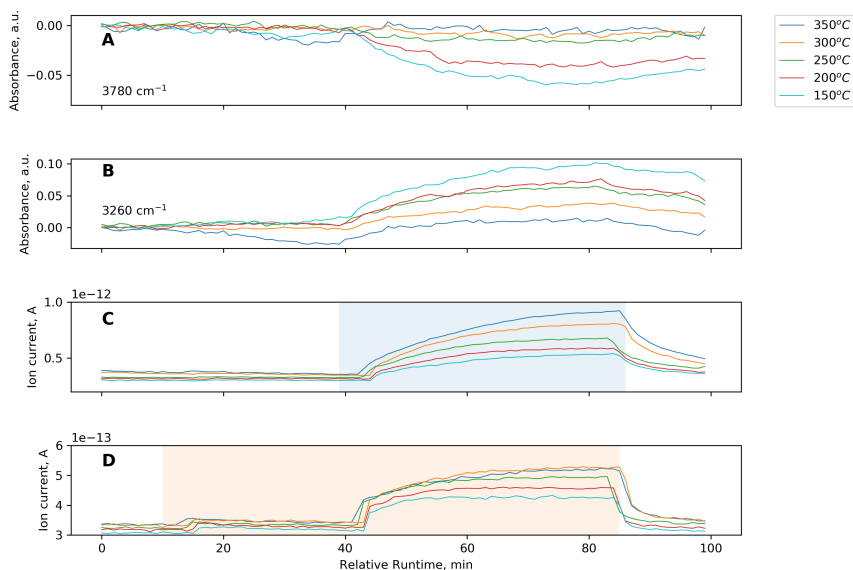
Figure 4.12: Cu/Al_2O_3 catalyst.**A**: Evolution of negative peak at 3780 cm^{-1}. **B**: Evolution in peak at 3260 cm^{-1}. **C**: MS signal for m18 and blue fill for NH_3 gas flow. **D**: MS signal for m28 and orange fill for NO gas flow
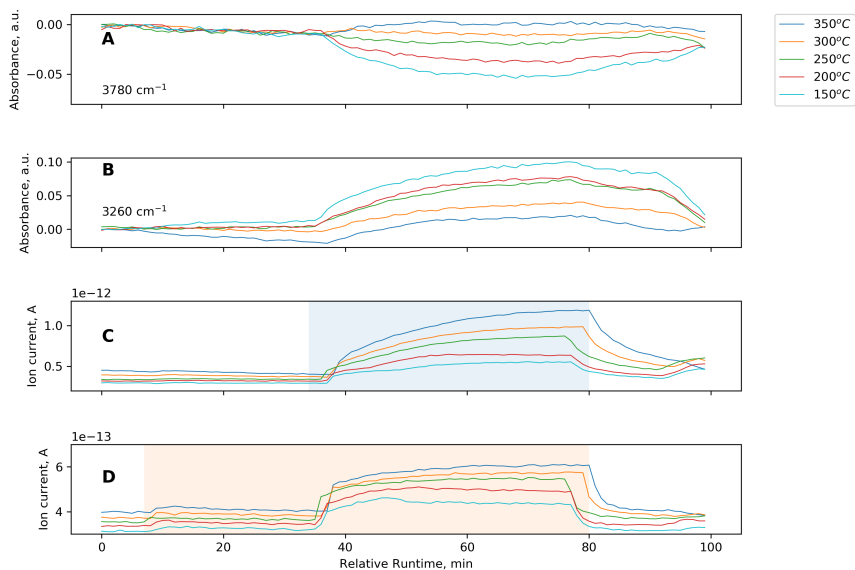
Figure 4.13: Fe/Al$_2$O$_3$ catalyst. **A**: Evolution of negative peak at 3780 cm^{-1}. **B**: Evolution of peak at 3260 cm^{-1}. **C**: MS signal for m18 and blue fill for NH$_3$ gas flow. **D**: MS signal for m28 and orange fill for NO gas flow
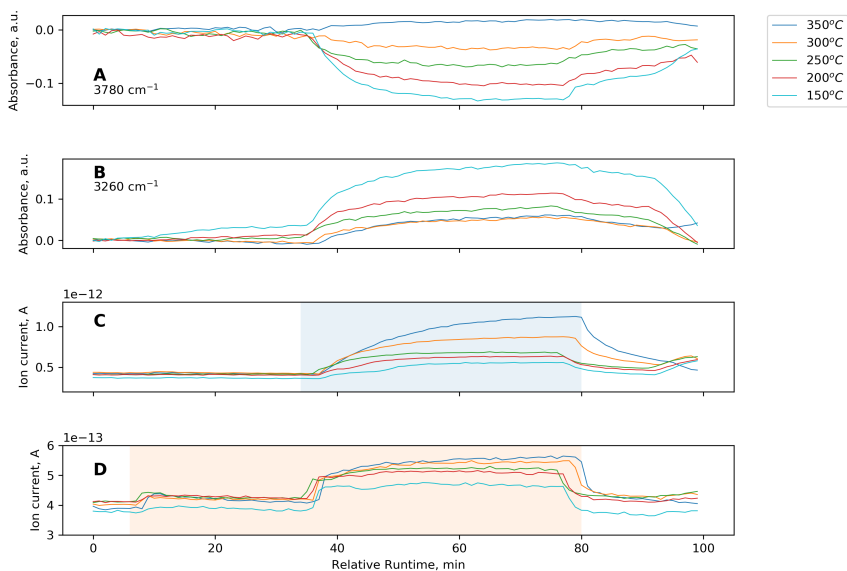
Figure 4.14: m-Al$_2$O$_3$ support. **A**: Evolution of negative peak at 3780 cm^{-1}. **B**: Evolution of peak at 3260 cm^{-1}. **C**: MS signal for m18 and orange fill for NH$_3$ gas flow. **D**: MS signal for m28 and blue fill for NO gas flow

The peak identification of **a** and **b** correspond well with literature as the appearance of the negative peak in the same area and the increase in the broad band have been reported by several scientists [8], [10], [12]. Centi *et.al* [8] reported similar results for alumina support, but not for copper-on-alumina. This could indicate that there were some Brønsted sites present on the alumina support that had not reacted with copper ions on the catalyst in use. Ruggeri et.al. [10] also reported a broad band between 3500-1550 cm^{-1} during NH$_3$ adsorption experiments on a Fe-ZSM-5 catalyst due to the formation of different kinds of adsorbed ammonia species, and a negative OH band at 3610 cm^{-1}. They associated the negative OH band to ammonium ions, NH$_4^+$, as the formation of ammonia ions compensated for the negative charge of the zeolite and thereby neutralized the hydroxyl bands (NH$_4^+$ + OH$^-$). Bands centered around 1450, 1700, and 3130 cm^{-1} are typical for ammonium ions. No Brønsted acid sites were observed on any of the samples as no bands were seen at 1450 or 1700 cm^{-1}, although one of the ammonia bands centered at around 3140 cm^{-1} could be due to the formation of ammonium ions. Jobson *et.al.* [12] also reported that hydroxyl bands on the alumina surface decreased in intensity upon ammonia adsorption and that the ammonia peaks increased in intensity with decreasing temperatures, as the ammonia desorbed from the surface at high temperatures. Only weak signals from ammonia adsorbed on Lewis acid sites were left on the surface at temperatures above 200°C.

For all three samples, a strong band occur between 1300 cm^{-1} and 1200 cm^{-1}, marked by **g**, that can be associated with coordinated ammonia on Lewis acid sites [8], [12]. The intensity of the peaks increases with decreasing temperatures in all three cases. This peak follows the same pattern as the ammonia peaks found in the broad band marked by **b**, where the coordinated ammonia gives a clear peak for the m-Al$_2$O$_3$ support already at 300°C, while it does not become clear for the Cu and Fe catalysts before the temperature reaches 200°C and below. An example of the temperature difference in peak **g** can be seen later on Cu/Al$_2$O$_3$ in Figure 4.19 and 4.20.

Peak **c** is also found in all three samples, located around 2340 cm^{-1}. This peak was not mentioned in published studies of the NH$_3$-SCR reaction as far as the author is aware, but it is believed that this peak can also be assigned to the formation of hydroxyl bands. The reason for this is that the peak is most intense for the Cu and Fe catalysts where it is believed that more H$_2$O is formed. Also, the intensity of the peak decreases at temperatures below 200°C where less water is formed, and less ammonia is desorbed from the surface. In other words, peak **c** follows the same pattern as the previously mentioned peak marked by **a** for all samples. Figures 4.15, 4.16 and 4.17 show how peak **c** changes from 300°C to 150°C for the three samples.

The MS signal for m18 and m17 is also included to show that the biggest change in the MS for the two temperatures is seen in m18 (H_2O), while the ammonia content in m17 almost doesn't change. The MS data thereby supports that the peak comes from the production of water from the SCR reaction. The NIST database [46] also confirms that water gives a small signal between 2400-2000 cm^{-1} as seen in figure C.3 in Appendix C. Peak **c** is a bit more visible at 300°C for Fe/Al$_2$O$_3$ in Figure 4.16 than for Cu/Al$_2$O$_3$, which could indicate that the Fe catalyst was a bit more active for the SCR reaction than the Cu catalyst, which was also indicated in the MS signals in chapter 4.2. However, the signals are in general very weak, so this could also just be because of noise.
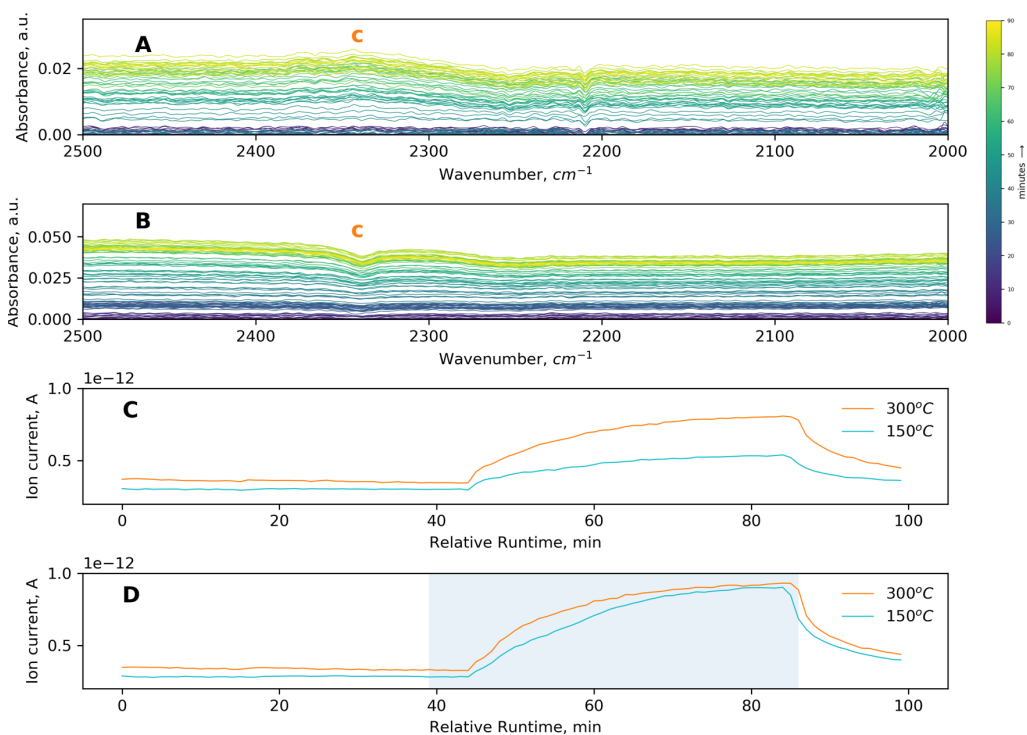
Figure 4.15: **A**: Peak **c** at 300°C on Cu/Al$_2$O$_3$. **B**:Peak **c** at 150°C on Cu/Al$_2$O$_3$. **C**: MS signal for m18. **D**: MS signal for m17 and blue fill for NH$_3$ gas flow
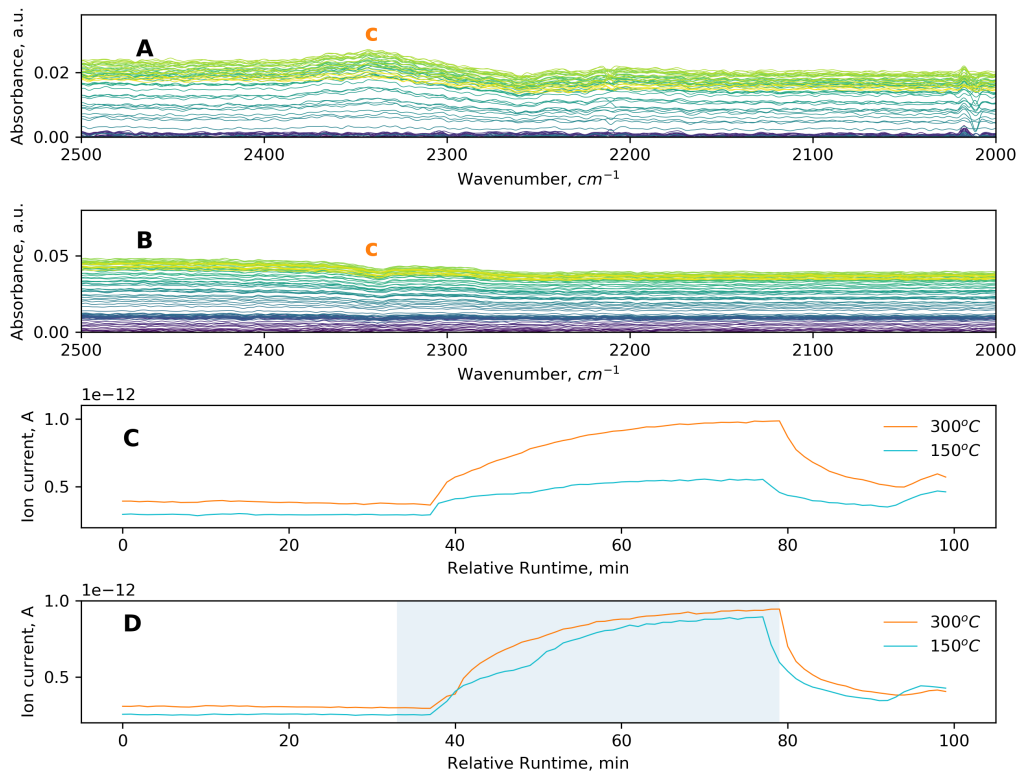
Figure 4.16: **A**: Peak **c** at 300°C on Fe/Al$_2$O$_3$. **B**:Peak **c** at 150°C on Fe/Al$_2$O$_3$. **C**: MS signal for m18. **D**: MS signal for m17 and blue fill for NH$_3$ gas flow
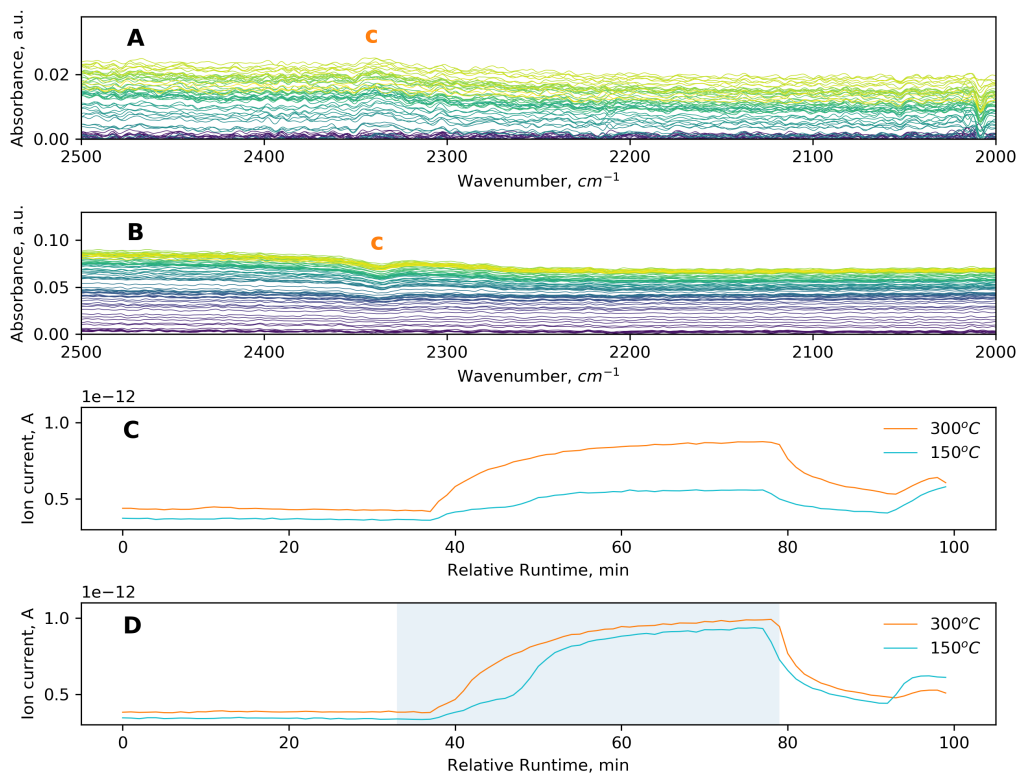
Figure 4.17: **A**: Peak **c** at 300°C on m-Al$_2$O$_3$. **B**:Peak **c** at 150°C on m-Al$_2$O$_3$. **C**: MS signal for m18. **D**: MS signal for m17 and blue fill for NH$_3$ gas flow

No production of N_2O was detected in the IR data in any of the samples as N_2O would give a peak mainly around 2222 cm^{-1} [11], [46], [48]. This shows that the catalysts have a high selectivity to N_2. N_2O could contribute to some of the intensity of peak **g** in the spectra as N_2O is also known to give a peak around 1282 cm^{-1} [48]. However, the intensities of peak **g** increase with lower temperatures. N_2O is a product of high temperature combustion of fossil fuels, and as the MS data of m44 in chapter 2.7 also illustrates, very little is produced at low temperatures. Also, no obvious detection of NO_2 was found in the spectra, but it is expected that there is a thermodynamic equilibrium between NO and NO_2 and that there is a gas phase reaction taking place between the two. Some of the contribution to the peaks assigned to NO will therefore also be from NO_2, as was also seen in the MS signals of m46 in chapter 4.2.

4.3.4 Differences between the Samples

The introduction of NO on Cu/Al$_2$O$_3$ can be seen clearly in figure 4.6 as a broad peak centered at 1555 cm^{-1} appears (**e**). The NO seems to be weakly chemisorbed to the surface as the peak disappears shortly after NH_3 is introduced and two new peaks are formed instead at 1625 cm^{-1} (**d**) and 1498 cm^{-1} (**f**). The peak at 1625 cm^{-1} (**d**) can be assigned to ammonia on lewis acid sites [8], [12], [39]. Figure 4.18 shows the evolution of peak **d** and **e** at 300°C compared to the MS signal of m17 (mainly NH_3) and m30 (mainly NO). Peak **d** starts to appear when the NH_3 gas is turned on and stays on the surface after the gas is turned off. A simultaneous drop in the NO signal can also be seen as the NO reacts with ammonia and the peak at 1555 cm^{-1} (**e**) decreases in panel B.
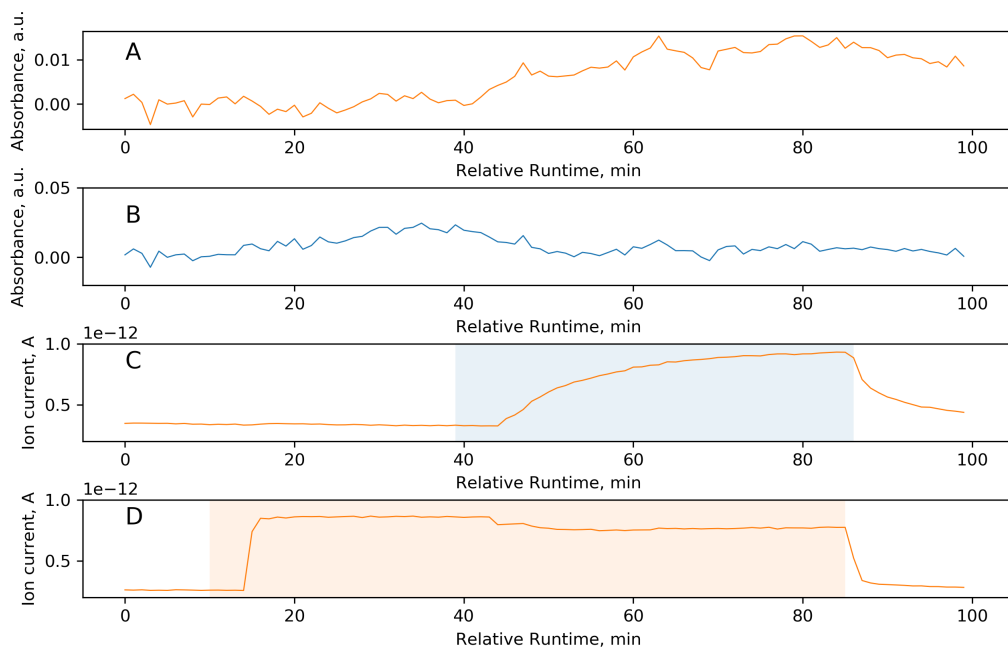
Figure 4.18: Cu/Al$_2$O$_3$ **A**: Evolution of peak **d** with maximum at 1625 cm^{-1} at 300°C. **B**: Evolution of peak **e** with maximum at 1555 cm^{-1} at 300°C. **C**: MS signal of m17 and blue fill for NH$_3$ gas flow at 300°C, **D**: MS signal of m30 and orange fill for NO gas flow at 300°C.

The peak centered at 1498 cm^{-1} (**f**) decreases in intensity at lower temperatures. The band can therefore not be assigned to species that are adsorbed to Brønsted sites, as they would have desorbed from the surface at temperatures above 200°C [12]. In accordance with Jobson *et.al.* [12], the peak can be assigned to ammonia molecules that are strongly bonded to positively charged Cu^{2+} sites. The area between 1700-1200 cm^{-1} at 300°C is presented as a lineplot in Figure 4.19 where the NO was introduced after 10 minutes while the NH$_3$ was introduced after 40 minutes. The peaks are addressed with the same letters as in Figure 4.6. Figure 4.20 shows the same area but at 200°C to see the difference in peak **f** at lower temperatures. Compared to Figure 4.19, the peak is gone at 200°C. Another difference in the two figures is that less NO reacts with NH$_3$ at lower temperatures, and therefore peak **e** is still present after 80 minutes in Figure 4.20 whereas this peak disappears when the NH$_3$ is introduced at 300°C in figure 4.20. Also, the figures show the formation of the previously addressed peak **g** at 200°C due to ammonia adsorbed on Lewis acid sites together with peak **d** at 1625 cm^{-1}.
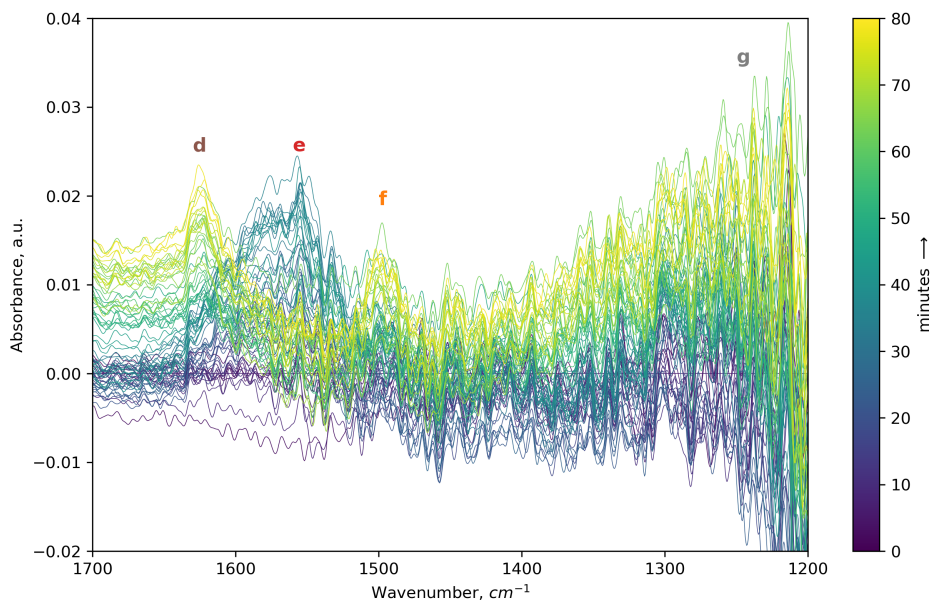
Figure 4.19: Line plot of SCR reaction at 300°C Cu/Al$_2$O$_3$ catalyst between 1700-1300 cm^{-1}. NO was introduced after 10 minutes and NH$_3$ was introduced after 40 minutes.
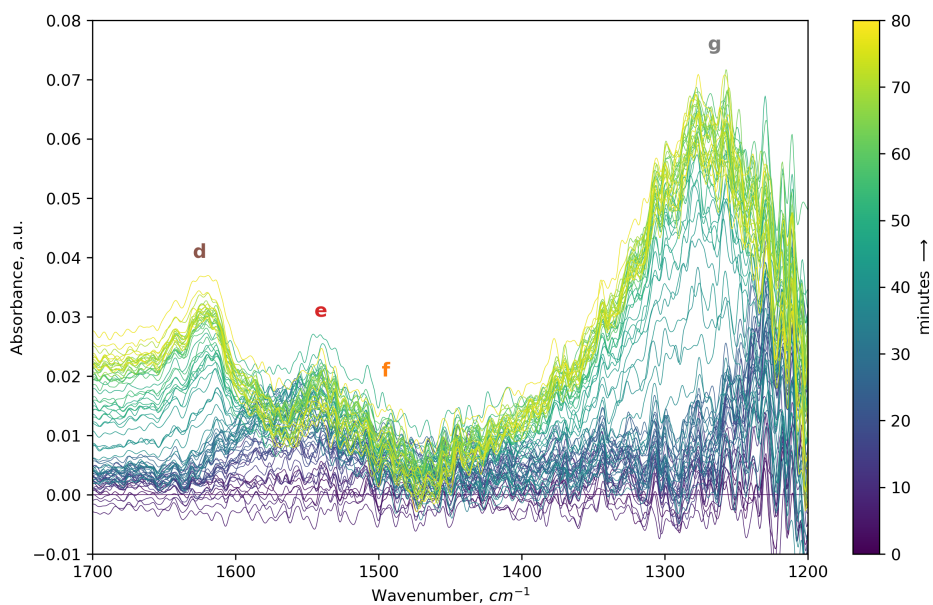
Figure 4.20: Line plot of SCR reaction at 200°C. Evolution of peaks between 1700-1300 cm^{-1}. NO was introduced after 10 minutes and NH$_3$ was introduced after 40 minutes.

The introduction of NO, and how it reacts with the surface, seems to differ between the samples. For the Fe catalyst in Figure 4.7 the introduction of NO gives a distinct peak around 1574 cm^{-1} (**d**), which is a little bit higher than for the Cu catalyst. In accordance with Ruggeri *et. al.* [10] this peak can be associated to the formation of ferric nitrates. Figure 4.21 shows a closeup of peak **d**. In this figure, one can also see the formation of a shoulder at 1620 cm^{-1}, marked by d2, which was also one of the peaks that Ruggeri *et. al.* assigned to ferric nitrates. The ferric nitrates are removed from the surface as they react with NH_3 to form H_2O and N_2.
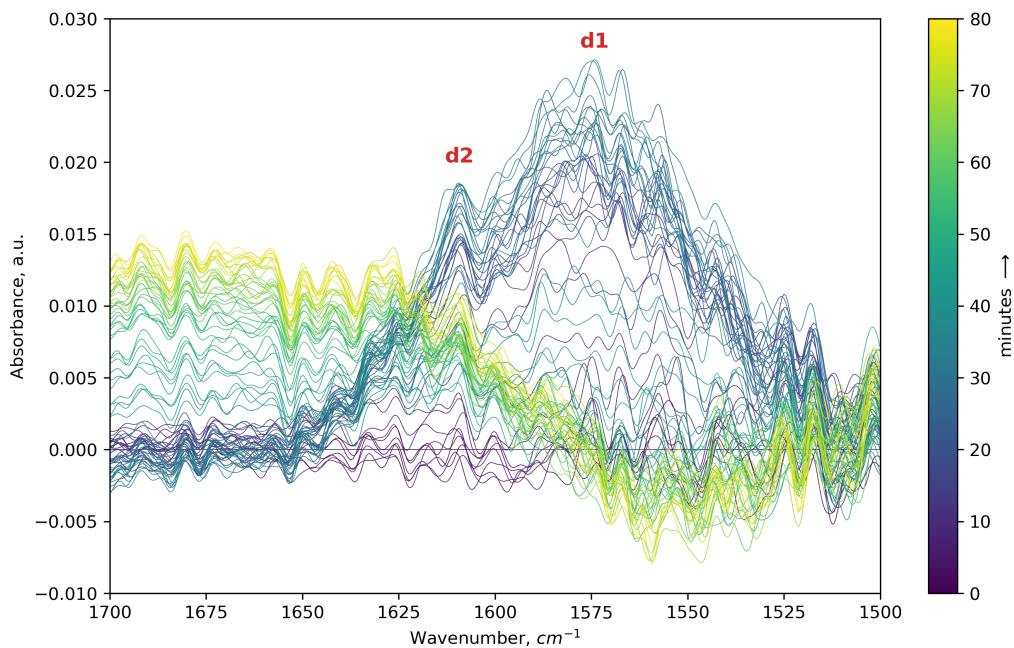
Figure 4.21: Lineplot of SCR reaction at 300°C on Fe/Al_2O_3 catalyst showing evolution of peak d1: 1574 cm^{-1} and d2: 1620 cm^{-1}. NO was introduced after 10 minutes and NH_3 was introduced after 40 minutes

To get a closer look at the formation of peak **d** the evolution of peak **d1** with time, compared to the MS signal of m28 and m30 is shown in Figure 4.22. As also seen in Figure 4.20, the peak appears when the NO is flowed in panel C, and the peak disappeared as soon as the NH_3 gas was introduced in panel B.
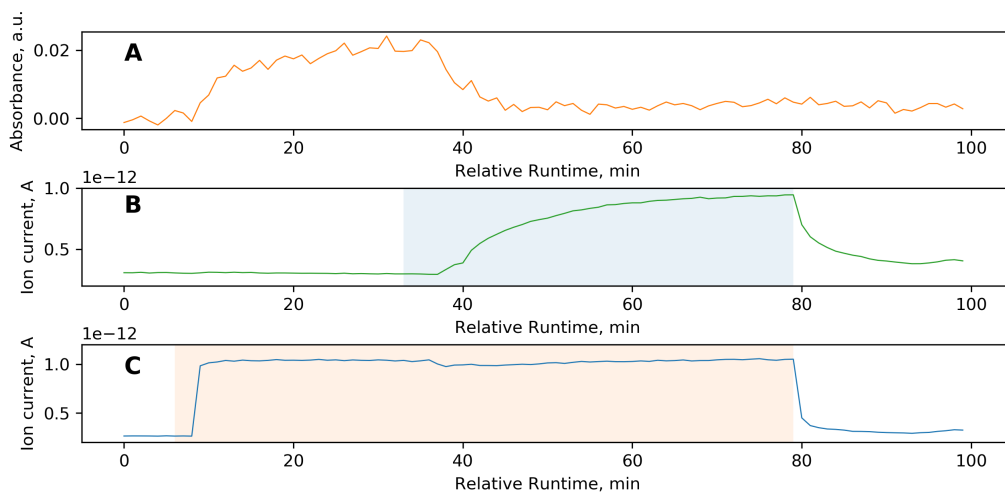
Figure 4.22: Fe/Al_2O_3 **A**: Evolution of peak d1 with respect to time. **B**: MS signal of m28 at 300°C and blue fill for NH_3 gas flow. **C**: MS signal of m30 at 300°C and orange fill for NO gas flow.

As for the m-Al$_2$O$_3$ support in Figure 4.8, the introduction of NO, marked by **e**, is almost not noticeable compared to the two other catalysts. This shows that NO does not chemisorb to the support alone, but to the Cu and Fe sites on the two other samples. The spectra are quite noisy below 1700 cm^{-1} for the alumina support, and it is therefore hard to address the peaks. Some assumptions can still be made. The area below 1700 cm^{-1} is shown in Figure 4.23, and the peaks are marked with the same letters as in the contour plot in figure 4.8. There are no big changes in the spectra as the NO is introduced. The NO would normally cause a peak to appear between 1515-1560 cm^{-1} [46], here marked by **e**. Two negative peaks could also be seen in Figure 4.8 around 1580 cm^{-1}, marked by **d**, and around 1460 cm^{-1}, marked by **f**. The same two peaks are barely visible in Figure 4.23. No literature was found on these two negative peaks, but Jobson *et.al.* [12] reported that they found an OH group at 1580 cm^{-1} on pure alumina. Data from NIST also shows that OH groups give a small peak in this area [46]. It can therefore be assumed that the negative peaks on the m-Al$_2$O$_3$ are due to OH groups that are reduced as ammonia is adsorbed in the same way as the previously mentioned negative peak **a** on all catalysts. Also, it makes sense that these negative peaks only occur on the alumina support and not for the Cu or Fe samples, as there are more sites available for OH groups without the copper and iron ions.
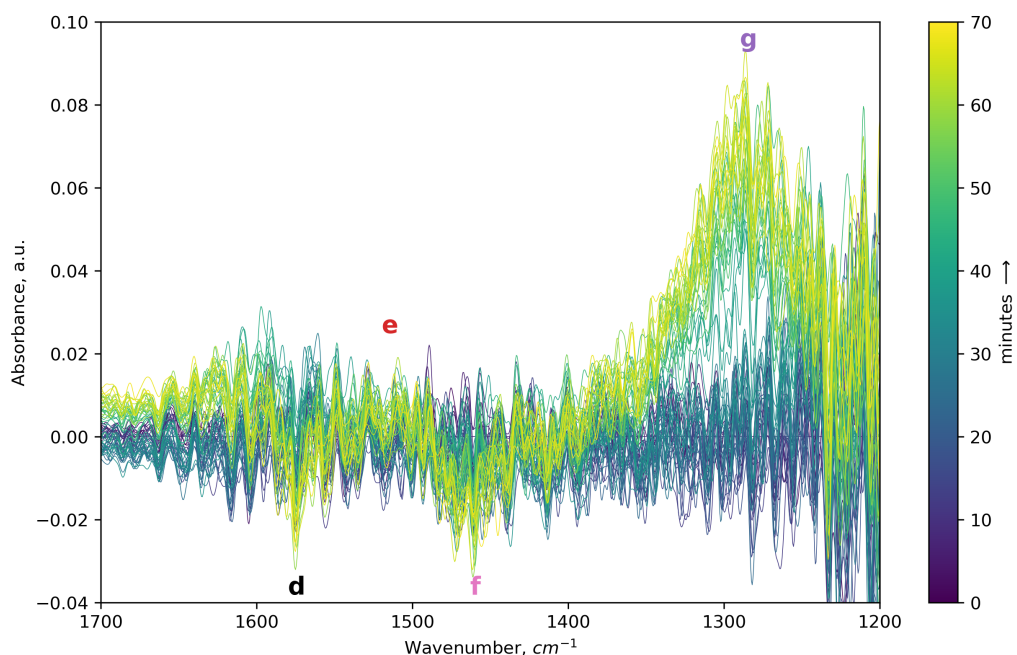
Figure 4.23: Lineplot of SCR reaction at 300°C on m-Al$_2$O$_3$ support. NO stream was started after 10 minutes, and NH$_3$ stream after 40 minutes.

The IR signals in the results are generally noisy. Infrared spectroscopy is a non-zero-background technique where the absorption of light is measured as the change in intensity from that of the original IR beam. The problem with such high intensities is the fact that the signal-to-noise (S/N) becomes large. This sensitivity problem is especially found in FTIR because white light is used, which contains frequencies that are not adsorbed, but still adds to the noise of the signals [15]. Time resoulution could also be a reason for the high level of noise. If one would use longer time to obtain spectra, they would also have been less noisy, but then it would not be possible to see the changes that occur quickly when the reaction is taking place. The detector used in this particulate apparatus is also not optimal for max intensity. The sensitivity problem sometimes makes it hard to determine if it is actually a peak occurring or just noise. It was however easier to separate the peaks from the noise when the data treatment was tackled by Python scripting in order to visualize the peaks and see the changes occurring with time as seen in the line plots presented previously in this chapter. The program FITYK was used as a tool to deconvolute peaks and reduce noise in the specialization project done prior to this thesis. This was however not an option in this *operando* study as the procedure generates over 1400 spectra for each experiment, and it would therefore be too time-consuming to deconvolute every spectrum.

Chapter 5

Summary and Conclusion

The goal of this thesis was to investigate if it was possible to do an *operando* study of the NH_3-SCR reaction using FTIR and simultaneous monitoring of the gas composition by using a mass spectrometer. The MS calibration did not work the way it was initially intended because the instrument was very sensitive to changes from oxidative to reductive environments. Information about consumption, conversion and selectivity of the gases could therefore not be retrieved from the MS data, and it was thus only used as a qualitative measurement. The MS results could still be used as an indication of what was going on in the system, and be used to verify the assumptions made about peaks formed in the FTIR results. The MS results indicated that the conversion level of the SCR reaction was quite low as the difference in the three samples was quite small. The MS data only presented a small difference in H_2O production between the three samples, although it was expected to see more activity in the Cu and Fe catalysts than on the support alone. However, the MS signal of m28 was smaller for the support, which confirms that the support was less active as less N_2 was produced. Both the MS signals and the IR spectra indicated that the Fe/Al_2O_3 was slightly more active for converting NO_x into H_2O and N_2 which had also been reported in literature.

The study revealed that there were some limitations in the technique with the equipment used in this thesis. The signals from the FTIR were generally weak and a bit noisy. It was still possible to extract information from the results, but resources should be used in order to improve the signal-to-noise. Although the results are not optimal, they will be of help in choosing more suitable tools/conditions in the future. The FTIR spectra revealed that the NO gas seemed to react differently with the surface of the different catalysts. For the Cu sample, the NO seemed to be weakly chemisorbed

to the surface as a peak at 1555 cm^{-1} disappeared as soon as the ammonia gas was introduced to the system. Two new peaks were formed instead located at 1625 cm^{-1}, which is typical for ammonia on Lewis acid sites, and a peak at 1498 cm^{-1}, which was identified as ammonia molecules that are strongly bonded to positively charged Cu^{2+} sites in accordance with Jobson *et.al.* [12]. For the Fe catalyst, the introduction of NO gave a peak around 1575 cm^{-1} along with a shoulder at 1620 cm^{-1}. These peaks were associated to the formation of ferric nitrates in accordance with Ruggeri *et.al.* [10]. The ferric nitrates were removed from the surface as they reacted with NH$_3$ to form H$_2$O and N$_2$. As for the m-Al$_2$O$_3$ support, the introduction of NO was almost not noticeable in the spectra. This shows that the NO did not adsorb to the support alone, but to the Cu and Fe sites on the two other catalysts. The IR results indicated that less reaction products were formed on the support as the N-H vibrations from ammonia located between 3600-3000 cm^{-1} and between 1300-1200 cm^{-1} could barely be seen on the Cu and Fe catalysts at 300°C but were very clear for the support alone at 300°C. These peaks looked more alike when the Cu and Fe samples had reached 200°C and about 50% less H$_2$O and N$_2$ formation was seen in the MS results. This showed that the Cu/Al$_2$O$_3$ and the Fe/Al$_2$O$_3$ catalysts were more active for the NH$_3$-SCR reaction than the support.

Chapter 6

Future Work

For future work on FTIR *operando* studies it should be a focus to reduce the signal-to-noise in the spectra. This could perhaps be done by lowering the resolution of the FTIR, or it could be interesting to try a transmission cell instead of the diffuse reflectance cell used in this thesis. In the specialization project done prior to this thesis, FITYK was used to deconvolute the peaks and reduce noise, but this would be way too time-consuming in an *operando* study, as this procedure generates over 1400 spectra for each experiment. Averaging and improving the S/N, or finding a way to deconvolute the spectra in for instance python would therefore help on the noise reduction. It would also be interesting to use a sparger to introduce water directly to the feed in order to see what part of the system that gives a signal to water in order to see where the NH_3 and NO binds, and what is actually produced. NTNU has recently purchased a new MS that can better differentiate the masses from each other, and that is less susceptible to oxidative and reductive environments. It would therefore be interesting to use this MS when it is up and running, in order to see if one could see a better correlation between the two measurements and to calculate consumption, conversion and selectivity of the gases.

Bibliography

[1] Calvert, J. G. and Stockwell, W. R., "Acid generation in the troposphere by gas-phase chemistry," *Environmental science & technology*, vol. 17, no. 9, 428A–443A, 1983.

[2] Fritz, A and Pitchon, V, "The current state of research on automotive lean nox catalysis," *Applied Catalysis B: Environmental*, vol. 13, no. 1, pp. 1–25, 1997.

[3] Logan, J. A., "Tropospheric ozone: Seasonal behavior, trends, and anthropogenic influence," *Journal of Geophysical Research: Atmospheres*, vol. 90, no. D6, pp. 10 463–10 482, 1985.

[4] Sandoval Rangel, L, Lucio-Ortiz, C., Rosa, J Rivera de la, and Castaldi, M., "Selective catalytic reduction of NO_x with NH_3 using ZSM5 with low content of copper," *Superficies y vacío*, vol. 29, no. 1, 2016.

[5] Chen, Z., Wang, F., Li, H., Yang, Q., Wang, L., and Li, X., "Low-temperature selective catalytic reduction of NO_x with NH_3 over Fe–Mn mixed-oxide catalysts containing $Fe_3Mn_3O_8$ phase," *Industrial & Engineering Chemistry Research*, vol. 51, no. 1, pp. 202–212, 2011.

[6] Brandenberger, S., Kröcher, O., Tissler, A., and Althoff, R., "The state of the art in selective catalytic reduction of NO_x by Ammonia using metal-exchanged zeolite catalysts," *Catalysis Reviews*, vol. 50, no. 4, pp. 492–531, 2008.

[7] Lai, S., She, Y., Zhan, W., Guo, Y., Guo, Y., Wang, L., and Lu, G., "Performance of Fe-ZSM-5 for Selective Catalytic Reduction of NOx with NH_3: Effect of the Atmosphere during the Preparation of Catalysts," *Journal of Molecular Catalysis A: Chemical*, vol. 424, pp. 232–240, 2016.

[8] Centi, G., Perathoner, S., Biglino, D., and Giamello, E., "Adsorption and reactivity of no on copper-on-alumina catalysts: I. formation of nitrate species and their influence on reactivity in no and NH_3 conversion," *Journal of Catalysis*, vol. 152, no. 1, pp. 75–92, 1995.

[9]   Long, R. and Yang, R., "FTIR and Kinetic Studies of the Mechanism of Fe_3^+-exchanged TiO_2-pillared Clay Catalyst for Selective Catalytic Reduction of NO with Ammonia," *Journal of catalysis*, vol. 190, no. 1, pp. 22–31, 2000.

[10] Ruggeri, M. P., Grossale, A., Nova, I., Tronconi, E., Jirglova, H., and Sobalik, Z., "FTIR in situ Mechanistic Study of the NH_3-NO/NO_2 "Fast SCR" reaction over a commercial Fe-ZSM-5 catalyst," *Catalysis Today*, vol. 184, no. 1, pp. 107–114, 2012.

[11] Liu, Z., Millington, P. J., Bailie, J. E., Rajaram, R. R., and Anderson, J. A., "A comparative study of the role of the support on the behaviour of iron based ammonia scr catalysts," *Microporous and mesoporous materials*, vol. 104, no. 1-3, pp. 159–170, 2007.

[12] Jobson, E., Baiker, A., and Wokaun, A., "Adsorption of ammonia and methylamines on alumina and copper/alumina studied by dynamic fourier-transform infrared experiments," *Journal of the Chemical Society, Faraday Transactions*, vol. 86, no. 7, pp. 1131–1137, 1990.

[13] Howe, R. F., "In-situ spectroscopy in heterogeneous catalysis," in. Wiley-VCH Verlag GmbH & Co. KGaA, 2004, pp. 139–177.

[14] Bañares, M. A., Guerrero-Pérez, M. O., Fierro, J. L. G., and Cortez, G. G., "Raman spectroscopy during catalytic operations with on-line activity measurement (operando spectroscopy): A method for understanding the active centres of cations supported on porous materials," *Journal of Materials Chemistry*, vol. 12, no. 11, pp. 3337–3342, 2002.

[15] Zaera, F., "New advances in the use of infrared absorption spectroscopy for the characterization of heterogeneous catalytic reactions," *Chemical Society Reviews*, vol. 43, no. 22, pp. 7624–7663, 2014.

[16] Niemantsverdriet, J. W., "Spectroscopy in catalysis," in. John Wiley & Sons, 2007, pp. 217–249.

[17] Barzetti, T., Selli, E., Moscotti, D., and Forni, L., "Pyridine and ammonia as probes for ftir analysis of solid acid catalysts," *J. Chem. Soc., Faraday Trans.*, vol. 92, pp. 1401–1407, 8 1996. DOI: `10.1039/FT9969201401`. [Online]. Available: `http://dx.doi.org/10.1039/FT9969201401`.

[18] MECA, *U.S. EPA 2007/2010 heavy-duty engine and vehicle standards and highway diesel fuel sulfur control requirements*, `http://www.meca.org/regulation/us-epa-20072010-heavyduty-engine-and-vehicle-standards-and-highway-diesel-fuel-sulfur-control-requirements`, Accessed 13.06.2018.

[19] Held, W., Koenig, A., Richter, T., and Puppe, L., "Catalytic NO_x reduction in net oxidizing exhaust gas," *SAE transactions*, pp. 209–216, 1990.

[20] Bovens, L., "The ethics of dieselgate," *Midwest studies in philosophy*, vol. 40, no. 1, pp. 262–283, 2016.

[21] Österman, C. and Magnusson, M., "A systemic review of shipboard scr installations in practice," *WMU Journal of Maritime Affairs*, vol. 12, no. 1, pp. 63–85, 2013.

[22] Amiridis, M. D., Duevel, R. V., and Wachs, I. E., "The effect of metal oxide additives on the activity of v2o5/tio2 catalysts for the selective catalytic reduction of nitric oxide by ammonia," *Applied Catalysis B: Environmental*, vol. 20, no. 2, pp. 111–122, 1999.

[23] Chorkendorff, I and Niemantsverdriet, J. W., "Concepts of modern catalysis and kinetics," in. John Wiley & Sons, 2017, ch. Catalyst Characterization, pp. 129–170.

[24] Kamasamudram, K., Currier, N., Szailer, T., and Yezerets, A., "Why cu-and fe-zeolite scr catalysts behave differently at low temperatures," *SAE International Journal of Fuels and Lubricants*, vol. 3, no. 2010-01-1182, pp. 664–672, 2010.

[25] Koebel, M., Elsener, M., and Kleemann, M., "Urea-SCR: a promising Technique to reduce NO_x Emissions from Automotive Diesel Engines," *Catalysis today*, vol. 59, no. 3-4, pp. 335–345, 2000.

[26] Shelef, M, "Selective catalytic reduction of nox with n-free reductants," *Chemical Reviews*, vol. 95, no. 1, pp. 209–225, 1995.

[27] Ravishankara, A., Daniel, J. S., and Portmann, R. W., "Nitrous oxide (N_2O): the dominant ozone-depleting substance emitted in the 21st century," *science*, vol. 326, no. 5949, pp. 123–125, 2009.

[28] Miljødirektoratet, *Lystgass (n_2o)*, `http://www.miljostatus.no/tema/klima/norske-klimagassutslipp/lystgass-utslipp/`, Accessed 23.05.2018, 2018.

[29] Larkin, P., "Infrared and raman spectroscopy: Principles and spectral interpretation," in. Elsevier, 2017, pp. 1–25.

[30] Colthup, N., Daly, L. H., and Wiberley, S. E., "Introduction to infrared and raman spectroscopy," in. Elsevier, 1990, ch. Vibrational and Rotational spectra, pp. 1–73.

[31] Ebsworth, E. A. V., Rankin, D. W., and Cradock, S., "Structural methods in inorganic chemistry," in. Blackwell Scientific Publications, 1987, ch. Vibrational Spectroscopy, pp. 173–246.

[32] Pasquini, C., "Near infrared spectroscopy: Fundamentals, practical aspects and analytical applications," *Journal of the Brazilian Chemical Society*, vol. 14, no. 2, pp. 198–219, 2003.

[33] *The Praying Mantis^{TM} user´s manual.* Harrick Scientific Products, Inc.

[34] Swinehart, D., "The beer-lambert law," *Journal of chemical education*, vol. 39, no. 7, p. 333, 1962.

[35] Vimont, A., Thibault-Starzyk, F., and Daturi, M., "Analysing and understanding the active site by ir spectroscopy," *Chem. Soc. Rev.*, vol. 39, pp. 4928–4950, 12 2010. DOI: `10.1039/B919543M`. [Online]. Available: `http://dx.doi.org/10.1039/B919543M`.

[36] Hattori, H. and Ono, Y., "Solid acid catalysis: From fundamentals to applications," pp. 93–99, 2015.

[37] Mapes, J. and Eischens, R., "The infrared spectra of ammonia chemisorbed on cracking catalysts," *The Journal of Physical Chemistry*, vol. 58, no. 12, pp. 1059–1062, 1954.

[38] Shen, Y.-F., Suib, S. L., Deeba, M, and Koermer, G., "Luminescence and ir characterization of acid sites on alumina," *Journal of Catalysis*, vol. 146, no. 2, pp. 483–490, 1994.

[39] Peri, J., "Infrared study of adsorption of ammonia on dry γ-alumina1," *The Journal of Physical Chemistry*, vol. 69, no. 1, pp. 231–239, 1965.

[40] Topsøe, N.-Y., "Mechanism of the selective catalytic reduction of nitric oxide by ammonia elucidated by in situ on-line fourier transform infrared spectroscopy," *Science*, vol. 265, no. 5176, pp. 1217–1219, 1994.

[41] Yang, S., Wang, C., Ma, L., Peng, Y., Qu, Z., Yan, N., Chen, J., Chang, H., and Li, J., "Substitution of WO_3 in V_2O_5/WO_3-TiO_2 by Fe_2O_3 for selective catalytic reduction of NO with NH_3," *Catalysis Science & Technology*, vol. 3, no. 1, pp. 161–168, 2013.

[42] Pontis, H. G., "Methods for analysis of carbohydrate metabolism in photosynthetic organisms: Plants, green algae and cyanobacteria," in. Academic Press, 2016, pp. 71–76.

[43] Reusch, W., *Mass spectrometry*, `https://www2.chemistry.msu.edu/faculty/Reusch/VirtTxtJml/Spectrpy/MassSpec/masspec1.htm`, Accessed 01.05.2018, 2013.

[44] NIST Mass Spec Data Center and Stein director, S., *Mass spectra*. NIST Chemistry WebBook, NIST Standard Reference Database Number 69, Eds. P.J. Linstrom, W.G. Mallard, National Institute of Standards, and Technology, Gaithersburg MD, 20899, doi:10.18434/T4D303, (retrieved march 11, 2018). [Online]. Available: `https://webbook.nist.gov/`.

[45] Meunier, F., "Pitfalls and benefits of in situ and operando diffuse reflectance ft-ir spectroscopy (drifts) applied to catalytic reactions," *Reaction Chemistry & Engineering*, vol. 1, no. 2, pp. 134–141, 2016.

[46] NIST Mass Spec Data Center and Stein director, S., *Infrared Spectra*. NIST Chemistry WebBook, NIST Standard Reference Database Number 69, Eds. P.J. Linstrom, W.G. Mallard, National Institute of Standards, and Technology, Gaithersburg MD, 20899, doi:10.18434/T4D303, (retrieved march 11, 2018). [Online]. Available: `https://webbook.nist.gov/`.

[47] Knözinger, H and Ratnasamy, P., "Catalytic aluminas: Surface models and characterization of surface sites," *Catalysis Reviews Science and Engineering*, vol. 17, no. 1, pp. 31–70, 1978.

[48] Montgomery, T. A., Samuelsen, G. S., and Muzio, L. J., "Continuous infrared analysis of N_2O in combustion products," *JAPCA*, vol. 39, no. 5, pp. 721–726, 1989.

Appendix A

Temperature Calibration

The following appendix presents some of the results generated in a specialization project leading up to this thesis. The project proved that there was a need to correct for temperature deviations in the IR cell in order to get accurate data. This chapter show how the temperature was calibrated, and the results were used in the experimental work done in this thesis as well.

A.1 Temperature Calibration Experimental

In order to see if the suspicions about the temperature control being off was correct, it was attempted to reproduce the work of Meunier [45]. This was done by using both a FLUKE 566 IR thermometer and a FLUKE 289 True RMS multimeter thermocouple. The cell was filled with pure grinded KBr and the thermocouple was installed onto the sample surface as shown in figure A.2. The IR thermometer was attached to a stand in a fixed position as shown in figure A.1 and the temperature was measured at the same point for every 50 degrees from 50°C to 500°C. The results were compared to the temperature given by the installed termocouple in the cell. The emissivity of KBr was assumed to be $\epsilon = 0.95$ when using the IR thermometer.
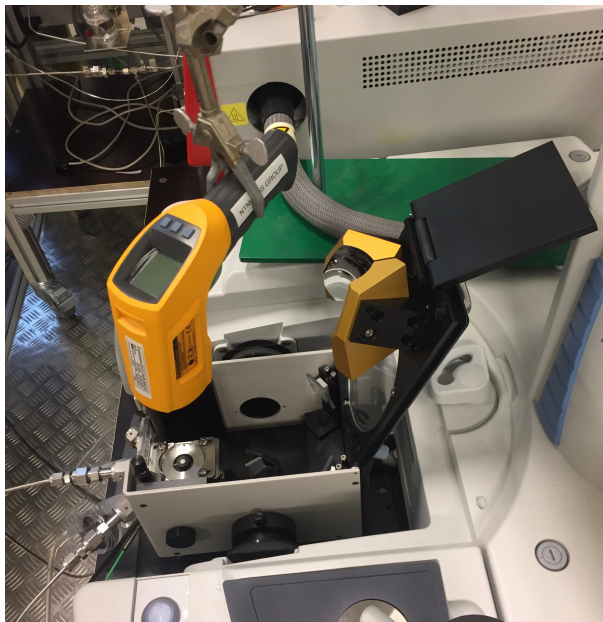
Figure A.1: FLUKE 566 IR thermometer used for temperature calibration
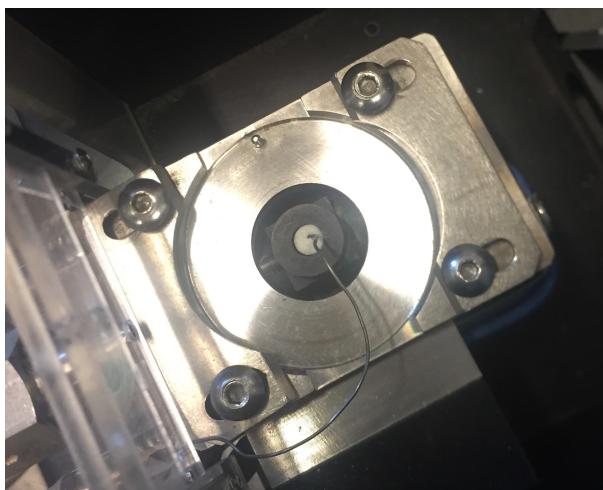
Figure A.2: Thermocouple installed on sample surface for temperature calibration

An average value of the temperatures measured by the IR thermometer and the thermocouple was found and plotted against the temperature setpoint values of the heater (50-500°C). The slope and intercept of the curve was found and used to find a linear temperature calibration curve as shown in equation A.1.

$$x = \frac{y}{m} - b \qquad \text{(A.1)}$$

where x is the corrected temperature, y is the wanted temperature, m is the slope of the curve and b is the intercept.

A.2   Temperature Calibration Results

The results from the temperature measurements are shown in figure A.3. The measured temperatures from the IR thermometer and the thermocouple placed on the KBr surface was very similar, which shows that the results are reliable and that there is a need to correct for the temperature controller in order to also get reliable results from the adsorption experiments. The results also showed a good correlation to the work of Meunier. Meunier reported that the temperature of the cell was about 100°C cooler when the temperature was set to 460°C. These results shows a difference of about 103°C at the same temperature.
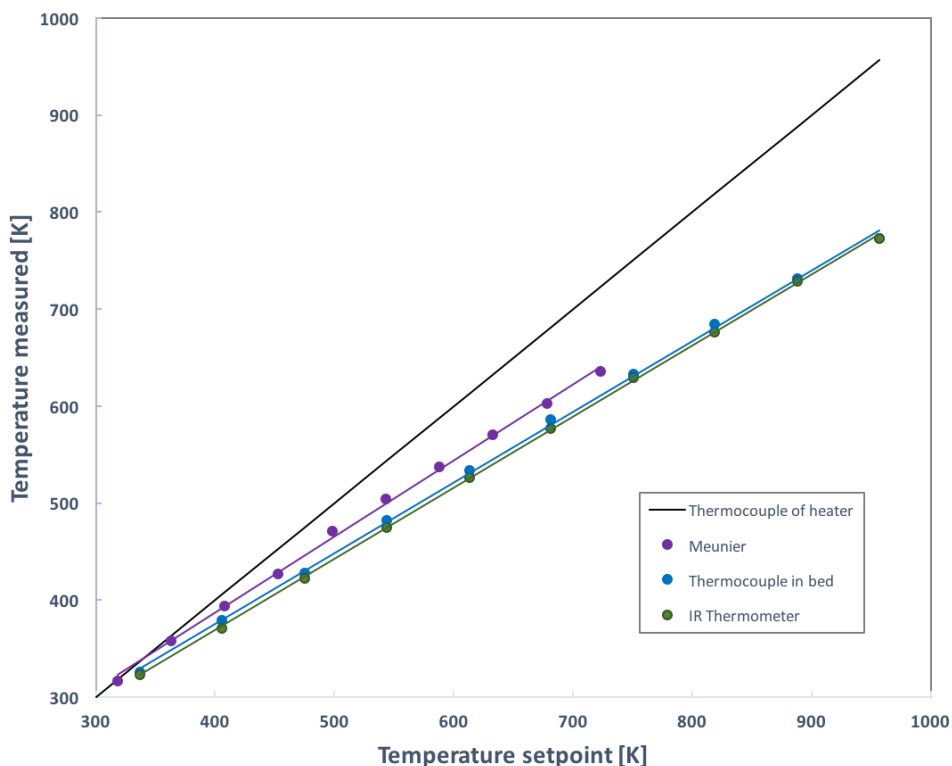
Figure A.3: Temperature measurements using a thermocouple on the sample surface, IR thermometer and comparing results to the work of Meunier *et. al* [45].

An average of the measured temperatures of the two methods was used to find new temperature points to correct for this deviation. The corrected temperatures are shown in table A.1 and the calibration curve is shown in figure A.4. The corrected temperatures was used in all adsorption experiments.

One must take in to account that there will still be some deviation from the real temperature as the dome was off the sample bed under the temperature measurements. Also the emissivity might not be correct, but the strong correlation between the temperatures measured from the two methods used and the strong accordance to the findings of Meunier shows that it is within range.

Table A.1: Temperature calibration

Target temperature [°K]	Corrected setpoint of heater [°K]
300	333
350	402
400	470
450	538
500	606
550	674
600	743
650	811
700	879
750	947
773	978
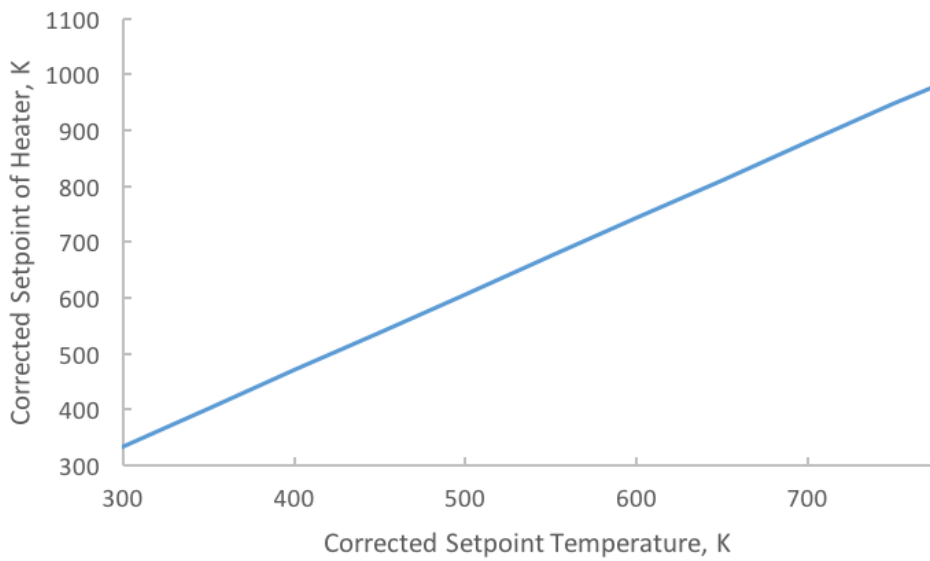
Figure A.4: Temperature curve

Appendix B

Mass Spectrums from NIST database

Reference mass spectrums of NO, N_2, NO_2, O_2, H_2O, Ar, N_2O obtained by NIST Chemistry Webbook are presented in this appendix.
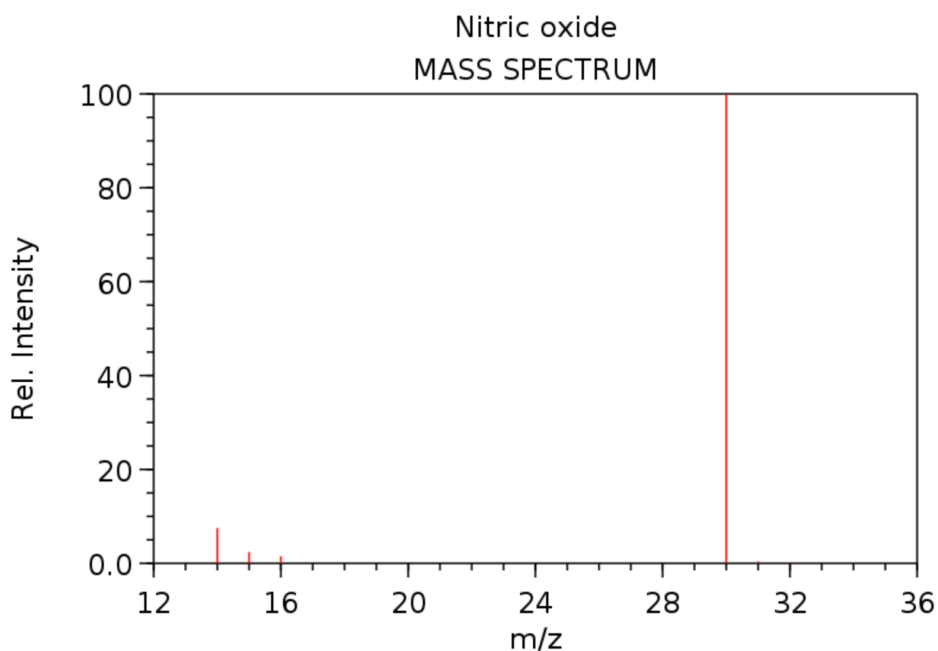
Figure B.1: NO mass spectrum from NIST Chemistry WebBook [44]
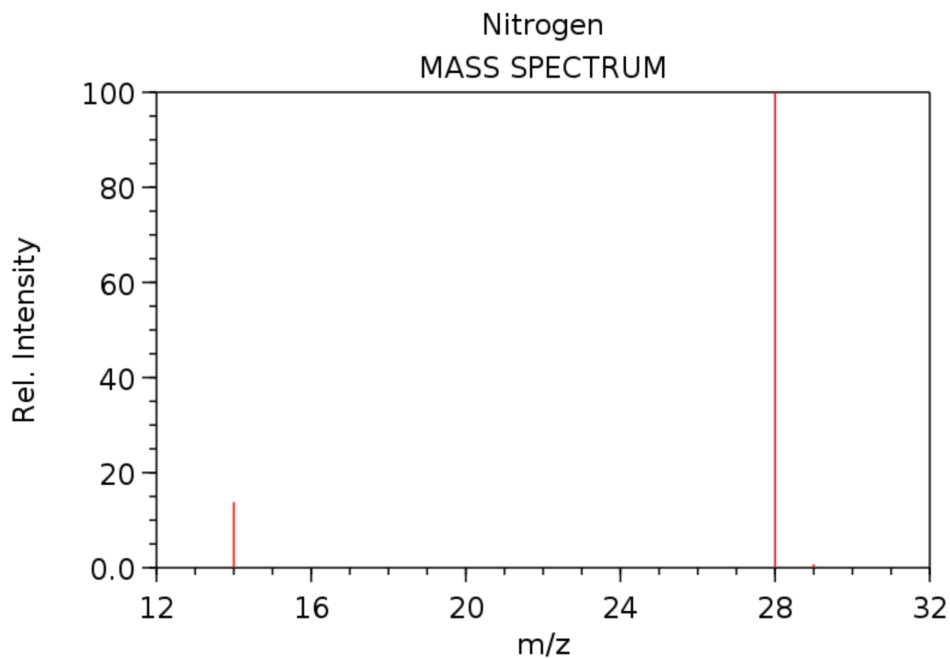
Figure B.2: N2 mass spectrum from NIST Chemistry WebBook [44]
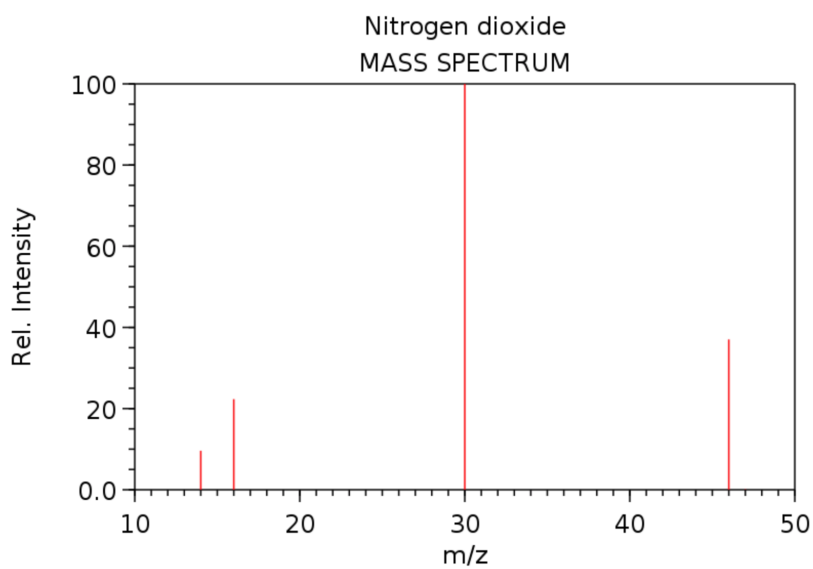
Figure B.3: NO_2 mass spectrum from NIST Chemistry WebBook [44]
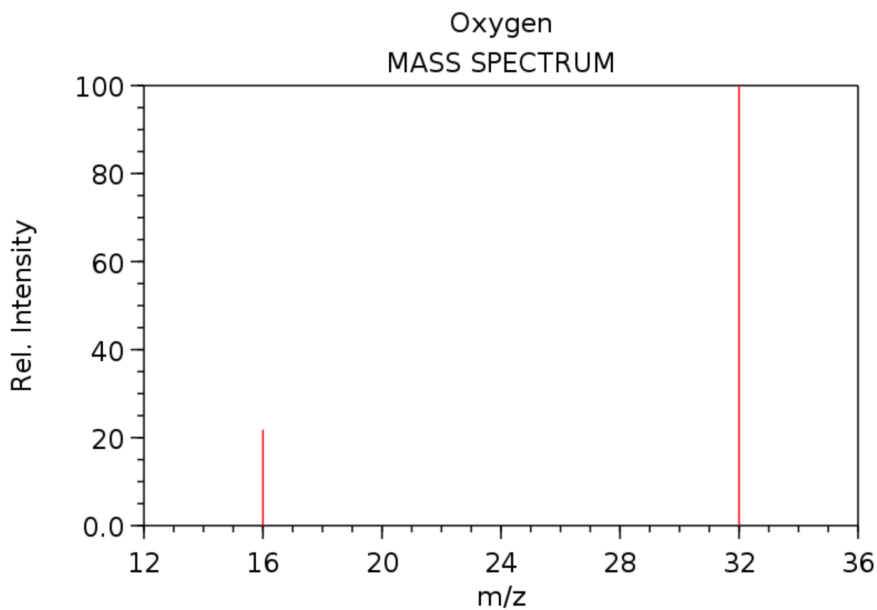
Figure B.4: O_2 mass spectrum from NIST Chemistry WebBook [44]
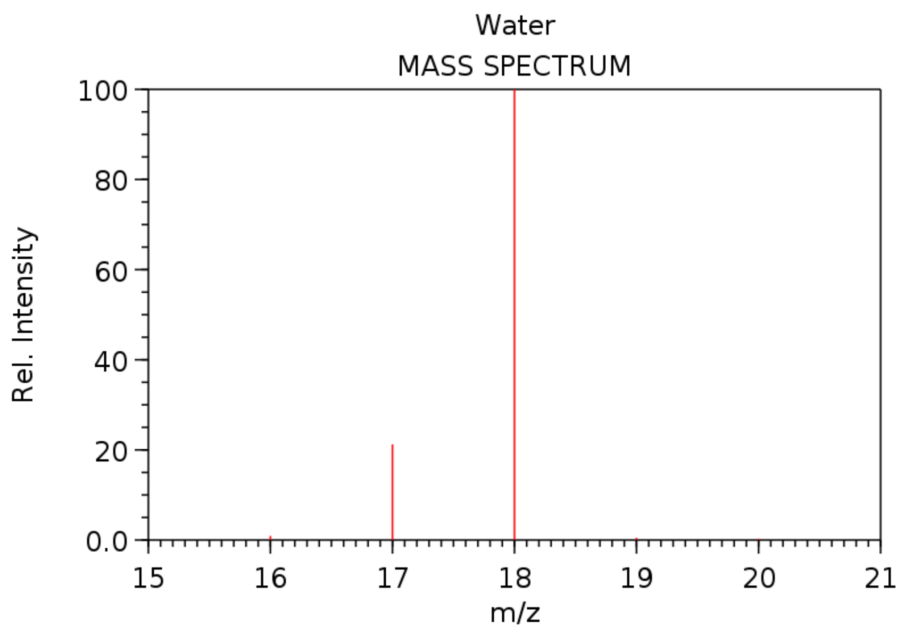
Figure B.5: H_2O mass spectrum from NIST Chemistry WebBook [44]
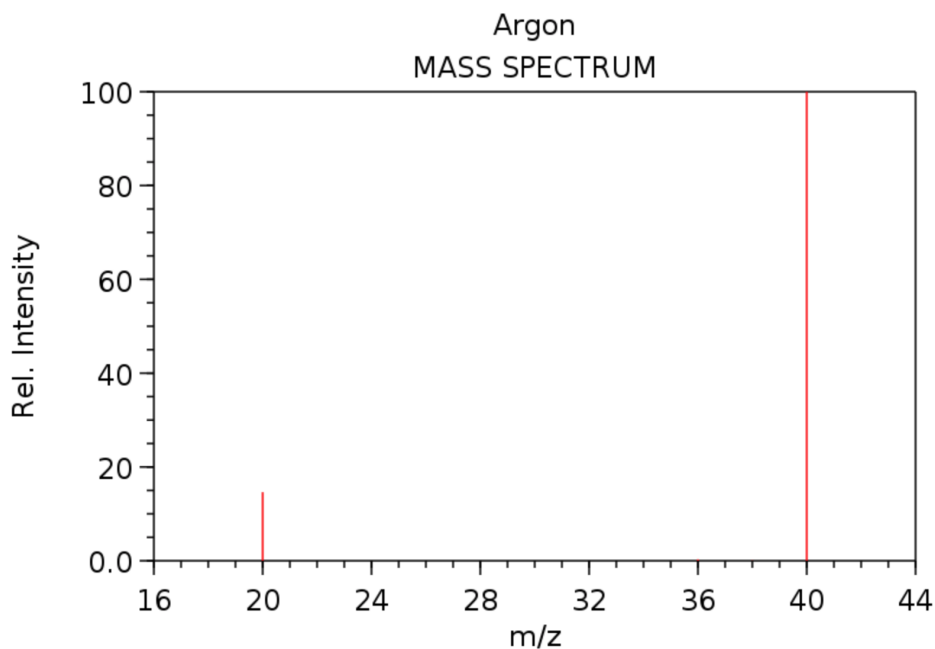
Figure B.6: Ar mass spectrum from NIST Chemistry WebBook [44]
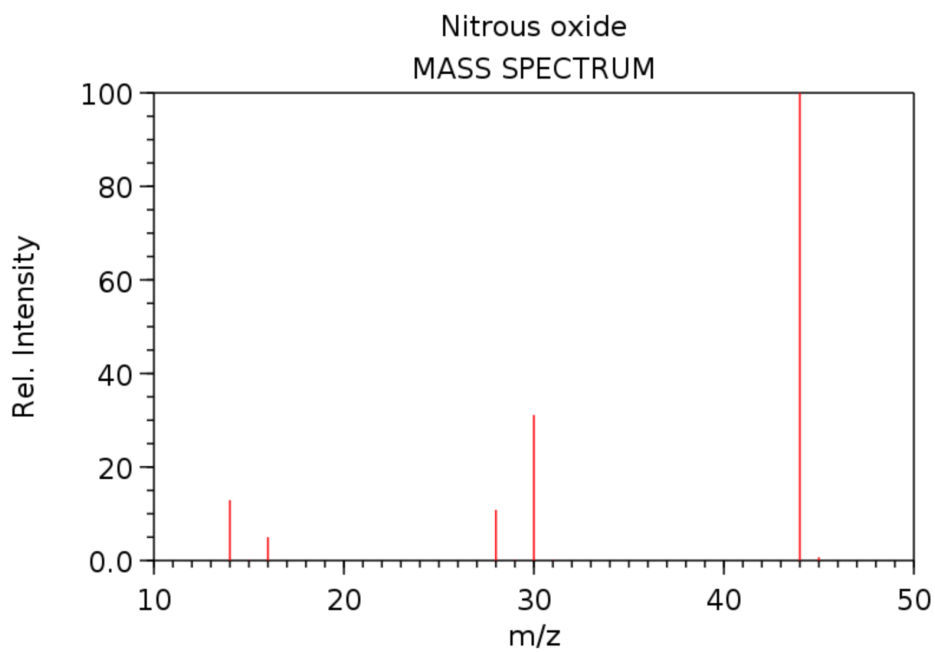
Figure B.7: N_2O mass spectrum from NIST Chemistry WebBook [44]

Appendix C

IR Spectrums from NIST Database

Reference IR spectrums of NH_3, NO, H_2O and N_2O obtained by NIST Chemistry Webbook are presented in this appendix.
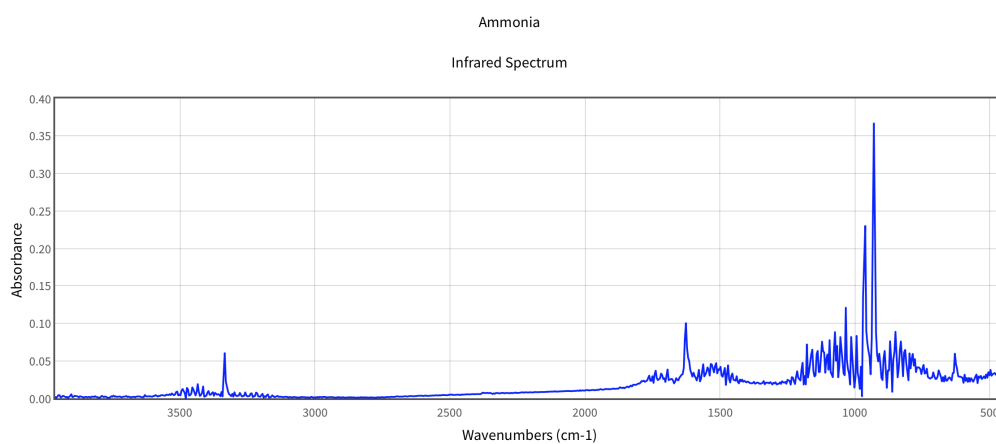
Figure C.1: Infrared spectrum of ammonia from NIST [46]
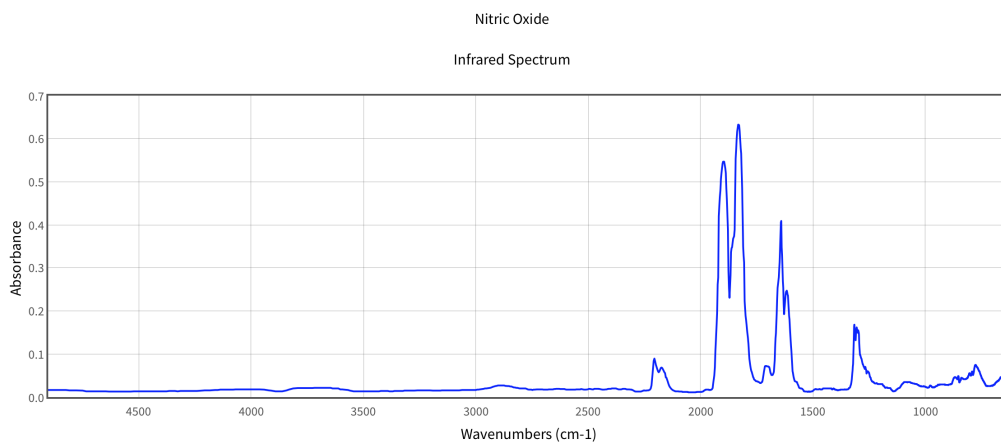
Figure C.2: Infrared spectrum of NO from NIST [46]
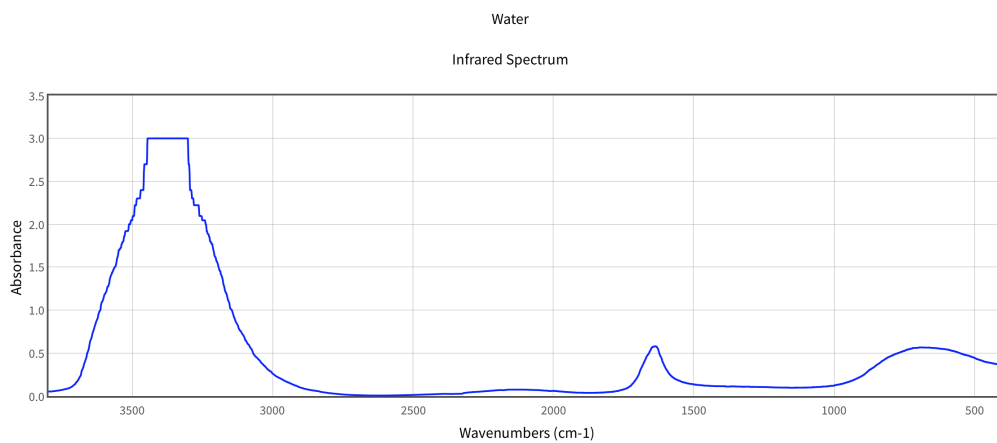
Figure C.3: Infrared spectrum of water from NIST [46]
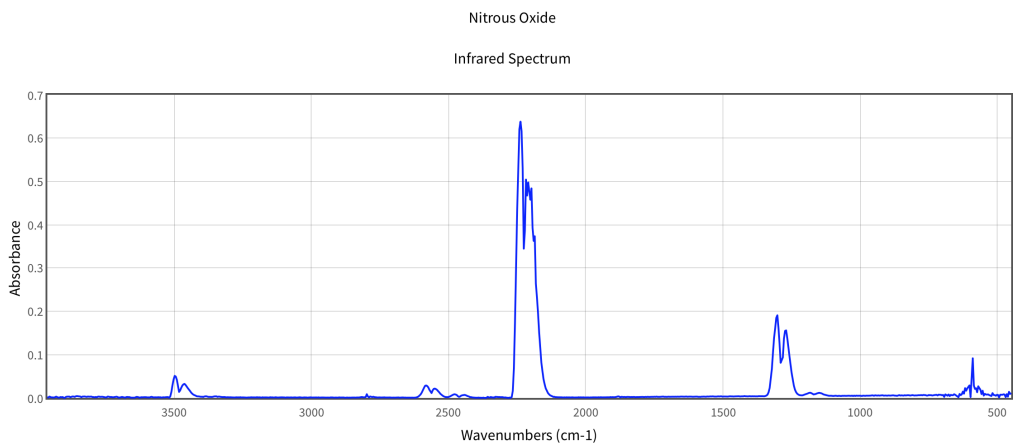
Figure C.4: Infrared spectrum of NO_2 from NIST [46]

Appendix D

Line plots of SCR reaction at 350°C and at room temperature

This appendix is included to show why the SCR reaction was mainly studied at 300°C. The line plots of all spectra generated at 350°C were very noisy. A reason for this could be that the sample itself starts to send out IR radiation, or it could be due to a poorly chosen background spectrum. The intensity of the absorbance was much higher at room temperature than for the other temperatures, probably because the sample was not reheated after reaction which caused the signal to increase. Also it is not expected to see much production of reaction products at room temperature as the SCR reaction usually takes place between 300-400°C. The line plots of the absorbance over the whole range is shown in Figures D.1 and D.2 for Cu/Al_2O_3.

Figure D.1: Line plot of absorbance spectra generated at 350°C
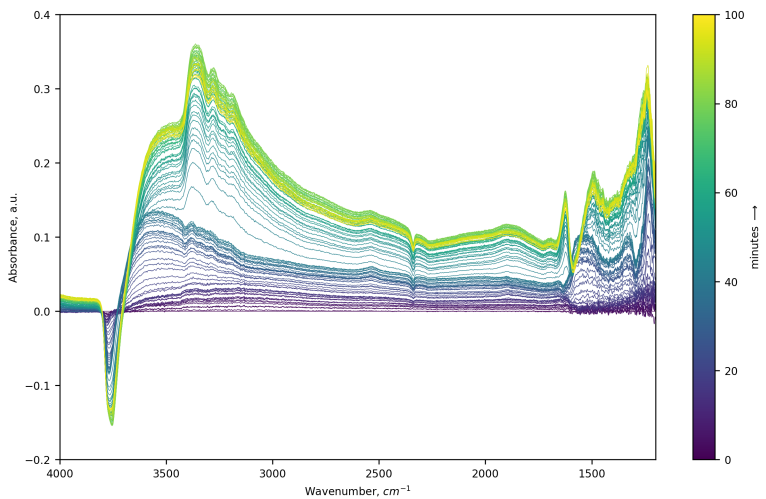
Figure D.2: Line plot of absorbance spectra generated at room temperature

Appendix E

Python Script

The Python script used for data analysis is given in this appendix. The script is for the Cu/Al$_2$O$_3$ catalyst, but the same code was used for all three samples.

E.1 MS data

The first script shows how the MS data was imported, separated and plotted.

```python
#import MS data
#import ASCII
Folder="/Users/jane/Documents/NTNU_master_2018/Experiments3/
2018-05-11_3CuAl"
Filename="20180511 141708 NH3-SCR_DRIFTS.asc"
os.chdir(Folder)
df_importedData=pd.read_csv(Filename, skiprows=7, header=0, delimiter='\t')

#select relevant columns and concatenate
df_Time=df_importedData.iloc[:-1,0:2]
df_Data=df_importedData.iloc[:-1,2::3]
df_Data=pd.concat([df_Time, df_Data], axis=1)

df_Time

#Sycnhronize with DRIFTS Data
df_Data=df_Data.iloc[3:,1:]

#Column Titles
df_Data.columns=['Runtime_MS[min]', '2', '4', '14', '15',
'16', '17', '18', '28', '30', '32', '40', '44', '46','Pressure']

#remove commas replace with dots
df_Data=df_Data.stack().str.replace(',','.').unstack()

#transform to numpy array
np_Data=df_Data.as_matrix().astype(np.float)
MS_time=np_Data[:,0]
MS_runtime=np.empty(len(MS_time))
for i in range(len(MS_time)):
    MS_runtime[i]=(MS_time[i]-MS_time[0])/60

m4=np_Data[:,2]
m14=np_Data[:,3]
```

```
m15=np_Data[:,4]
m16=np_Data[:,5]
m17=np_Data[:,6]
m18=np_Data[:,7]
m28=np_Data[:,8]
m30=np_Data[:,9]
m32=np_Data[:,10]
m40=np_Data[:,11]
m44=np_Data[:,12]
m46=np_Data[:,13]
Pressure=np_Data[:,14]
m2=np_Data[:,1]

LV_runtime,temperature,O2_conc,NO_conc,NH3_conc,MFC_He,Total_FLow,
SV=np.loadtxt("2018-05-11_SCR_DRIFTS_LabVIEW_log-sync.txt", unpack=True)

#MS_runtime,m4,m14,m15,m16,m17,m18,m28,m30,m32,m40,m44,m46,m2=np.loadtxt
("2018-02-18_SCR_DRIFTS_CeZrW_2nd_MS-Log.txt", unpack=True, skiprows=1)
m4=griddata(MS_runtime,m4,LV_runtime,method='linear')
m14=griddata(MS_runtime,m14,LV_runtime,method='linear')
m15=griddata(MS_runtime,m15,LV_runtime,method='linear')
m16=griddata(MS_runtime,m16,LV_runtime,method='linear')
m17=griddata(MS_runtime,m17,LV_runtime,method='linear')
m18=griddata(MS_runtime,m18,LV_runtime,method='linear')
m28=griddata(MS_runtime,m28,LV_runtime,method='linear')
m30=griddata(MS_runtime,m30,LV_runtime,method='linear')
m32=griddata(MS_runtime,m32,LV_runtime,method='linear')
m40=griddata(MS_runtime,m40,LV_runtime,method='linear')
m44=griddata(MS_runtime,m44,LV_runtime,method='linear')
m46=griddata(MS_runtime,m46,LV_runtime,method='linear')
m2=griddata(MS_runtime,m2,LV_runtime,method='linear')
Pressure=griddata(MS_runtime,Pressure,LV_runtime,method='linear')

#Import MS data




#plot
fig=plt.figure(figsize=(15,15), dpi=300)
```

```python
plt.style.use('default')
mpl.rcParams.update({'font.size': 8})

gs=mpl.gridspec.GridSpec(15,1)
gs.update(wspace=0.3, hspace=0.4, bottom=0,top=1)

#Panel 1: Temperature
panel1 = plt.subplot(gs[0:1,0:1])
plt.plot(LV_runtime, temperature, 'k', label='Temperature')
#plt.xlabel('Runtime, min')
plt.tick_params(labelbottom=False)
plt.ylabel('Temperature')
plt.xlim(0,1150)
plt.legend(frameon=False)

#Panel 2: NO
panel2 = plt.subplot(gs[1:2,0:1])
plt.plot(LV_runtime, m30, color='C0', label='m30', linewidth=0.3)
#plt.plot(LV_runtime, MFC_NH3, color='C0', label='m30', linewidth=0.3)
panel2.fill_between(LV_runtime,NO_conc,facecolor='C1', alpha=0.1,
interpolate=True)
#plt.xlabel('Time on Stream, min')
plt.tick_params(labelbottom=False)
plt.ylabel('Ion current, A')
#plt.xlim(0,1000)
plt.legend(frameon=False)
plt.ylim(0,2e-12)


#Panel 3: NH3
panel3 = plt.subplot(gs[2:3,0:1])
plt.plot(LV_runtime, m17,'C2', label='m17', linewidth=0.3)
panel3.fill_between(LV_runtime,NH3_conc,facecolor='C0', alpha=0.1,
interpolate=True)
plt.tick_params(labelbottom=False)
#plt.xlabel('Time on Stream, min')
plt.ylabel('Ion current, A')
plt.xlim(0,1150)
```

```
plt.ylim(2e-13,1e-12)
plt.legend(frameon=False)


#Panel 4: H2O
panel4 = plt.subplot(gs[3:4,0:1])
plt.plot(LV_runtime, m18,'C7', label='$m18$', linewidth=0.3)
plt.tick_params(labelbottom=False)
#plt.xlabel('Time on Stream, min')
plt.ylabel('Ion current, A')
plt.xlim(0,1150)
plt.ylim(2e-13,1e-12)
plt.legend(frameon=False)



#Panel 5: O2
panel5 = plt.subplot(gs[4:5,0:1])
plt.plot(LV_runtime, m32,'C3', label='$m32$', linewidth=0.3)
panel5.fill_between(LV_runtime,O2_conc,facecolor='C2', alpha=0.1,
interpolate=True)
plt.tick_params(labelbottom=False)
#plt.xlabel('Time on Stream, min')
plt.ylabel('Ion current, A')
plt.xlim(0,1150)
plt.ylim(0,5e-11)
plt.legend(frameon=False)


#Panel 6: NO2
panel6 = plt.subplot(gs[5:6,0:1])
plt.plot(LV_runtime, m46,'C5', label='$m46$', linewidth=0.3)
#plt.xlabel('Time on Stream, min')
plt.tick_params(labelbottom=False)
plt.ylabel('Ion current, A')
plt.xlim(0,1150)
plt.legend(frameon=False)



#Panel 7:
panel7 = plt.subplot(gs[6:7,0:1])
```

```
plt.plot(LV_runtime, m4, label='m4', linewidth=0.3)
#plt.xlabel('Time on Stream, min')
plt.tick_params(labelbottom=False)
plt.ylabel('Ion current, A')
plt.xlim(0,1150)
plt.legend(frameon=False)


#Panel 8:
panel8 = plt.subplot(gs[7:8,0:1])
plt.plot(LV_runtime, m14, label='$m14$', linewidth=0.3)
#plt.xlabel('Time on Stream, min')
plt.tick_params(labelbottom=False)
plt.ylabel('Ion current, A')
plt.xlim(0,1150)
plt.legend(frameon=False)


#Panel 9:
panel9 = plt.subplot(gs[8:9,0:1])
plt.plot(LV_runtime, m15, label='$m15$', linewidth=0.3)
#plt.xlabel('Time on Stream, min')
plt.tick_params(labelbottom=False)
plt.ylabel('Ion current, A')
plt.xlim(0,1150)
plt.legend(frameon=False)


#Panel 10:
panel10 = plt.subplot(gs[9:10,0:1])
plt.plot(LV_runtime, m16, label='$m16$', linewidth=0.3)
#plt.xlabel('Time on Stream, min')
plt.tick_params(labelbottom=False)
plt.ylabel('Ion current, A')
plt.xlim(0,1150)
plt.legend(frameon=False)


#Panel 11:
panel11 = plt.subplot(gs[10:11,0:1])
plt.plot(LV_runtime, m28, label='$m28$', linewidth=0.3)
#plt.xlabel('Time on Stream, min')
```

```python
plt.tick_params(labelbottom=False)
plt.ylabel('Ion current, A')
plt.xlim(0,1150)
plt.legend(frameon=False)


#Panel 12:
panel12 = plt.subplot(gs[11:12,0:1])
plt.plot(LV_runtime, m40, label='$m40$', linewidth=0.3)
#plt.xlabel('Time on Stream, min')
plt.tick_params(labelbottom=False)
plt.ylabel('Ion current, A')
plt.xlim(0,1150)
plt.legend(frameon=False)


#Panel 13: N2O
panel13 = plt.subplot(gs[12:13,0:1])
plt.plot(LV_runtime, m44, label='$m44$', linewidth=0.3)
#plt.xlabel('Time on Stream, min')
plt.tick_params(labelbottom=False)
plt.ylabel('Ion current, A')
plt.xlim(0,1150)
plt.ylim(2.2e-13,4e-13)
plt.legend(frameon=False)


#Panel 14: m2
panel14 = plt.subplot(gs[13:14,0:1])
plt.plot(LV_runtime, m2, label='$m2$', linewidth=0.3)
#plt.xlabel('Time on Stream, min')
plt.tick_params(labelbottom=False)
plt.ylabel('Ion current, A')
plt.xlim(0,1150)
plt.legend(frameon=False)

#Panel 15: Pressure
panel15 = plt.subplot(gs[14:15,0:1])
plt.plot(LV_runtime, Pressure, label='$Pressure$', linewidth=0.3)
plt.xlabel('Time on Stream, min')
plt.ylabel('Ion current, A')
```

```
plt.xlim(0,1150)
plt.legend(frameon=False)
```

```
plt.show()
```
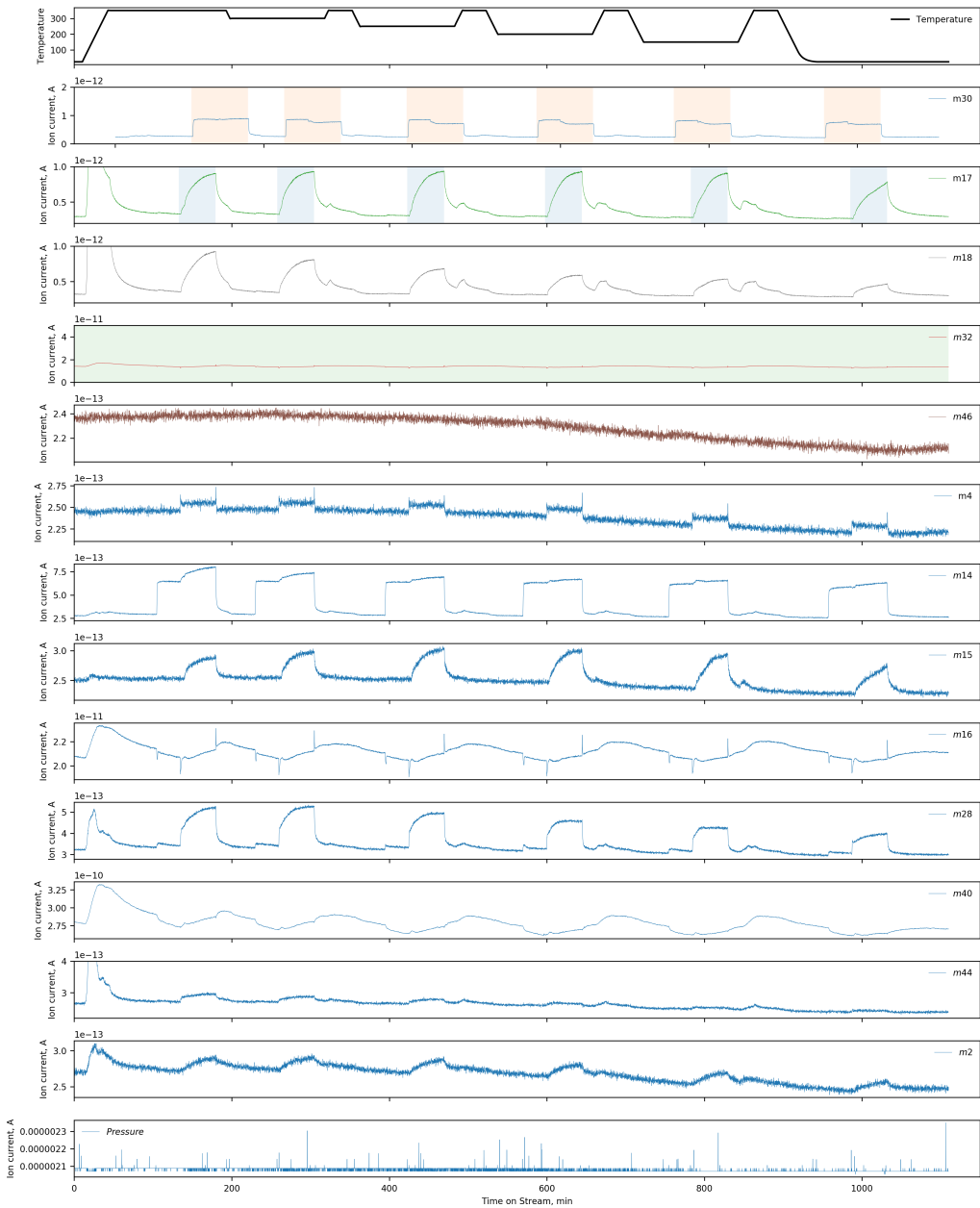
E.2 IR data

The script presented in this chapter show how the IR data was imported and how the absorbance was calculated. The absorbance was recalculated with new background spectrum for each temperature. The LabVIEV runtime was regridded to fit the runtime of the IR data.

```
#IR data

#Read in Data
os.chdir("/Users/jane/Documents/NTNU_master_2018/Experiments3
/2018-05-11_3CuAl/output")
#list all files
filelist=sorted(os.listdir(os.getcwd()))
num_files=range(len(filelist))

time0=dt.datetime.strptime(filelist[0], "%Y-%m-%d_T%H-%M-%S.drifts")

wavenumber,background=np.loadtxt(filelist[80], skiprows=1, unpack=True)
IRdata=np.empty([len(filelist),len(wavenumber)])
runtime=np.empty(len(filelist))

for num, filename in enumerate(filelist,0):
    wavenumber,data=np.loadtxt(filelist[num], skiprows=1, unpack=True)
    #IRdata[num]=np.log10(background/data)
    IRdata[num]=data
    delta=(dt.datetime.strptime(filename,
                                "%Y-%m-%d_T%H-%M-%S.drifts"))-time0
    minutes=delta.total_seconds()/60
    runtime[num]=minutes

#regrid temperature
temperatureIR=griddata(LV_runtime,temperature,runtime,method='linear')
df_temperature=pd.DataFrame(data=temperatureIR)

df_temperature.iplot(kind='scatter',xTitle='Dates',yTitle='Returns',
title='Cufflinks - Line Chart')
#regrid runtime
temperatureIR=griddata(LV_runtime,temperature,runtime,method='linear')
```

```
df_runtime=pd.DataFrame(data=runtime)

df_runtime.iplot(kind='scatter', xTitle='Dates', yTitle='Returns',
                 title='Cufflinks - Line Chart')
```

Importing raw IR data:

```
#Make DataFrame with Pandas
df_datamatrix=pd.DataFrame(data=absorbance, index=runtime,
columns=AbsWavenumber)

#split dataframe
#df_datamatrix=df_datamatrix.iloc[0:1500,1500:10000:5]
df_datamatrix=df_datamatrix.iloc[::3,::5]
#plot setup——————————————————————————
fig=plt.figure(figsize=(12,12), dpi=200)
fsize=6
plt.rc('axes', linewidth=0.5)
plt.rc('ytick', labelsize=6)
#——————————————————————————————————

#Plot time resolved lineplot
X,Y=np.meshgrid(df_datamatrix.columns, df_datamatrix.index)
Z=df_datamatrix
ax = fig.gca(projection='3d')
ax.plot_surface(X,Y,Z, rstride=1, cstride=1, cmap=cm.viridis, shade=True,
                antialiased=True, alpha=1)
ax.set_xlabel('Wavenumber, $cm^{-1}$')
ax.set_ylabel('Runtime, min')
ax.set_zlabel('Absorption, -')
#plt.xlim(2650, 1650)
#plt.ylim(285,)
ax.view_init(azim=0)
plt.show()
```
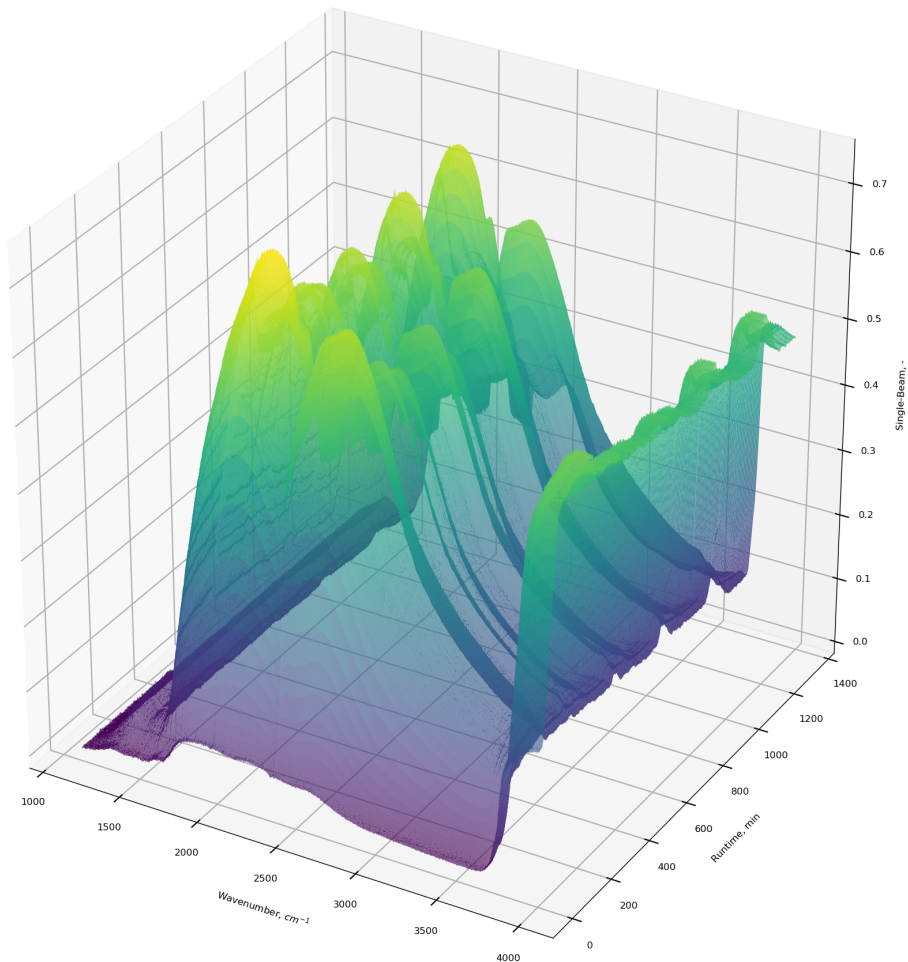
Calculating absorbance at 350°C:

```
df_rawIR=pd.DataFrame(data=IRdata,index=runtime,columns=wavenumber)
df_cutIR=df_rawIR.iloc[::,100::]  #[::,1600::]



AbsData=df_cutIR.as_matrix()
#wavenumber_abs=wavenumber[1500,:]
abs_wavenumber=pd.DataFrame(data=wavenumber)
df_wavenumber_abs=abs_wavenumber.iloc[100::]
```

```
AbsWavenumber=df_wavenumber_abs.as_matrix()

#AbsWavenumber=df350.columns

#C: calculate absorbance a=log(I0/I)
I0=AbsData[90,:] #endret fra 180
ratio=np.empty(np.shape(AbsData))
for i in range(len(AbsData)):
    ratio[i,:]=np.divide(I0,AbsData[i,:])
absorbance=np.log10(ratio)
absorbance=np.nan_to_num(absorbance, copy=False)
#absorbance[np.where(absorbance<0)]=0
#absorbance[np.where(absorbance>1)]=1



    #ratio[i,:]=np.divide(I0,AbsData[i,:])
#absorbance=-np.log10(ratio)
#absorbance[np.where(absorbance<0)]=0




#Make DataFrame with Pandas
df_datamatrix=pd.DataFrame(data=absorbance,index=runtime,
                            columns=AbsWavenumber)

#split dataframe
#df_datamatrix=df_datamatrix.iloc[0:1500,1500:10000:5]
df_datamatrix=df_datamatrix.iloc[::3,::5]
#plot setup————————————————————————
fig=plt.figure(figsize=(12,12), dpi=200)
fsize=6
plt.rc('axes', linewidth=0.5)
plt.rc('ytick', labelsize=6)
#————————————————————————————————————

#Plot time resolved lineplot
X,Y=np.meshgrid(df_datamatrix.columns,df_datamatrix.index)
Z=df_datamatrix
```

xxviii

```
ax = fig.gca(projection='3d')
ax.plot_surface(X,Y,Z, rstride=1, cstride=1, cmap=cm.viridis, shade=True,
                antialiased=True, alpha=1)
ax.set_xlabel('Wavenumber, $cm^{-1}$')
ax.set_ylabel('Runtime, min')
ax.set_zlabel('Absorption, -')
#plt.xlim(2650, 1650)
#plt.ylim(285,)
ax.view_init(azim=0)
plt.show()
```

E.2.1 Contour plots and line plots for each temperature

The script in this chapter show an example of how the absorbance was calculated at each temperature, and contour plots and line plots were made in order to better see the changes occurring at each temperature step. The following example is at 300°C.

```
df300=pd.DataFrame(data=IRdata,index=runtime,columns=wavenumber)
df300cut=df300.iloc[::,100::]

AbsData300=df300cut.as_matrix()
```

xxx

```
abs_wavenumber300=df300cut.columns
runtime300=df300cut.index


#C: calculate absorbance a=log(I0/I)
I0=AbsData300[215,:]
ratio=np.empty(np.shape(AbsData300))
for i in range(len(AbsData300)):
    ratio[i,:]=np.divide(I0,AbsData300[i,:])
absorbance300=np.log10(ratio)
absorbance300=np.nan_to_num(absorbance300, copy=False)


#Contourplot 300deg
fig=plt.figure(figsize=(10,6), dpi=300)
plt.style.use('default')
mpl.rcParams.update({'font.size': 8})
df_datamatrix=pd.DataFrame(data=absorbance300,
                           index=runtime300,columns=abs_wavenumber300)


#split dataframe
#df_datamatrix=df_datamatrix.iloc[0:1500,1500:10000:5]
df_datamatrix=df_datamatrix.iloc[210:320:,100::]
#plot setup----------------------------------

#--------------------------------------------

#Plot time resolved lineplot
X,Y=np.meshgrid(df_datamatrix.columns,df_datamatrix.index)
Z=df_datamatrix

plt.contourf(X,Y,Z,100, cmap=cm.jet, antialiased=True, alpha=1)
plt.xlabel('Wavenumber, $cm^{-1}$')
plt.ylabel('Runtime, min')
plt.text(3790,310, 'a', fontsize=14, fontweight='bold')
plt.text(3200,310, 'b', fontsize=14, color='C0', fontweight='bold')
plt.text(2350,310, 'c', fontsize=14, color='C1', fontweight='bold')
plt.text(1640,310, 'd', fontsize=14, color='C5', fontweight='bold')
plt.text(1585,249, 'e', fontsize=14, color='C3', fontweight='bold')
```

```
plt.text(1510,310, 'f', fontsize=14, color='C1', fontweight='bold')
plt.text(1300,295, 'g', fontsize=14, color='C7', fontweight='bold')
plt.text(3900,230, 'NO was introduced', fontsize=12)
plt.text(3900,260, 'NH$_3$ was introduced', fontsize=12)
plt.text(3900,302, 'Both gases were turned off', fontsize=12)
plt.text(3900,220, '"Clean sample"', fontsize=12)

plt.xlim(4000, 1200)

plt.colorbar()
plt.plot([3100,1300], [231,231], 'k-', lw=1)
plt.plot([3100,1300], [261,261], 'k-', lw=1)
plt.plot([2700,1300], [303,303], 'k-', lw=1)
plt.show()
```
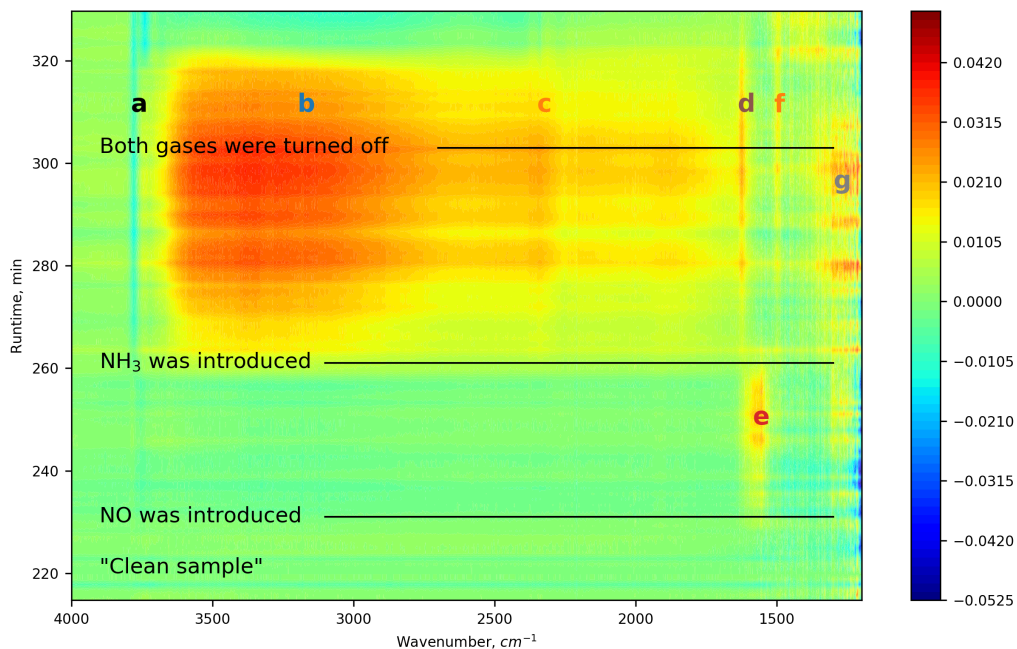
```
#Lineplot 300
df_datamatrix=pd.DataFrame(data=absorbance300,
                           index=runtime300,columns=abs_wavenumber300)

df_datamatrix=df_datamatrix.iloc[210:290:,100::]
#plot setup————————————————————————————
fig=plt.figure(figsize=(10,6), dpi=300)
plt.style.use('default')
mpl.rcParams.update({'font.size': 10})
#————————————————————————————————————————

#Plot time resolved lineplot
X=df_datamatrix.columns #wavenumber
Y=df_datamatrix.index #time
Z=df_datamatrix.as_matrix() #data

norm=mpl.colors.Normalize(0,len(df_datamatrix.index))
c_m=mpl.cm.viridis
s_m=mpl.cm.ScalarMappable(cmap=c_m, norm=norm)
s_m.set_array([])

for time, Y in enumerate(Y, 0):
    plt.plot(X,Z[time], label=time, color=s_m.to_rgba(time), linewidth=0.4)
plt.xlabel('Wavenumber, $cm^{-1}$')
plt.ylabel('Absorbance, a.u.')
#plt.text(3770,-0.015, 'a', fontsize=12)
#plt.text(3570,0.036, 'b', fontsize=12)
#plt.text(3450,0.038, 'c', fontsize=12)
#plt.text(3260,0.038, 'd', fontsize=12)
#plt.text(1630,0.025, 'd', fontsize=12, color='C5', fontweight='bold')
#plt.text(1560,0.025, 'e', fontsize=12, color='C3', fontweight='bold')
#plt.text(1500,0.019, 'f', fontsize=12, color='C1', fontweight='bold')
#plt.text(1250,0.035, 'g', fontsize=12, color='C7', fontweight='bold')
#plt.text(1560,0.025, 'i', fontsize=12)
#plt.text(1500,0.021, 'j', fontsize=12)
```

```
#ax.set_zlabel('Absorption, −')
plt.xlim(4000, 1200)
plt.ylim(−0.02,0.04)
#ax.view_init(azim=0)
cbar=plt.colorbar(s_m, label='minutes $\longrightarrow$')
plt.show()
```
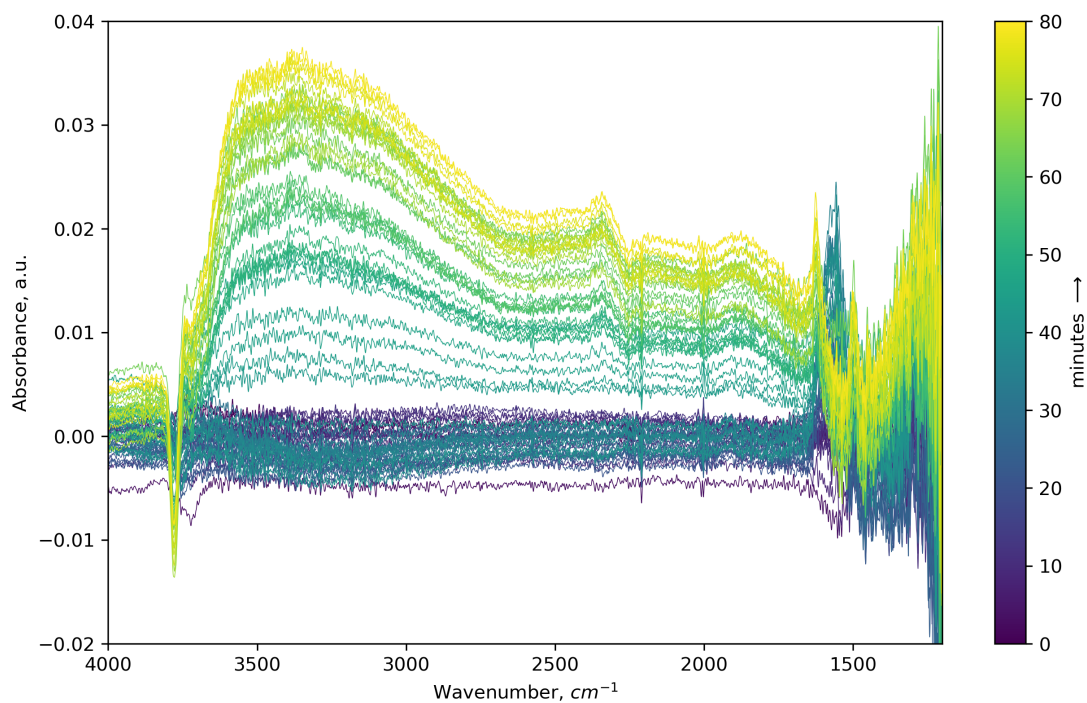
E.3   Correlation between MS and IR data

Selected data points from the two data sets were then plotted against each other in order to highlight the evolution of various peaks and see the correlation between IR data and MS data. Here is an example of one of these codes.

```
#plot setup————————————————————————————
fig=plt.figure(figsize=(10,6), dpi=300)
plt.style.use('default')
mpl.rcParams.update({'font.size': 10})
#————————————————————————————————————————
gs=mpl.gridspec.GridSpec(4,1)
gs.update(wspace=0.4, hspace=0.6, bottom=0,top=1)


#panel 1: 300 deg
panel1 = plt.subplot(gs[0:1,0:1])
df_datamatrix=pd.DataFrame(data=absorbance300,index=runtime300,
                            columns=abs_wavenumber300)
df_datamatrix=df_datamatrix.iloc[210:300:,100::]
X=df_datamatrix.columns #wavenumber
Y=df_datamatrix.index #time
Z=df_datamatrix.as_matrix() #data
norm=mpl.colors.Normalize(0,len(df_datamatrix.index))
c_m=mpl.cm.viridis
s_m=mpl.cm.ScalarMappable(cmap=c_m, norm=norm)
s_m.set_array([])
for time, Y in enumerate(Y, 0):
    plt.plot(X,Z[time], label=time, color=s_m.to_rgba(time), linewidth=0.4)
plt.xlabel('Wavenumber, $cm^{-1}$')
plt.ylabel('Absorbance, a.u.')
plt.xlim(2500,2000)
plt.text(2345,0.028, 'c', fontsize='14', color='C1', fontweight='bold')
plt.text(2470,0.025, 'A', fontsize=14, fontweight='bold')
plt.ylim(0,0.035)
#ax.view_init(azim=0)

#panel 2: 150deg
panel2 = plt.subplot(gs[1:2,0:1])
```

```
df_datamatrix=pd.DataFrame(data=absorbance150,index=runtime150,
                            columns=abs_wavenumber150)
df_datamatrix=df_datamatrix.iloc[700:790:,100::]
X=df_datamatrix.columns #wavenumber
Y=df_datamatrix.index #time
Z=df_datamatrix.as_matrix() #data
norm=mpl.colors.Normalize(0,len(df_datamatrix.index))
c_m=mpl.cm.viridis
s_m=mpl.cm.ScalarMappable(cmap=c_m, norm=norm)
s_m.set_array([])
for time, Y in enumerate(Y, 0):
    plt.plot(X,Z[time], label=time, color=s_m.to_rgba(time),
             linewidth=0.4)
plt.xlabel('Wavenumber, $cm^{-1}$')
plt.ylabel('Absorbance, a.u.')
plt.xlim(2500, 2000)
plt.ylim(0,0.07)
plt.text(2345,0.05, 'c', fontsize='14', color='C1', fontweight='bold')
plt.text(2470,0.055, 'B', fontsize=14, fontweight='bold')


#panel 3: m18, water
panel3 = plt.subplot(gs[2:3,0:1])
x=range(0,100)

m18max2=np.empty([100,1])
m18max5=np.empty([100,1])



for i in range(0,100):
    m18max2[i] = np.max(m18_rg[i+210])
    m18max5[i] = np.max(m18_rg[i+697]) #530


plt.plot(x, m18max2, color='C1', linewidth=0.7, label='300$^oC$')
plt.plot(x, m18max5, color='C9', linewidth=0.7, label='150$^oC$')
```

```
#ax2.set_ylabel('Ion current, A')
plt.xlim(-5,105)
#ax2.set_ylim(0,2e-12)
plt.legend(frameon=False, loc=1)

plt.xlabel('Relative Runtime, min')
plt.text(0,8e-13, 'C', fontsize=14, fontweight='bold')
plt.ylim(0.2e-12,1e-12)
plt.ylabel('Ion current, A')

#panel 4: m28, ammonia
#Ammonia MS
panel4 = plt.subplot(gs[3:4,0:1])
x=range(0,100)

Amax2=np.empty([100,1])
Amax5=np.empty([100,1])


for i in range(0,100):
    Amax2[i] = np.max(Ammonia[i+210])
    Amax5[i] = np.max(Ammonia[i+697])


plt.plot(x, Amax2, color='C1', linewidth=0.7, label='300$^oC$')
plt.plot(x, Amax5, color='C9', linewidth=0.7, label='150$^oC$')

#ax2.set_ylabel('Ion current, A')
plt.xlim(-5,105)
#ax2.set_ylim(0,2e-12)
plt.legend(frameon=False)

plt.xlabel('Relative Runtime, min')
plt.text(0,8e-13, 'D', fontsize=14, fontweight='bold')
plt.ylim(0.2e-12,1e-12)
plt.ylabel('Ion current, A')
panel4.fill_between(x,NH3_conc_rg[90:190],facecolor='C0', alpha=0.1,
```

```
                    interpolate=True)
```

```
plt.show()
```
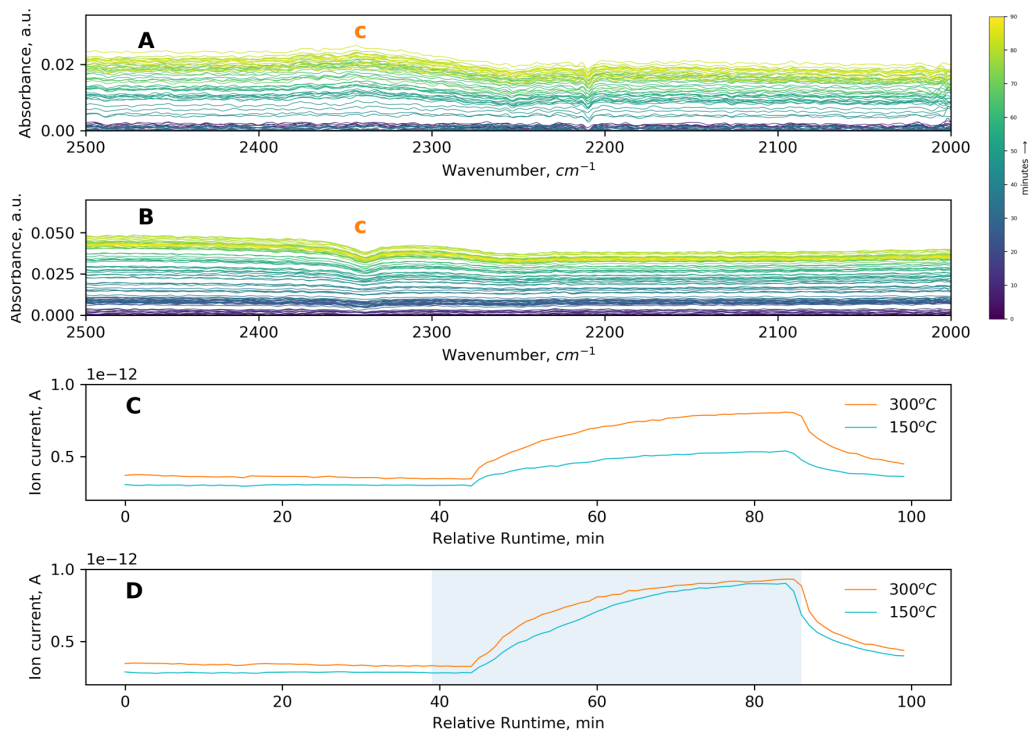
Appendix F

Risk Assessment

A risk assessment for the laboratory work were performed and is given in this appendix.

ID	23707	**Status**	**Dato**
Risikoområde	Risikovurdering: Helse, miljø og sikkerhet (HMS)	Opprettet	04.10.2017
Opprettet av	Jane Eiane Aarsland	Vurdering startet	04.10.2017
Ansvarlig	Jane Eiane Aarsland	Tiltak besluttet	04.10.2017
		Avsluttet	

Risikovurdering:

CAT, Master Student, 2017, Jane Eiane Aarsland

Gyldig i perioden:
9/4/2017 - 6/25/2018

Sted:
Gløshaugen - Kjemi 5

Mål / hensikt
This risk assessment contains the activities that the master student Jane Eiane Aarsland will perform in the labs of the Catalysis group.

Bakgrunn
The project aims to to use FTIR to study industrial catalysts in their actual work environment (in situ).

Beskrivelse og avgrensninger
Will determine acid sites on different catalysts made of Al_2O_3, ZrO_3, Pt, WO_3 mixed with KBr at different dilution ratios and temperature. Pyridine and NH_3 is used as probe molecules. In master thesis, SCR reaction experiments will be done using bottles of NH_3, NO, O_2 and Ar gas.

Forutsetninger, antakelser og forenklinger
[Ingen registreringer]

Vedlegg
[Ingen registreringer]

Referanser
[Ingen registreringer]

xl

Oppsummering, resultat og endelig vurdering

I oppsummeringen presenteres en oversikt over farer og uønskede hendelser, samt resultat for det enkelte konsekvensområdet.

Farekilde: **In-situ DRIFTS**

Uønsket hendelse: **Leakage**

Konsekvensområde: Helse   Risiko før tiltak: 🟡   Risiko etter tiltak: ⚪

Uønsket hendelse: **Uncontrolled heating**

Konsekvensområde: Helse   Risiko før tiltak: 🟢   Risiko etter tiltak: ⚪
                       Materielle verdier   Risiko før tiltak: 🟢   Risiko etter tiltak: ⚪

Uønsket hendelse: **Forget to turn on Nitrogen**

Konsekvensområde: Materielle verdier   Risiko før tiltak: 🟢   Risiko etter tiltak: ⚪

Uønsket hendelse: **Pyridine vapor into rig**

Konsekvensområde: Helse   Risiko før tiltak: 🟢   Risiko etter tiltak: ⚪
                       Materielle verdier   Risiko før tiltak: 🟢   Risiko etter tiltak: ⚪

Uønsket hendelse: **Forget to turn on water pump**

Konsekvensområde: Materielle verdier   Risiko før tiltak: 🟢   Risiko etter tiltak: ⚪

Farekilde: **Sample preparation**

Uønsket hendelse: **Spillage**

Konsekvensområde: Helse   Risiko før tiltak: 🟢   Risiko etter tiltak: ⚪

Uønsket hendelse: **Dust formation**

Konsekvensområde: Helse   Risiko før tiltak: 🟢   Risiko etter tiltak: ⚪

	Utskriftsdato:	Utskrift foretatt av:	Side:
Norges teknisk-naturvitenskapelige universitet (NTNU)			
Unntatt offentlighet jf. Offentlighetsloven § 14	07.06.2018	Jane Eiane Aarsland	2/15

xli

APPENDIX F. RISK ASSESSMENT

Farekilde:	Leakage of ammonia		

Uønsket hendelse: Leakage of ammonia gas into rig

Konsekvensområde: Helse   Risiko før tiltak: 🟢 Risiko etter tiltak: ⚪

Uønsket hendelse: Leakage of ammonia gas from gas bottle

Konsekvensområde: Helse   Risiko før tiltak: 🟢 Risiko etter tiltak: ⚪

Farekilde:	Leakage of NO		

Uønsket hendelse: Leakage of NO gas into rig

Konsekvensområde: Helse   Risiko før tiltak: 🟡 Risiko etter tiltak: ⚪

Uønsket hendelse: Leakage of NO from gas bottle

Konsekvensområde: Helse   Risiko før tiltak: 🟡 Risiko etter tiltak: ⚪

Endelig vurdering

Norges teknisk-naturvitenskapelige universitet (NTNU)	Utskriftsdato:	Utskrift foretatt av:	Side:
Unntatt offentlighet jf. Offentlighetsloven § 14	07.06.2018	Jane Eiane Aarsland	3/15

xlii

Involverte enheter og personer

En risikovurdering kan gjelde for en, eller flere enheter i organisasjonen. Denne oversikten presenterer involverte enheter og personell for gjeldende risikovurdering.

Enhet /-er risikovurderingen omfatter

- NTNU

Deltakere

Samuel K. Regli

Lesere

Karin Wiggen Dragsten

Magnus Rønning

Andre involverte/interessenter

[Ingen registreringer]

Følgende akseptkriterier er besluttet for risikoområdet Risikovurdering: Helse, miljø og sikkerhet (HMS):

Helse   **Materielle verdier**   **Omdømme**   **Ytre miljø**

Norges teknisk-naturvitenskapelige universitet (NTNU)

Unntatt offentlighet jf. Offentlighetsloven § 14

Utskriftsdato: 07.06.2018

Utskrift foretatt av: Jane Eiane Aarsland

Side: 4/15

xliii

APPENDIX F. RISK ASSESSMENT

Oversikt over eksisterende, relevante tiltak som er hensyntatt i risikovurderingen

I tabellen under presenteres eksisterende tiltak som er hensyntatt ved vurdering av sannsynlighet og konsekvens for aktuelle uønskede hendelser.

Farekilde	Uønsket hendelse	Tiltak hensyntatt ved vurdering
In-situ DRIFTS	Leakage	Safety goggles
	Leakage	Lab coat
	Leakage	Nitrile gloves
	Leakage	Emergency Eye shower and flask
	Leakage	Emergency shower
	Uncontrolled heating	Thermocouple
	Forget to turn on Nitrogen	
	Pyridine vapor into rig	Venting system
	Forget to turn on water pump	Procedure
Sample preparation	Spillage	Safety goggles
	Spillage	Lab coat
	Spillage	Nitrile gloves
	Spillage	Emergency Eye shower and flask
	Spillage	Venting system
	Dust formation	Safety goggles
	Dust formation	Lab coat
	Dust formation	Nitrile gloves
	Dust formation	Venting system
Leakage of ammonia	Leakage of ammonia gas into rig	Venting system
	Leakage of ammonia gas from gas bottle	Venting system
Leakage of NO	Leakage of NO gas into rig	Safety goggles
	Leakage of NO gas into rig	Lab coat
	Leakage of NO gas into rig	Nitrile gloves
	Leakage of NO gas into rig	Venting system
	Leakage of NO gas into rig	Gas Detectors
	Leakage of NO from gas bottle	Venting system
	Leakage of NO from gas bottle	Gas Detectors
	Leakage of NO from gas bottle	Open windows

Eksisterende og relevante tiltak med beskrivelse:

Safety goggles
Eye protection to be worn at all times while working in lab.

Norges teknisk-naturvitenskapelige universitet (NTNU)	Utskriftsdato:	Utskrift foretatt av:	Side:
Unntatt offentlighet jf. Offentlighetsloven § 14	07.06.2018	Jane Eiane Aarsland	5/15

xliv

Lab coat
Protection of skin against spills, chemicals, etc.

Nitrile gloves
Hand protection against chemicals

Emergency Eye shower and flask
In case chemicals come in contact with eyes. Rinse with plenty of water, consult medical personnell

Emergency shower
In case of serious spills, or clothing on fire. Located in lab.

Fire Extinguisher
In case of fire, located in lab

Venting system
The system is inside a rig with ventilation

Thermocouple
Thermocouple in cell will monitor the temperature

Procedure
Follow FTIR method procedure. Check that everything is ready prior to an experiment

Gas Detectors
Can use gas detectors which will tell if the NO concentration in the air exceeds the limit

Open windows
Open the windows to ventilate the room

Norges teknisk-naturvitenskapelige universitet (NTNU)	**Utskriftsdato:**	**Utskrift foretatt av:**		**Side:**
Unntatt offentlighet jf. Offentlighetsloven § 14	07.06.2018	Jane Eiane Aarsland		6/15

xlv

Risikoanalyse med vurdering av sannsynlighet og konsekvens

I denne delen av rapporten presenteres detaljer dokumentasjon av de farer, uønskede hendelser og årsaker som er vurdert. Innledningsvis oppsummeres farer med tilhørende uønskede hendelser som er tatt med i vurderingen.

Følgende farer og uønskede hendelser er vurdert i denne risikovurderingen:

- **In-situ DRIFTS**
  - Leakage
  - Uncontrolled heating
  - Forget to turn on Nitrogen
  - Pyridine vapor into rig
  - Forget to turn on water pump
- **Sample preparation**
  - Spillage
  - Dust formation
- **Leakage of ammonia**
  - Leakage of ammonia gas into rig
  - Leakage of ammonia gas from gas bottle
- **Leakage of NO**
  - Leakage of NO gas into rig
  - Leakage of NO from gas bottle

Detaljert oversikt over farekilder og uønskede hendelser:

Farekilde: In-situ DRIFTS

Infrared spectra were collected using the OMNIC v.9.0 software in connection with a 912A0763 Nicolet iS50 FTIR KBr Gold Spectrometer and pyridine

Uønsket hendelse: Leakage

Leakage of pyridine into the surrounding area.

Årsak: Bad Connection between bubbler and pipes

Årsak: Residuals of pyridine in reaction chamber

Sannsynlighet for hendelsen (felles for alle konsekvensområder): **Sannsynlig (3)**

Kommentar:
Limited volume in pyridine bottle (ca 30 ml)

Konsekvensområde: Helse   *Risiko:*

Vurdert konsekvens: **Middels (2)**

Kommentar: R-11 Highly flammable.
R-20/21/22 Harmful by inhalation, in contact with skin and if swallowed.

Uønsket hendelse: Uncontrolled heating

Årsak: Uncontrolled heating of temperature controller

Sannsynlighet for hendelsen (felles for alle konsekvensområder): **Svært lite sannsynlig (1)**

Kommentar:
[Ingen registreringer]

Konsekvensområde: Helse   *Risiko:*

Vurdert konsekvens: **Liten (1)**

Kommentar: [Ingen registreringer]

Norges teknisk-naturvitenskapelige universitet (NTNU)	**Utskriftsdato:**	**Utskrift foretatt av:**	**Side:**
Unntatt offentlighet jf. Offentlighetsloven § 14	07.06.2018	Jane Eiane Aarsland	8/15

xlvii

APPENDIX F. RISK ASSESSMENT

Konsekvensområde: Materielle verdier

Vurdert konsekvens: **Middels (2)**

Kommentar: [Ingen registreringer]

Risiko:

Uønsket hendelse: Forget to turn on Nitrogen

Disturbs measurements. Have to repeat experiments. Will cause more power consumption

Sannsynlighet for hendelsen (felles for alle konsekvensområder): **Lite sannsynlig (2)**

Kommentar:
[Ingen registreringer]

Konsekvensområde: Materielle verdier

Vurdert konsekvens: **Liten (1)**

Kommentar: [Ingen registreringer]

Risiko:

Uønsket hendelse: Pyridine vapor into rig

Due to pressure in tubes if valves are not opened correctly. Will smell bad. Leave the rig and close the doors. Turn off nitrogen and ventilate the rig.

Årsak: Pressure in tubes if valves are not opened correctly

Sannsynlighet for hendelsen (felles for alle konsekvensområder): **Lite sannsynlig (2)**

Kommentar:
[Ingen registreringer]

Konsekvensområde: Helse

Vurdert konsekvens: **Middels (2)**

Kommentar: [Ingen registreringer]

Risiko:

Norges teknisk-naturvitenskapelige universitet (NTNU)	Utskriftsdato:	Utskrift foretatt av:	Side:
Unntatt offentlighet jf. Offentlighetsloven § 14	07.06.2018	Jane Eiane Aarsland	9/15

xlviii

Konsekvensområde: Materielle verdier

Vurdert konsekvens: **Middels (2)**

Kommentar: [Ingen registreringer]

Risiko:

Uønsket hendelse: Forget to turn on water pump

- -

Årsak: Damage to setup

Sannsynlighet for hendelsen (felles for alle konsekvensområder): **Lite sannsynlig (2)**

Kommentar:
Follow the procedure

Konsekvensområde: Materielle verdier

Vurdert konsekvens: **Middels (2)**

Kommentar: [Ingen registreringer]

Risiko:

Norges teknisk-naturvitenskapelige universitet (NTNU)	**Utskriftsdato:**	**Utskrift foretatt av:**	**Side:**
Unntatt offentlighet jf. Offentlighetsloven § 14	07.06.2018	Jane Eiane Aarsland	10/15

xlix

APPENDIX F. RISK ASSESSMENT

Farekilde: Sample preparation

All samples have to be diluted in KBr before analysis

Uønsket hendelse: Spillage

Spillage of samples

Sannsynlighet for hendelsen (felles for alle konsekvensområder):   **Sannsynlig (3)**

    Kommentar:
    [Ingen registreringer]

Konsekvensområde: Helse   *Risiko:*

    Vurdert konsekvens: **Liten (1)**

      Kommentar: Very small amount of powder is used to fill the FTIR cell

Uønsket hendelse: Dust formation

Sannsynlighet for hendelsen (felles for alle konsekvensområder):   **Sannsynlig (3)**

    Kommentar:
    [Ingen registreringer]

Konsekvensområde: Helse   *Risiko:*

    Vurdert konsekvens: **Liten (1)**

      Kommentar: Very small amount of samples is used to fill the FTIR cell.

l

Farekilde: Leakage of ammonia

5000 ppm Ammonia gas in Argon was used in FTIR experiments

Uønsket hendelse: Leakage of ammonia gas into rig

Due to pressure in tubes if valves are not opened correctly. Will smell bad. Leave the rig and close the doors. Close gass bottle and ventilate the rig.

Årsak: Due to pressure in tubes if valves are not opened correctly

Sannsynlighet for hendelsen (felles for alle konsekvensområder): **Lite sannsynlig (2)**

Kommentar:
[Ingen registreringer]

Konsekvensområde: Helse

Risiko:

Vurdert konsekvens: **Middels (2)**

Kommentar: WIll smell the ammonia quickly. Can close bottle and ventilate.

Uønsket hendelse: Leakage of ammonia gas from gas bottle

Will smell bad. Open windows and ventilate

Sannsynlighet for hendelsen (felles for alle konsekvensområder): **Lite sannsynlig (2)**

Kommentar:
[Ingen registreringer]

Konsekvensområde: Helse

Risiko:

Vurdert konsekvens: **Middels (2)**

Kommentar: WIll smell the ammonia quickly. Can close bottle and ventilate.

Norges teknisk-naturvitenskapelige universitet (NTNU)	**Utskriftsdato:**	**Utskrift foretatt av:**		**Side:**
Unntatt offentlighet jf. Offentlighetsloven § 14	07.06.2018	Jane Eiane Aarsland		12/15

li

APPENDIX F. RISK ASSESSMENT

Farekilde: Leakage of NO

4000 ppm of NO gas in Argon was used for adsorption experiments

Uønsket hendelse: Leakage of NO gas into rig

Due to leakage from tubes. Leave the rig and close the doors. Close gas bottle and ventilate the rig.

Årsak: Leakage from tubes

Sannsynlighet for hendelsen (felles for alle konsekvensområder): **Lite sannsynlig (2)**

Kommentar:

[Ingen registreringer]

Konsekvensområde: Helse   *Risiko:*

Vurdert konsekvens: **Stor (3)**

Kommentar: Inhalation of NO is very toxic, but the chance of leakage into the rig is very
small.

Uønsket hendelse: Leakage of NO from gas bottle

Open windows and ventilate.

Årsak: Leakage from gas bottle

Sannsynlighet for hendelsen (felles for alle konsekvensområder): **Lite sannsynlig (2)**

Kommentar:

[Ingen registreringer]

Konsekvensområde: Helse   *Risiko:*

Vurdert konsekvens: **Stor (3)**

Kommentar: Inhalation of NO is very toxic

Norges teknisk-naturvitenskapelige universitet (NTNU)	Utskriftsdato:	Utskrift foretatt av:	Side:
Unntatt offentlighet jf. Offentlighetsloven § 14	07.06.2018	Jane Eiane Aarsland	13/15

lii

Oversikt over besluttede risikoreduserende tiltak:

Under presenteres en oversikt over risikoreduserende tiltak som skal bidra til å reduseres sannsynlighet og/eller konsekvens for uønskede hendelser.

Detaljert oversikt over besluttede risikoreduserende tiltak med beskrivelse:

Norges teknisk-naturvitenskapelige universitet (NTNU)	**Utskriftsdato:**	**Utskrift foretatt av:**	**Side:**
Unntatt offentlighet jf. Offentlighetsloven § 14	07.06.2018	Jane Eiane Aarsland	14/15

liii

APPENDIX F. RISK ASSESSMENT

Detaljert oversikt over vurdert risiko for hver farekilde/uønsket hendelse før og etter besluttede tiltak